RESERVOIR CHARACTERIZATION AND DEVELOPMENT OPPORTUNITIES IN JACOB FIELD, SOUTH-CENTRAL TEXAS

A Thesis

by

MIRKO JOSHOE HERNANDEZ DEPAZ

Submitted to the Office of Graduate Studies of
Texas A&M University
in partial fulfillment of the requirements for the degree of

MASTER OF SCIENCE

May 2004

Major Subject: Petroleum Engineering

RESERVOIR CHARACTERIZATION AND DEVELOPMENT

OPPORTUNITIES IN JACOB FIELD, SOUTH-CENTRAL TEXAS

A Thesis

by

MIRKO JOSHOE HERNANDEZ DEPAZ

Submitted to Texas A&M University
in partial fulfillment of the requirements
for the degree of

MASTER OF SCIENCE

Approved as to style and content by:

David S. Schechter (Chair of Committee)	Duane A. McVay (Member)
Steven L. Dorobek (Member)	Stephen A. Holditch (Head of Department)

May 2004

Major Subject: Petroleum Engineering

ABSTRACT

Reservoir Characterization and Development Opportunities

in Jacob Field, South-Central Texas. (May 2004)

Mirko Joshoe Hernandez Depaz, B.S., National University of Engineering, Peru

Chair of Advisory Committee: Dr. David S. Schechter

The Jacob field was discovered in the year 1931. In the year 2002, due to the low productivity of the field, the company wanted to determine whether to keep operating, abandon or sell the field. So they asked Texas A&M University to perform the study, determine the oil potential, and make recommendations to improve production.

Since no previous reservoir study was performed in this field, the original oil in place and the current status of depletion was unknown. Therefore a complete integrated study was needed in order to learn about the reservoir and evaluate it in a qualitative and quantitative manner, before making any recommendation.

The current pay zone underlying the Jacob field forms a monocline structure composed of unconsolidated young clastic sediments deposited in the Eocene epoch of the stratigraphic column of the Nueces River Basin, mainly due to a fluvial deltaic system developed in south Texas.

The original oil in place for this pay zone was estimated to be 18.12 MMSTB and the cumulative production as of October 2003, 3.8 MMSTB.

The analysis of the production data available had shown that the pay zone is being flooded by a strong water encroachment from the lower sides of the structure. This behavior was confirmed by the anisotropy analysis from core and log data, which shows that the reservoir tends to be more homogeneous in the direction of the water encroachment.

It seems that there is not much room for further development in the current pay zone in the Jacob field (the remaining reserves were estimated to be 10 MSTB as of October 2003). However, the presence of a continuous shallow clean sandstone, not properly

tested, of better reservoir properties than the actual pay zone was noticed. Moreover, this clean sandstone showed oil and gas presence in thirteen wells in the drilling cuttings.

Therefore further development should concentrate more on investigating and developing the oil potential of the latter sandstone as well as accelerating the reserves production in the actual pay zone by means of waterflooding and/or infill drilling.

DEDICATION

This thesis is dedicated to:

My beloved parents, Libia and Maximo, for their continuous emotional and financial support.

My brothers, Max and Ilich, my sisters, Libia, Thania, Carola and Carmen, for sharing wonderful moments of brotherhood.

My beloved Carolina for her love, care and inspiration shared.

ACKNOWLEDGEMENTS

I would like to express my sincere gratitude to Dr. David S. Schechter for his assistance, encouragement, guidance and financial support throughout this research.

I would also like to thank Dr. Duane A. McVay and Dr. Steven L. Dorobek for acting as committee members and helping me in my research.

Thanks to Mr. Jay Buzzini for letting me use the database of Loma Oil Co. for this research.

I would also like to thank the faculty members of the Harold Vance Department of Petroleum Engineering for the excellent courses taught, with special attention to Dr. Maria Barrufet, Dr. Akhil Datta-Gupta, Dr. Richard Startzman, Dr. Tom Blasingame, and Dr. Walter Ayers. The topics covered in those courses helped me to improve this research.

My sincere gratitude to each individual in the naturally fractured reservoir group and in the Petroleum Engineering department, especially to Dr. Erwin Putra, Christian Huapaya, Jorge Nieto, Adedayo Oyerinde, and Deepak Chakravarthy for their technical assistance and for sharing moments of joy.

TABLE OF CONTENTS

Page

CHAPTER Page

LIST OF FIGURES

FIGURE Page

FIGURE Page

FIGURE Page

LIST OF TABLES

CHAPTER I

INTRODUCTION

The Jacob field is located in McMullen County, 80 miles south of San Antonio, Texas (**Fig. 1-1**). The discovery well was drilled in 1931 finding gas in a shallow horizon (~700 ft). Just few months after the field discovery, the second well was drilled in 1932 finding oil in a deeper horizon (~900 ft). Since then, the exploitation of the oil field was concentrated in the latter horizon, even though there were attempts at trying to find deeper productive zones with no apparent success. More than 150 wells were drilled in an area of 3100 acres (**Fig. 1-2**).

The pay reservoir, known as Pettus, is a thin layer of unconsolidated shaly sands. The Pettus sand was originated in a fluvial deltaic system of the Yegua formation in the Nueces River Basin.

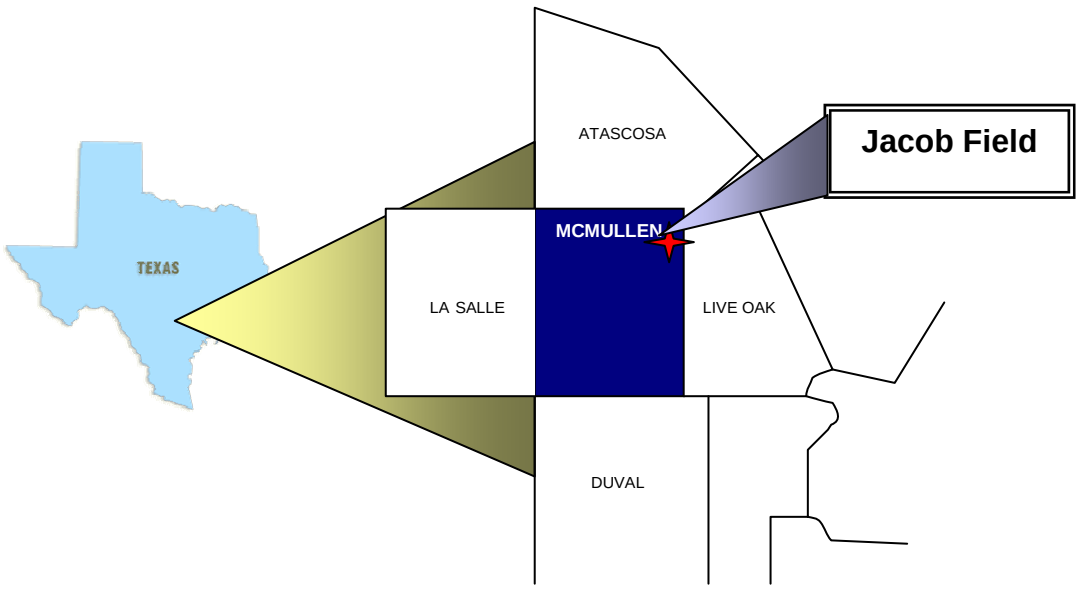

Fig. 1-1 – Location of the Jacob field.

This thesis follows the style and format of the *Journal of Petroleum Technology*.

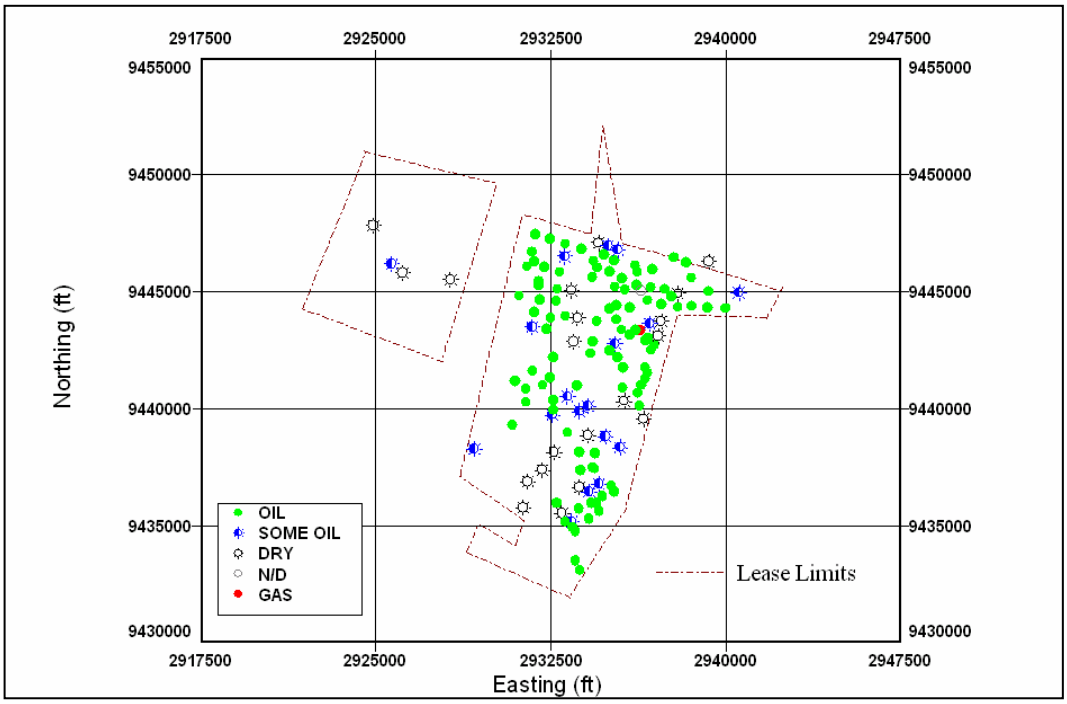

Fig. 1-2 – Area of study enclosed by lease limits.

The first well drilled in the Jacob field started producing 200 barrels of oil per day. Most of the drilling activity was concentrated at the first 10 years after discovery. From 1970 to 1990 not a single well was drilled. Since 1999 most of the wells producing at that time were gradually plugged and abandoned due to low oil rates or high water cuts, leaving only 8 wells pumping at late 2002. In the year 2002 two wells were drilled and they started producing less than 5 BOPD. Field practices avoided the proper record of production data on a well-by-well basis. Recorded production accounts for 2.0 MMSTB of cumulative oil for the period from 1932 to 1937 and from 1956 to 2003. For the 19 years gap, production data was not available in any accessible database.

The current production rates account for less than 1 barrel of oil per day per well. Due to that fact, the Jacob field might be an uneconomically prospect for continuing operating. And that is the main reason why this study was carried out: to determine

whether or not is possible to increment the oil production and/or identify alternatives to development.

1.1 Description of the problem

In order to determine whether is possible to increment oil production in the Jacob field and/or identify alternatives for development, it is necessary to evaluate the field in two aspects: quality and quantity. For quality meaning that we need to identify the main features of the geological structure, the facies distribution along the field, the vertical and horizontal anisotropy, etc. And for quantity meaning the original in place, the recovery factor and the remaining reserves. By integrating those two types of analyses we will have a better picture of the reservoir and therefore better recommendations will be drawn.

However while doing the research we have found that the lack of information and the quality of data is a major concern in the process of this study.

The study started basically from no previous knowledge, it was necessary to collect and organize data before performing any engineering study. The data set that was conveyed comprised 11 old gamma ray-resistivity-neutron logs, two wells containing modern gamma ray-resistivity-porosity logs, 25 core analyses, 4 sidewall cores, some production tests (oil and water rates) on a well basis, and monthly oil production for the whole field since 1956.

It is worth mentioning that the core data did not provide a proper geological description, only data of petrophysical parameters (porosity, permeability), so the determination of lithofacies derived from core descriptions was not possible.

1.2 Objectives of this research

The main goal of this research is to determine the hydrocarbons potential of the Jacob field and to find possible alternatives for improving production.

To obtain our goal, the following subordinate objectives have been established:

1. Estimate a static reservoir model that can describe the reservoir, identifying continuity of rock types, permeable and low-permeability strata as well as the distribution of fluids.
2. From the reservoir model built, estimate the original oil in place.
3. Evaluate the production history from the available data in order to determine the status of depletion as well as the movement of fluids along the field and the remaining reserves.

CHAPTER II

GEOLOGICAL DESCRIPTION

2.1 Introduction

The purpose of performing a geological description is to build the foundation for the subsequent sections. In doing this analysis we will be able to determine the continuity of the reservoir units along the field, the depositional environments for the sediments and the distribution of facies that characterizes the sediments.

A reservoir description is a comprehensive picture of the three-dimensional distribution and continuity of the rocks, pores, and fluids of the reservoir and aquifer system, including barriers to fluid flow[1]

In the reservoir description process, a critical first step is the recognition of all correlative reservoir layers of subzones and the intervening dense, impermeable or low-permeability strata. Knowledge of the depositional and diagenetic processes controlling both the reservoir and the non-reservoir rock units is essential to obtain a high degree of reliability in correlating these units from well to well[1].

Wilson[2] described a methodology of reservoir description (the schematic diagram is shown in **Fig 2-1**) that basically relies on the availability of a complete set of core, log, seismic and production data. What Wilson suggests is to integrate all the information from the sources mentioned and construct a comprehensive theoretical model. However, in the Jacob field the lack of data is a major concern. In the following sections we try to develop an estimation of the geological model that may reflect the formations of interest within Jacob field.

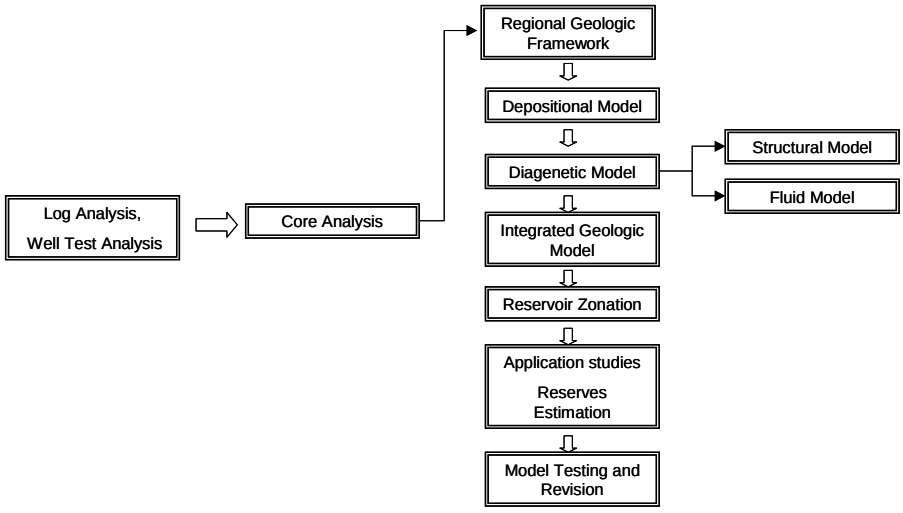

Fig. 2-1 – Stages in the generation of an integrated geological reservoir model.

2.2 Regional geology

Regional description of south central Texas suggests that the pay reservoirs in the Jacob field belong to the Eocene Series of the geologic column.[3]

The United States Geological Survey[4] (USGS) includes the study area as a part of the Northwestern Gulf Coast basin, which is bounded roughly on the west by the Rio Grande River and on the east by the Mississippi River.

The Northwestern Gulf basin has been a deposit for large amounts of clastic sediments since the beginning of the Tertiary. Sediments were derived mainly from the Cordilleran Foreland and other highland sources in western North America. The Tertiary sedimentary sequence is a repetitive series of progradational and transgressional phases of deposition.

The US Geological Survey in its report of the Western Gulf Province described two major Eocene plays that concern our study:

- Yegua Updip Fluvial-deltaic oil and gas play: “Reservoirs in this play are fluvial, deltaic, and shelf sandstones. Porosity ranges up to 37%, and permeability ranges up to 2,000 md. Depths of reservoirs range from 1,000 to 10,000 ft”

- Jackson Updip gas and oil play: “Reservoirs in this play are deltaic and strandplain sandstones. Porosity ranges up to 30% and permeability up to 800 md. Depths of reservoirs range from 500 to 6,000 ft”

The depths of the reservoirs of interest in the Jacob field as well as their quality suggest that they were deposited either in the Yegua or Jackson Group.

By doing an intensive literature review we found two geological studies from areas close to our area of interest. These were: The “Nueces River Cross Section” by Anderson et al.[5] And “Stratigraphy and Environment of deposition of The San Miguel Lignite Deposit Northern McMullen and Southeastern Atascosa Counties, Texas” by Snedden.[6]

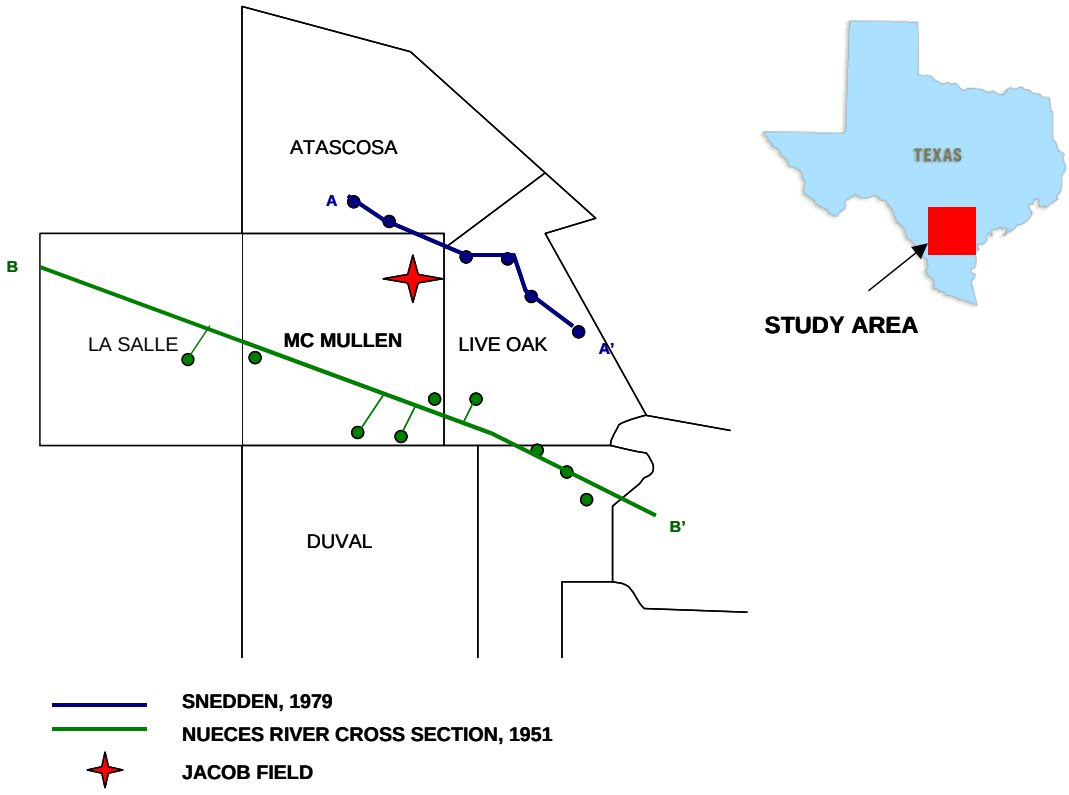

Fig. 2-2 – Regional cross sections close to the area of study.

We were interested in the cross sections constructed in those two studies. The cross section interpreted by Anderson et al.[5] crosses the McMullen County at approximately 29 miles away from the Jacob field (See **Fig 2-2**), whereas the Cross section interpreted by Snedden is even closer to the Jacob field: approximately 5 miles apart.

Anderson et al.[5] delimited the depth limits for the Jackson and Yegua groups for their area under study. That boundary is marked at approximately 3000 ft below sea level. A continuous shale body present in all the wells determines the change of geological formations.

Moreover, Anderson et al.[5] identified the Pettus sand as a Gamma Ray serrate shape located at the upper Yegua. That can be appreciated in the limit between McMullen and Live Oak counties (**Fig. 2-3**). Also, the Mirando Sand is identified on gamma ray logs as an upward trend in the lower part of the Jackson Group.

In determining the continuity of the San Miguel Lignite across South Texas, Snedden interpreted a cross section that crosses the upper part of McMullen County (**Fig. 2-4**). Because of his interest in the shallow occurrence of lignite across McMullen County, Snedden identified the Yegua formation and the Jackson Group and, again, delimited the change of geologic formations in a continuous shale interval. The Pettus sand was identified in the upper Yegua and the Mirando in the lower Jackson Group. As in Anderson's work, the Mirando Sand is characterized by an upward coarsening trend on SP logs and the Pettus by a serrated SP response. The depth at which Snedden interpreted the change of lithological behavior was approximately 1000 ft at the location marked as the limit between Atascosa and Live Oak County.

A continuous lignite layer across McMullen County provides key information about the depositional settings of the Jackson Group in the Jacob field and also serves as an excellent lithostratigraphic marker.

From the discussed cases, we might infer that the Jackson and Yegua formations are present all along McMullen County. Even more, we can infer that similar formations with the same name are continuous from North to South along McMullen County. The

next step is to compare similar behavior in the Jacob field electrical logs and determine whether our assumptions are correct or not.

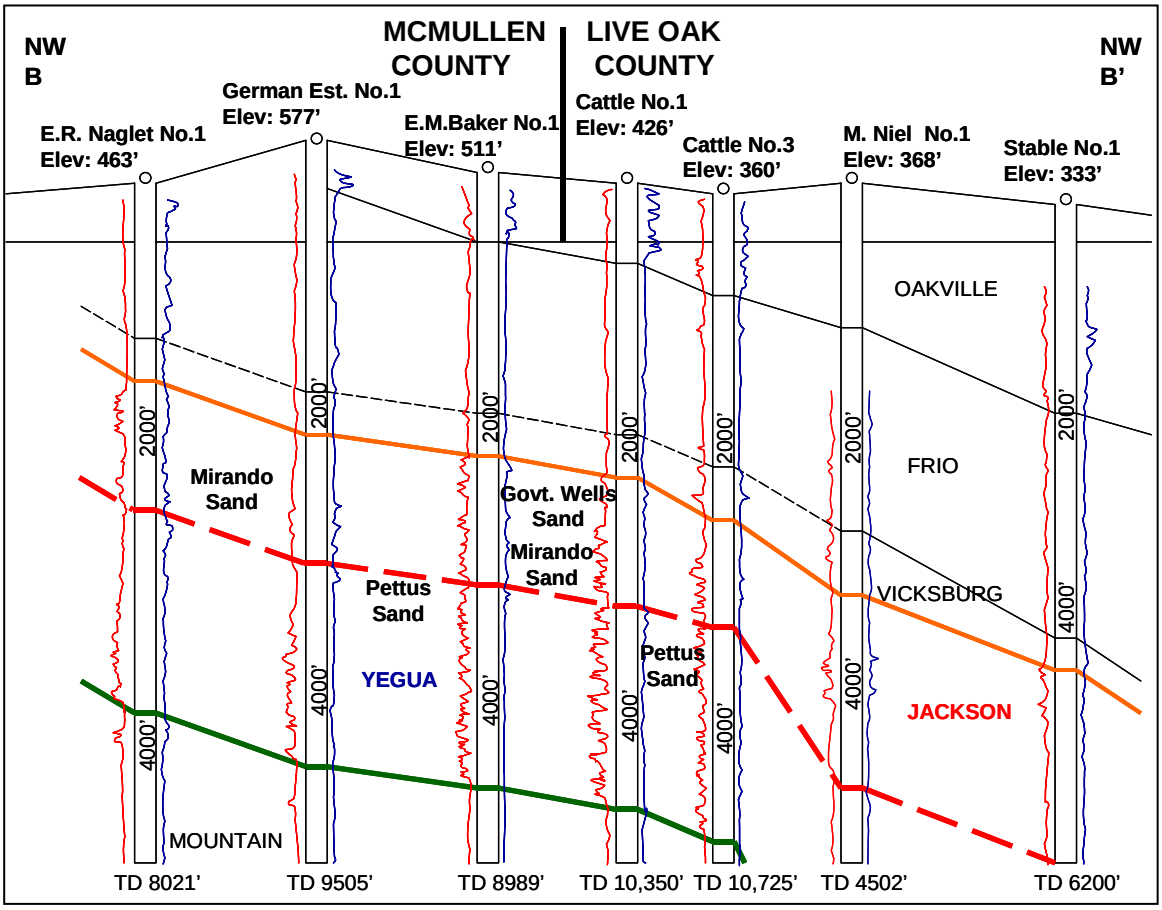

Fig. 2-3 – Nueces river cross section (modified from Anderson et al., 1951).

Fig. 2-5 shows a cross section of three well logs across McMullen County. It is included a "typical" well log from the Jacob field (Well 121A). Following the log signatures it could be correlated the electrical logs and determined the continuity of the Jackson and Yegua groups along McMullen County. Definitely the same Mirando sand is present along McMullen belonging to Lower Jackson. The change in geological groups is defined by the presence of a continuous shale between the Mirando and Pettus formations.

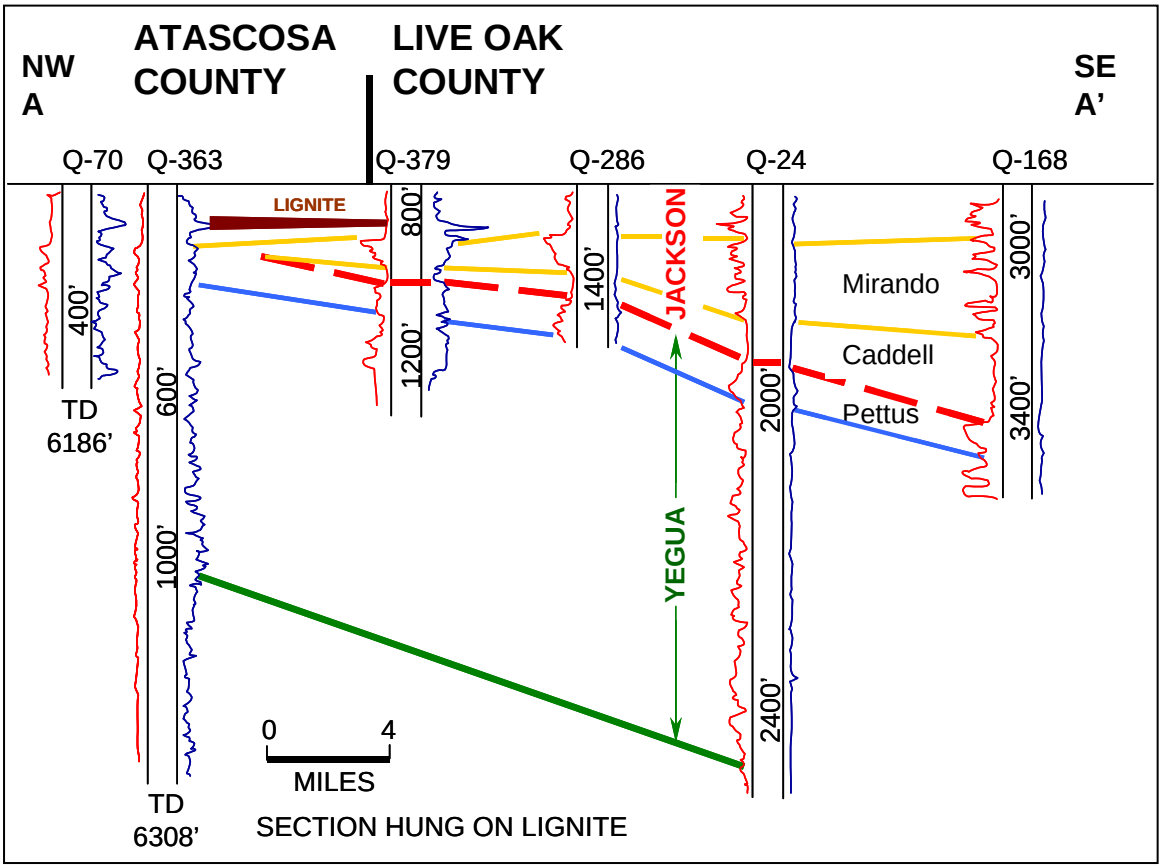

Fig. 2-4 – Atascosa-Live Oak cross section (modified from Snedden, 1979).

2.3 Environments of deposition of Yegua Formation and Jackson Group

Now that we have determined that the main reservoirs underlying the Jacob field belong to Jackson and Yegua formations, we need to go back to the description of what types of environments of deposition generated such formations.

Kaiser[7] defined the main facies that characterize the Eocene section and divided them into groups (**Fig. 2-6**). He included the Yegua Formation into the Claiborne Group and divided the Jackson Group into four different formations: Whitsett, Manning, Wellborn and Caddell.

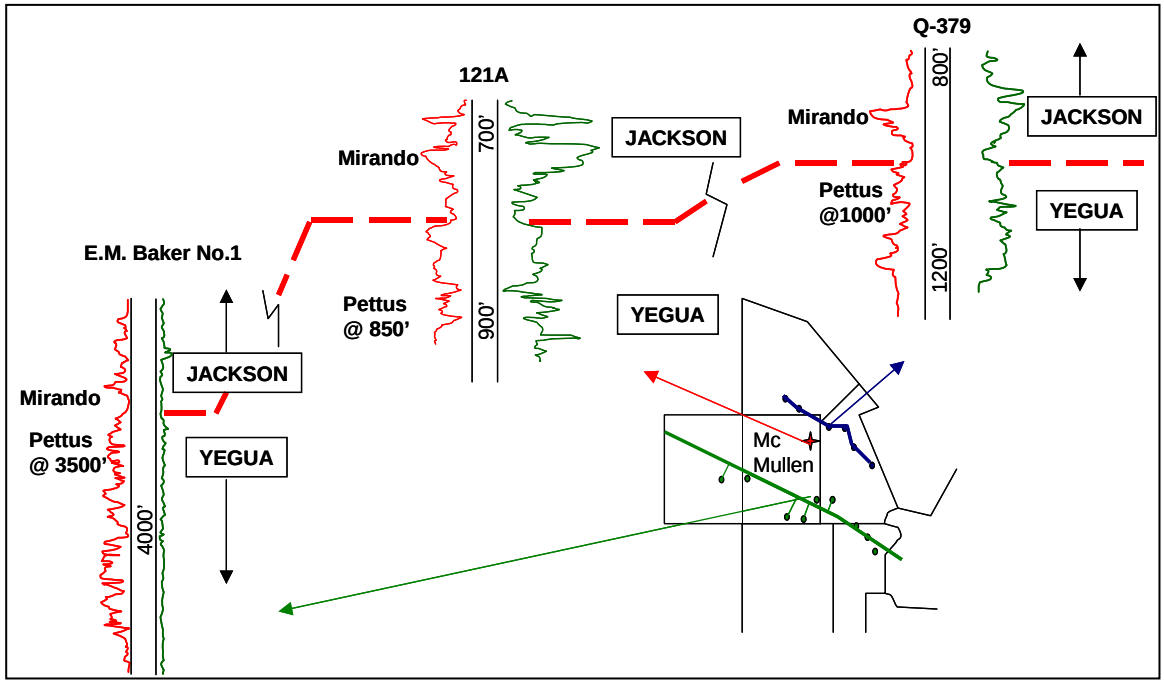

Fig. 2-5 – Regional correlation across McMullen County including the Jacob field typical well log.

As Fig. 2.6 illustrates, the environments of deposition changed with time but in a very systematic manner. The time-stratigraphic equivalents of each formation become progressively more marine downdip.

The Middle Eocene Yegua Formation is the uppermost unit of the Claiborne Group.

Two major systems deposited Yegua strata in Texas. In Southeast Texas, a large fluvio-deltaic system transported great amounts of continentally derived sand and clay into the basin (**Fig. 2-7**)

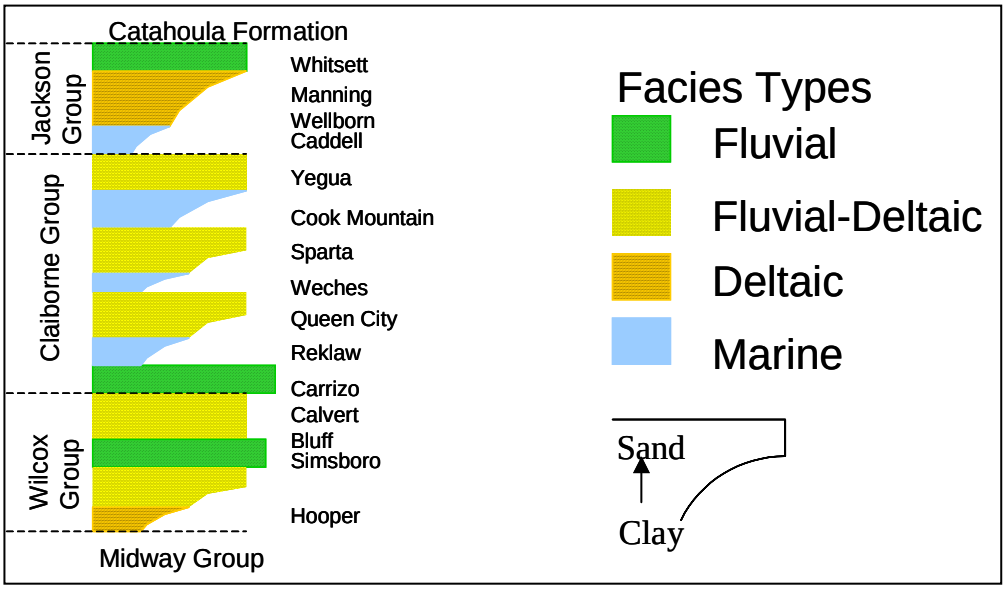

Fig. 2-6 – Lithostratigraphic column in the Texas Eocene (modified from Kaiser, 1977).

In South Texas, sand dispersal was largely strike-oriented and an extensive strandplain-barrier bar system developed. An additional source of sand may have been from a small river system situated along the present drainage of the Nueces and Frio Rivers in South Texas. However, the system was small and sediment influx to the area was minor. The Yegua Formation crops out in an arcuate band from the Rio Grande to the Sabine River. At the outcrop, it is about 1,100 ft thick in southeast Texas and then thins rapidly to the south and east. Outcrops of Yegua Formation in South Texas are mostly composed of clay and shale (Snedden, 1979).

The late Eocene Jackson Group is situated stratigraphically above the Middle Eocene Yegua Formation and below the Oligocene Catahoula Formation. The Jackson Group of South Texas is composed principally of interbedded sands and fossiliferous shales, with abundant volcanic ash and silicified wood. The Jackson Group is defined as a time-stratigraphic unit embracing all sediments deposited during the advance and retreat of the late Eocene Sea in the Gulf and Atlantic Coastal Region.

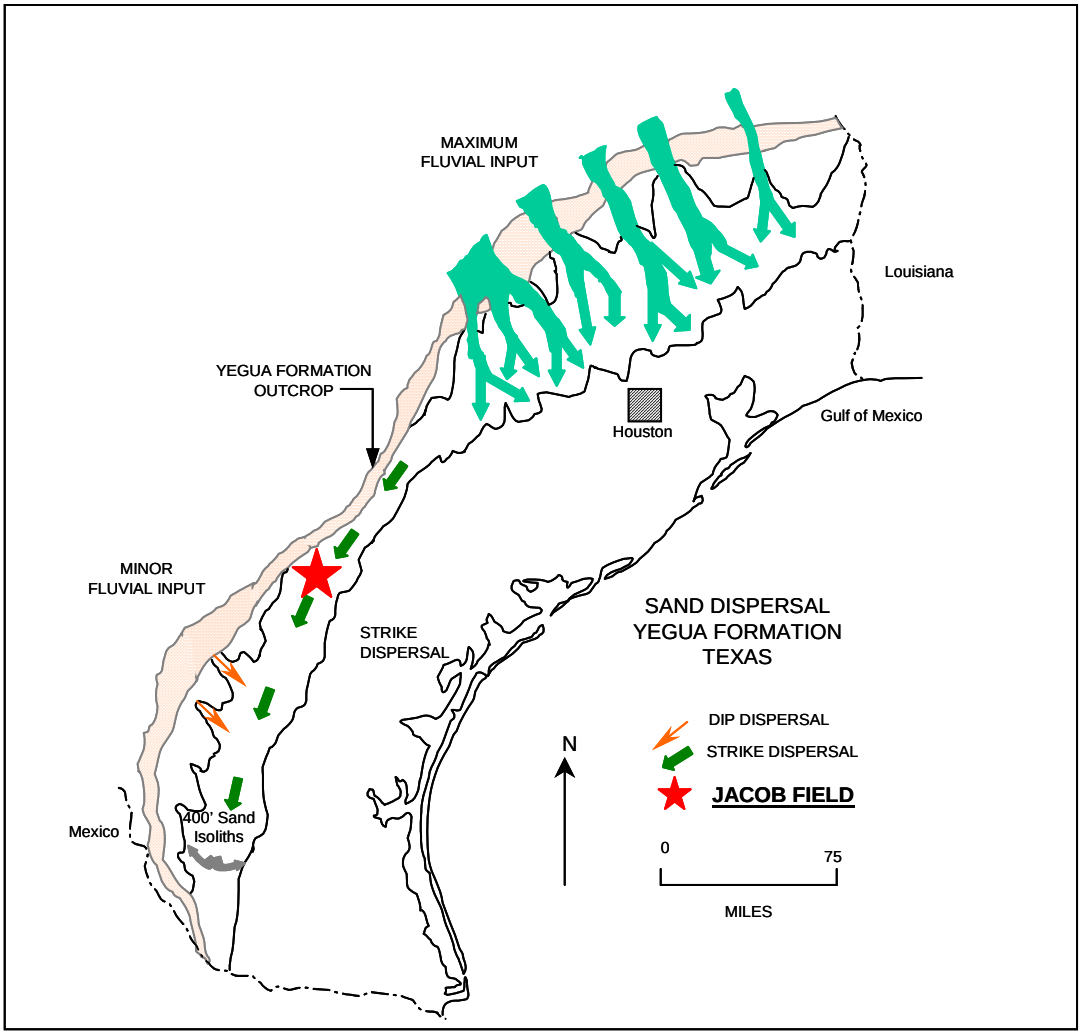

Fig. 2-7 – Sand dispersal systems in the Yegua Formation of Texas (modified from Snedden, 1979).

The regional facies pattern of the Jackson Group (**Fig. 2-8**) is very similar to the facies pattern of the Yegua Formation. But the Jackson Group is thinner than the Yegua Formation. The sedimentary sequence northwest of the southeast Texas facies contains lignite, which indicates that deltaic plain environments were located updip from the major sand deposits (Snedden, 1979).

The Jackson Group of South Texas was interpreted to have formed in a strandplain-barrier bar system with associated updip lagoonal and downdip shelf environments. As in the Yegua, sand was transported along strike to the south from the

major delta system (see Fig. 2-8). Additionally dip feeding of the strand plain system by minor fluvial systems occurred in the area of McMullen, Karnes, La Salle, and Webb Counties.

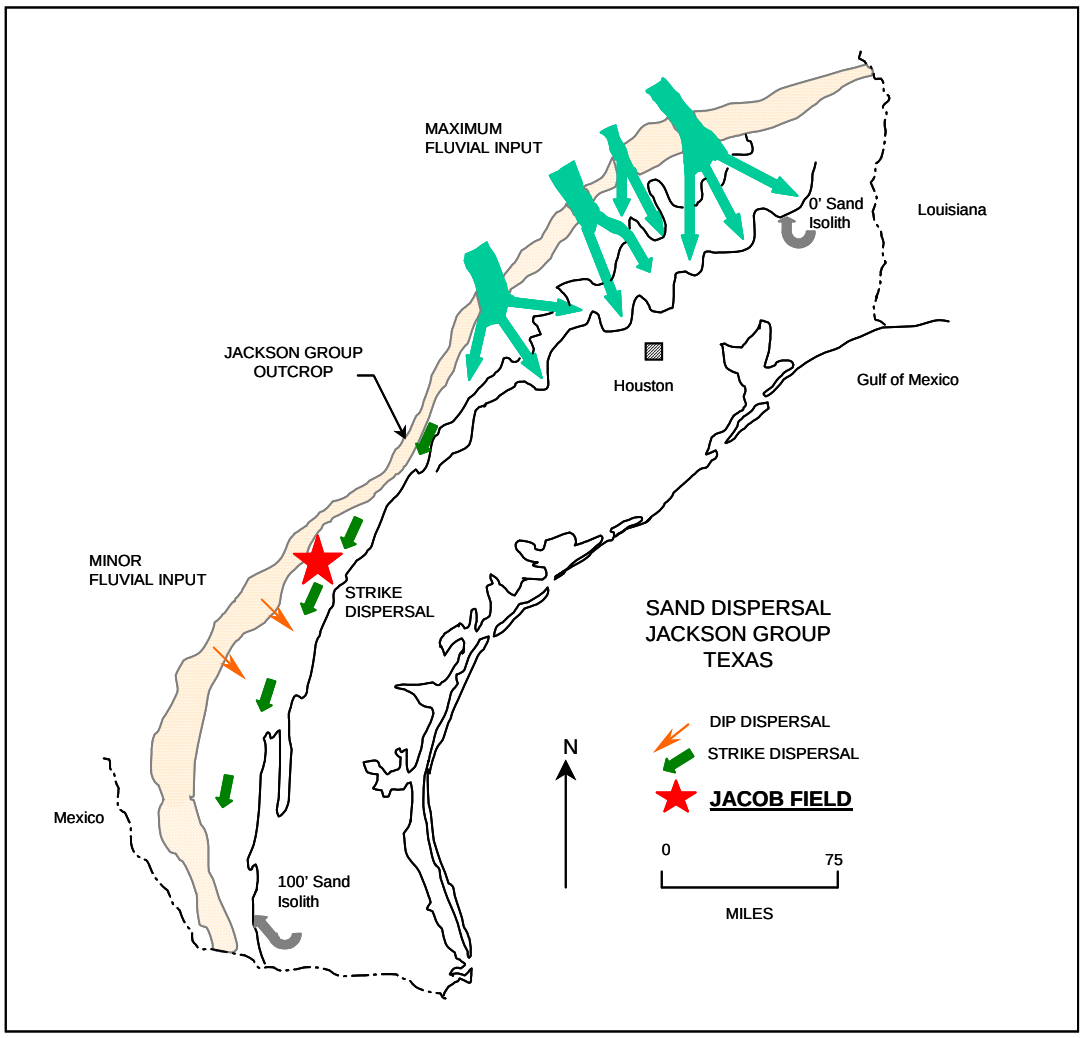

Fig. 2-8 – Sand dispersal systems in the Jackson Group of Texas (modified from Snedden, 1979).

2.4 Local geology

In terms of local geology I investigated the continuity of subsurface geological formations existing in the Jacob field that were identified in the log signatures recorded in well electrical logs. Two types of cross sections were developed: structural and stratigraphic. Also, the development of facies is performed and the concept of electrofacies is introduced.

2.4.1 Cross Sections

Geological cross sections are graphical representations of vertical slices through the earth used to clarify or interpret geological relationships. Cross sections are used to portray geological information in a visual form so that reservoir characteristics can be readily interpreted.

There are two major classes of cross sections used in understanding petroleum reservoirs[8]:

- Structural cross sections, which show the present day dip of strata across an area
- Stratigraphic cross sections, which show original stratal geometries and relationships by adjusting the elevation of stratigraphic units to some chosen geological horizon.

Fig. 2-9 shows the cross sections used in determining the continuity of the sand bodies in the Jacob field. It was possible to analyze two cross sections:

- Northeast – Southwest strike-oriented cross section, including wells 25W, 48A, 65A.
- Northwest – Southeast dip-oriented cross section, including wells 1C, 121A, 122A.

The logs used for correlation were SP and/or Gamma Ray in the correlation track and the deep resistivity in the resistivity track.

Previous to this job a normalization process of the log curves was done which is explained in a later section.

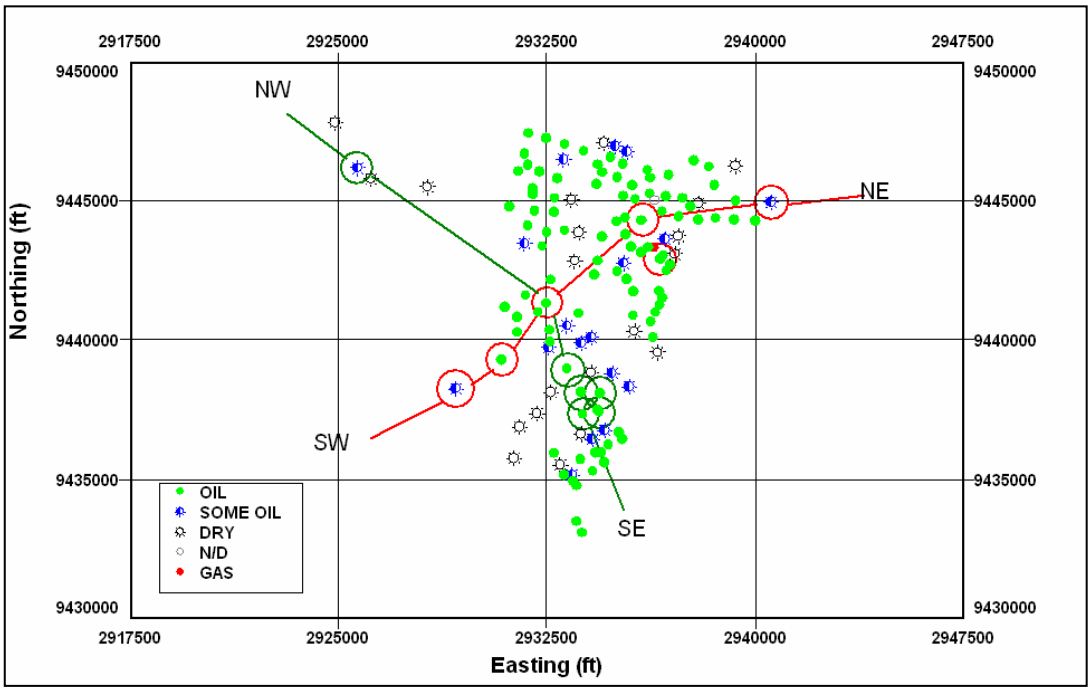

Fig. 2-9 – Cross sections: strike direction (NESW) and dip direction (NWSE).

Stratigraphic column

Previous to the analysis of structural and stratigraphic cross sections we need to identify the stratigraphic column used to build the cross sections.

As it was mentioned before, the vertical zone of interest includes as the top the San Miguel lignite and as the bottom the bottom of the Pettus shaly sand. In all the electrical logs, the following formations were present:

Lignite

Shale

Lignite

Mirando Sand

Shale

Shaly sand

Shale

Pettus shaly sand

The idea behind developing structural and stratigraphic cross sections is to determine the depositional trends and to try to establish a history of deposition of the sediments.

Structural cross sections

For the structure cross section, the datum is sea level, thus the data is plotted below that point. In our cross sections besides the sea level datum we choose to show the logs below 500 ft in order to show a better graphical quality.

The cross sections were oriented perpendicular to the major structural trends: strike (**Fig. 2-10**) and dip (**Fig. 2-11**)

Along the strike direction, all the formations are present. The lignite shows to be a good marker; the two lignite beds separated by a continuous shale body are present along the strike or at least are present in the wells selected. The Mirando sand becomes thicker towards the northeast direction, the same behavior seems to be true for the Pettus shaly sand; however, it is difficult to establish the continuity for the Pettus sand, since it seems that for well 48A the log total recorded depth does not cover all the Pettus sand. However it is appreciable that the Pettus sand is even shalier than the above shaly sand. The Pettus sand is a thinner body compared to the younger sediments.

Along the dip direction, again, all the formations are present. Since the logs were equally spaced, Fig. 2.11 shows an exaggerated change of the formations' dip. The distance between wells 1C and 121A is 10,400 ft and between 121A and 122A is 1,700 ft. By making a proportionally spaced distance it is possible to appreciate a better continuity, however a graphical representation is lost. In this direction better continuity is appreciated and the formation bodies are more constant in thickness than in the previous case. The continuity in the Mirando sand can be clearly appreciated and its thickness is almost constant, as well as in the Pettus shaly sand. In this case the shaliness of the Pettus sand is better appreciated.

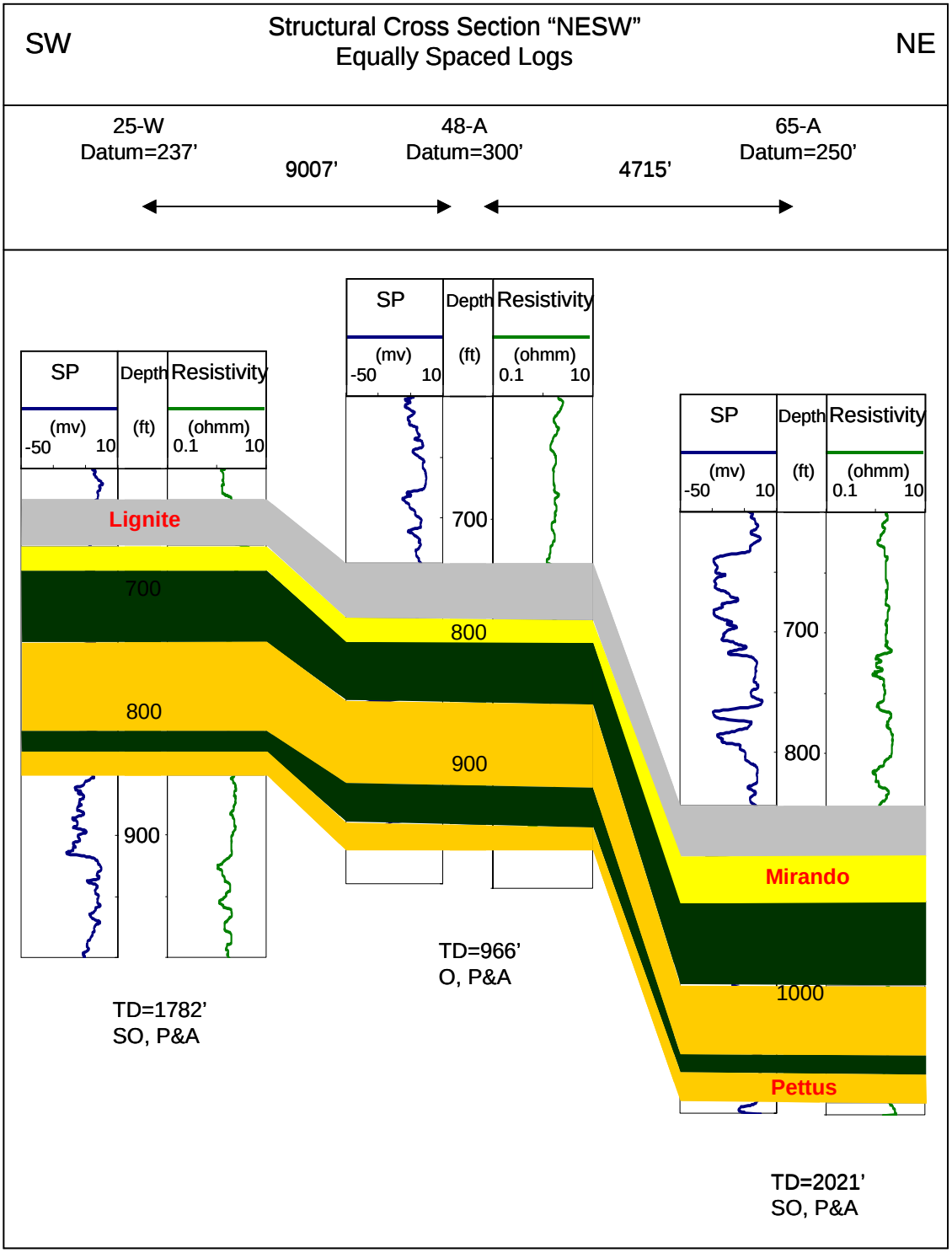

Fig. 2-10 – Structural cross section along strike – Northeast Southwest.

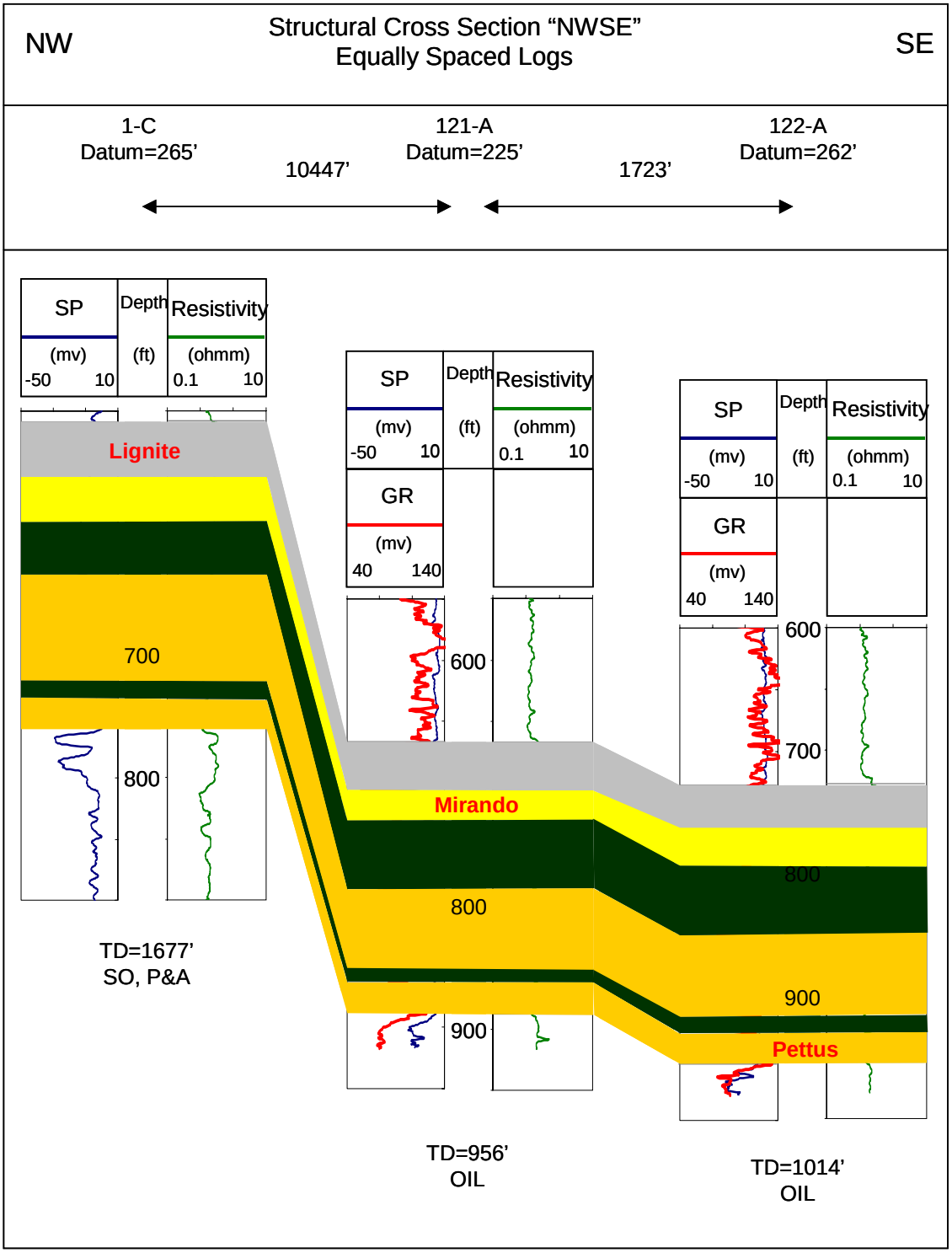

Fig. 2-11 – Structural cross section along dip – Northwest Southeast.

Stratigraphic cross sections

For the stratigraphic cross section, the datum is top of the San Miguel lignite. In this type of cross section all the vertical information is "hanged" from the stratigraphic horizon and following the principle of original horizontality we produce an interpretation of what the slice of the earth might have looked like at an earlier time (without deformation of any kind). The assumption that this surface was horizontal when deposited assumes no original depositional slope. We choose the San Miguel lignite as a datum basically because of its presence in all the wells in the Jacob field.

As in the structural case, two cross sections were built: along strike (**Fig. 2-12**) and dip (**Fig. 2-13**)

The intention of the cross section along the strike or parallel to the basin margin is to investigate lateral variations of the formation beds. In Fig. 2-12 we can observe that the Mirando sand shows a decrement in thickness from northeast to southwest, which is of particular interest. Again the same behavior observed in the structural cross section is observed in the Pettus shaly sand. The interval corresponding to the last formation could be erroneous and since the log was an old one and lacked quality control (repeated section) we can assume that the horizon shown in the last formation is arguable. However, the younger sediments, the shale below Mirando sand and the subsequent shaly sand show the same depositional trend. Anyway, the Pettus sand is shown to be a thin interval compared to the Mirando or the other geological formations.

The cross section oriented perpendicular to the depositional strike (dip section) tries to determine the change of facies toward or away from the basin margin. Fig. 2-13 shows this change of facies along the dip of the Jacob field. The Mirando sand is thicker in the Northwest part of the field while it decreases towards the basin margin. In can be appreciated that the Pettus sand keeps almost constant along the dip. It is important to make the reader aware that the apparent rapid change in the beds' slope is due to the graphical effects as a consequence of the equally spaced logs. As it was pointed out before, the distance between well 1C to 121A is almost 10 times the distance from 121A to 122A.

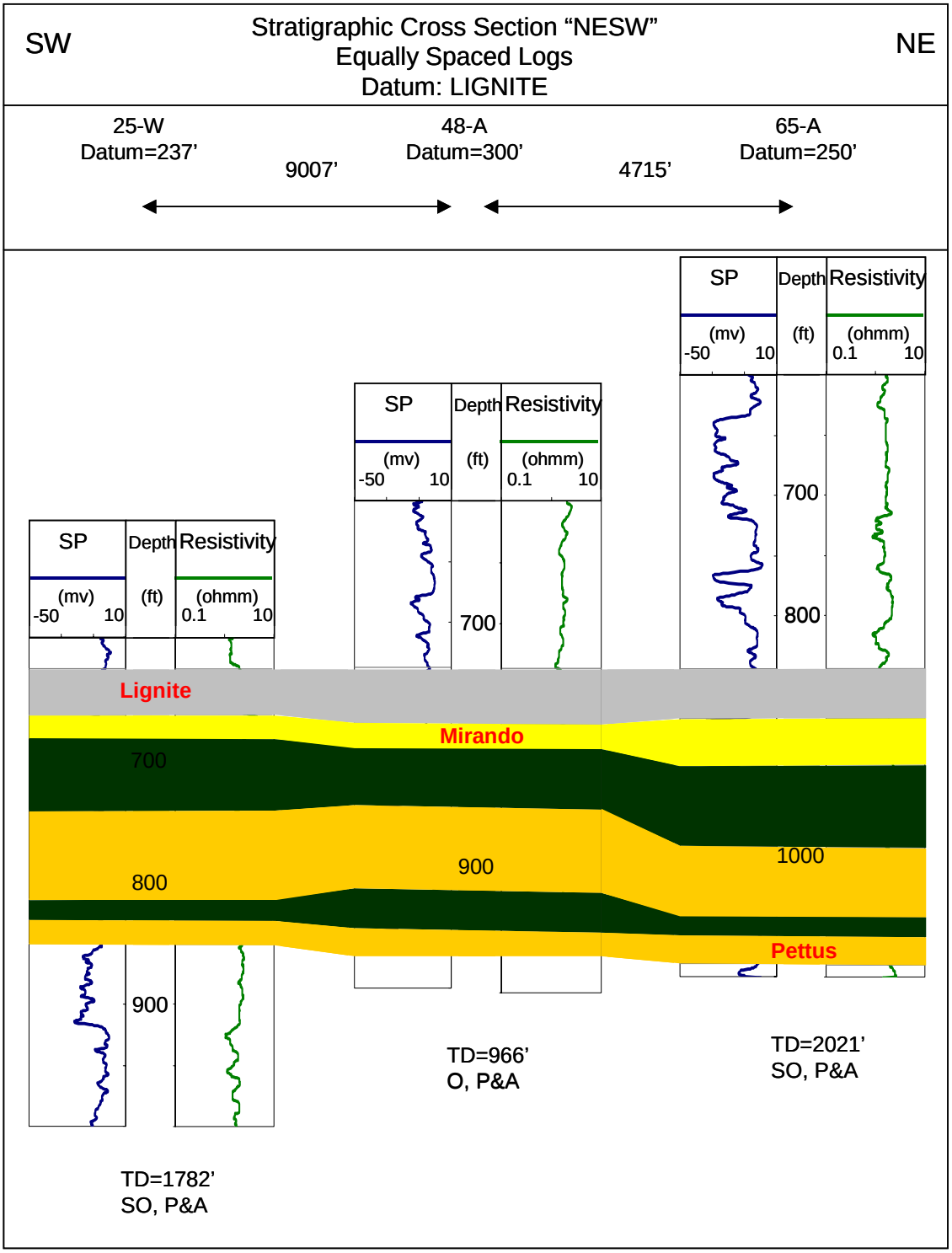

Fig. 2-12 – Stratigraphic cross section along strike – Northeast Southwest.

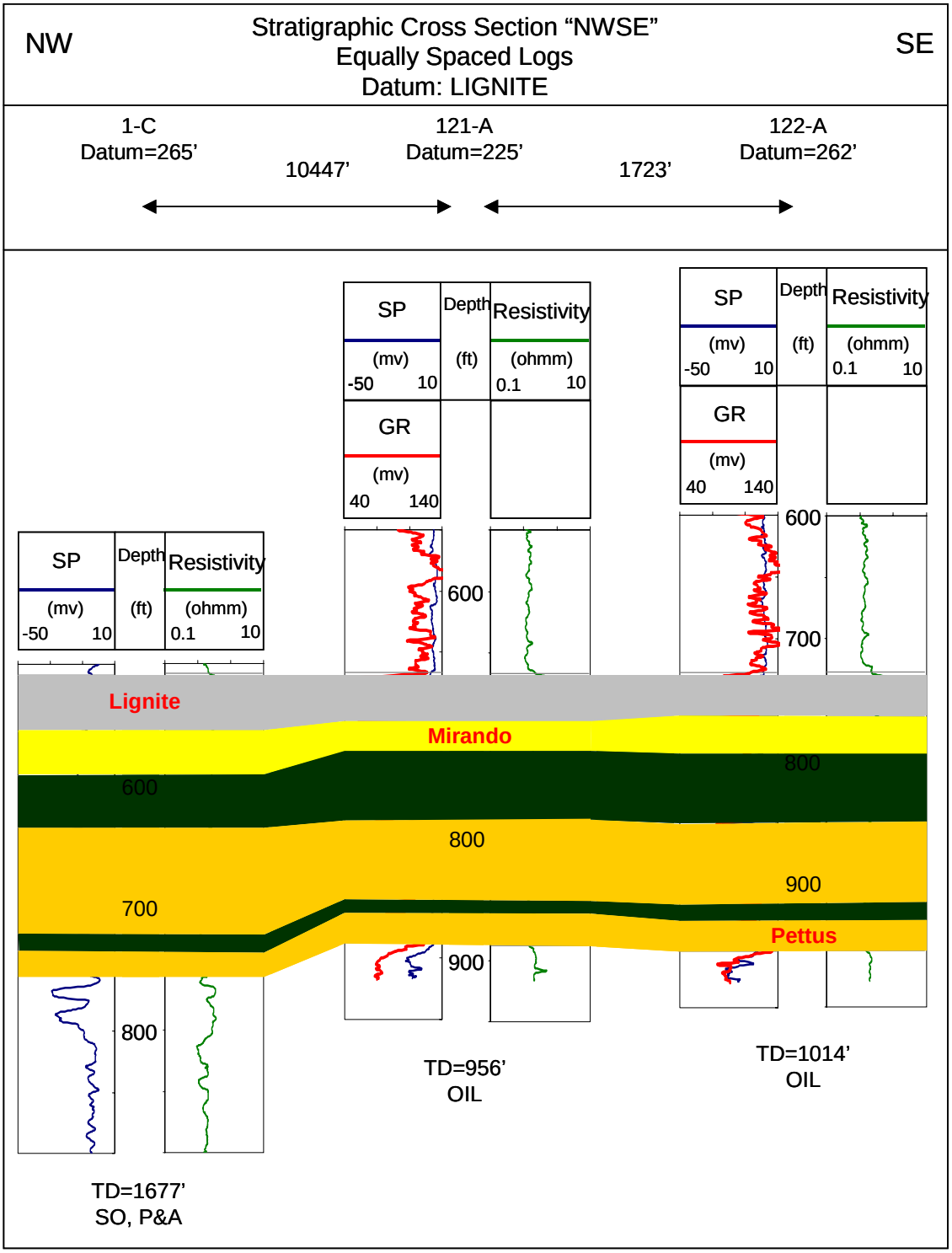

Fig. 2-13 – Stratigraphic cross section along dip – Northwest Southeast.

2.4.2 Interpreted depositional environments from log signatures

Within any given depositional environment, various physical and biological processes act to transport and deposit sediments. These processes result in various distributions of grain size and sedimentary structures that characterize the deposited sediment.

All of the characteristics of a particular rock unit are called “Facies”. Basic data requirements for facies analysis of subsurface rocks are: seismic, conventional core description, wireline logs. Conventional core is perhaps the most diagnostic for sedimentological interpretation of vertical sequences. One of the first steps in the facies analysis of a clastic reservoir is the description and interpretation of available conventional core. However as it was mentioned before, the lack of core samples undermines the reservoir description of the Jacob field.

Interpretation of the environment in which lithofacies were deposited from analysis of cored sequences involves relating the identified lithofacies to the physical and biological processes that produced them. For reservoirs in which no core is available, the wireline log shape is used to interpret sandstone body type and identify depositional environments[9]. In that sense I estimated a possible depositional environment from the log signatures present in the Jacob field. **Fig. 2-14** shows the interpreted depositional environments for well 121A that seems to have a typical GR behavior with respect to the other well logs. The Mirando sand is described as an upward coarsening shape. Upward coarsening log patterns exhibit an upward decrease in argillaceous content. It is estimated to have developed in a shoreline system, specifically in a strandplain-barrier bar beach sequence. Sands in the beach or foreshore are very well sorted, lack interstratified clay, and exhibit excellent reservoir properties. In general, barrier islands have the best reservoir quality rocks at the top of the sequence.

The Pettus sand has a serrate GR behavior; it is a tabular, sheet-like deposit of mudstone (clay and silt) interbedded with thin sandstones. The depositional environment can be marine shelf or lagoon. In the description of drilling cuttings in the wells of the Jacob field the presence of a continuous layer of oyster shells just above the Pettus sand

was noticed. That fact strengthens the lagoonal behavior of the depositional system of the Pettus sand: the presence of a continuous layer of shells suggests a rapid invasion of the sea in a fluvial deltaic system. As observed by Kaiser (1977) the Eocene formations are characterized by a cyclical deposition of sediments: after the rapid invasion of the sea just above the Pettus shaly sand a delta system was originated, above the delta a floodplain preceded the barrier system (Mirando sand). And finally the floodplain system allowed the deposition of ash or coal to form the lignite layers.

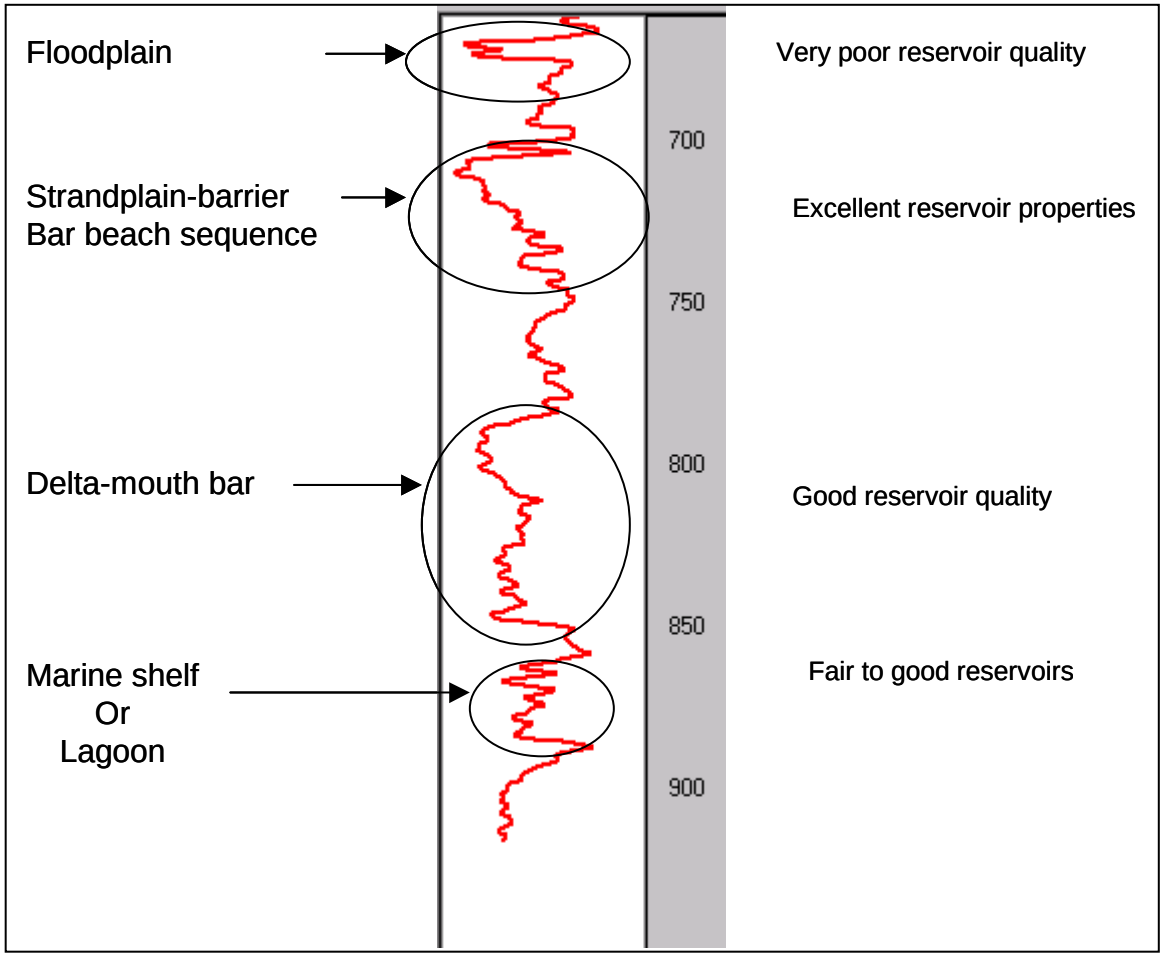

Fig. 2-14 – Interpreted depositional environments from log signatures.

2.4.3 Electrofacies characterization

The lack of core description undermines the lithofacies analysis for the determination of sedimentological interpretation; however, a new approach can be used taking advantage of the available wireline logs. The approach that we use is called Electrofacies and it has been demonstrated to be very useful in the characterization of complex reservoirs[10]

The term Electrofacies is defined as "a composite set of well log responses that characterizes a sediment and permits the sediment to be distinguished from others".

First we select a set of well logs. In our case we selected only the newest wireline logs, those of wells 121A and 122A (first it was necessary to perform the respective environment corrections and multiwell normalization). Among the curves used are: GR, SP, Resistivity (deep, medium and shallow), porosity (neutron and density). Once the logs are selected a principal component analysis is performed, PCA. The PCA is used to summarize the data effectively and to reduce the dimensionality of the data without a significant loss of information. **Fig. 2-15** shows the "screeplot," a bar plot of the variance of the principal components, which provides a convenient visual method of identifying the important components.

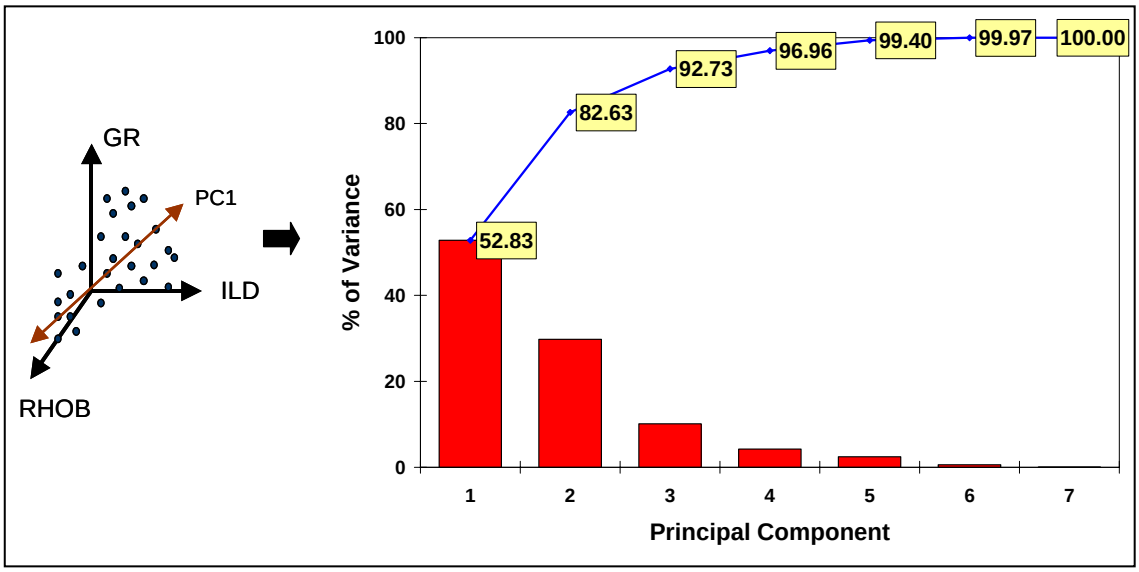

Fig. 2-15 – Principal component analysis: 3 first PC cover 92% of the data.

Only 3 principal components explain more than 92% of the variation for the whole data set. As a result of the principal component analysis we obtain the coefficients of the transformation (eigenvectors). **Table 2-1** summarizes the results after performing the PCA. The contribution of the first four PCs is highlighted.

Then, the PCs are reduced to the following expressions, for example:

$$PC1 = 0.40GR + 0.31SP - 0.49ILD - 0.49ILM - 0.48SFLR + 0.11\phi_N + 0.09\rho_D \ldots. (2.1)$$

$$PC2 = 0.24GR + 0.34SP + 0.17ILD + 0.16ILM + 0.11SFLR + 0.63\phi_N - 0.60\rho_D \ldots. (2.2)$$

$$PC3 == 0.38GR + 0.64SP + 0.19ILD + 0.22ILM + 0.33SFLR - 0.23\phi_N + 0.45\rho_D \ldots. (2.3)$$

TABLE 2-1 – RESULTS OF THE PRINCIPAL COMPONENT ANALYSIS

	PC1	PC2	PC3	PC4	PC5	PC6	PC7
GR	0.40	0.24	0.38	-0.76	0.24	0.04	-0.01
SP	0.31	0.34	0.64	0.61	0.07	0.02	0.00
ILD	-0.49	0.17	0.19	-0.07	0.04	0.52	-0.64
ILM	-0.49	0.16	0.22	-0.08	0.02	0.32	0.76
SFLR	-0.48	0.11	0.33	-0.12	-0.11	-0.78	-0.12
ϕ_N	0.11	0.63	-0.23	-0.08	-0.73	0.03	0.00
ρ_D	0.09	-0.60	0.45	-0.11	-0.63	0.15	0.00

Eigenvalue	4781.00	2696.00	914.00	383.00	221.00	51.82	2.40
Contribution	52.83	29.79	10.10	4.23	2.44	0.57	0.03
Cumulative contribution	52.83	82.63	92.73	96.96	99.40	99.97	100.00

Once the data was minimized in principal components, a cluster analysis is performed in order to define distinct groups based on the unique characteristics of the well-log measurements. The aim of cluster analysis is to classify a data set into groups that are internally homogeneous and externally isolated on the basis of a measure of similarity or dissimilarity between groups (Lee et al 2002).

In **Fig. 2-16**, each cluster can be treated as an electrofacies that reflects the hydrologic, lithologic, and diagenetic characteristics.

Now, that the electrofacies have been identified, we go back to the original logs and add another track in which to plot the electrofacies. **Fig. 2-17** shows the corresponding electrofacies to the rock units identified in previous sections.

The main electrofacies are EF3 corresponding to a continuous shale layer having characteristic low gamma ray, SP and resistivity, EF4 corresponding to the layer of lignite having a characteristic high neutron porosity and low density, EF6 that corresponds to the coarser part of the Mirando sand having a characteristic clean behavior, and EF3+EF5 that corresponds to the shaly Pettus sand. Notice that the electrofacies observed in the Pettus sand is not equally identified to the electrofacies corresponding to the shale layer (EF3).

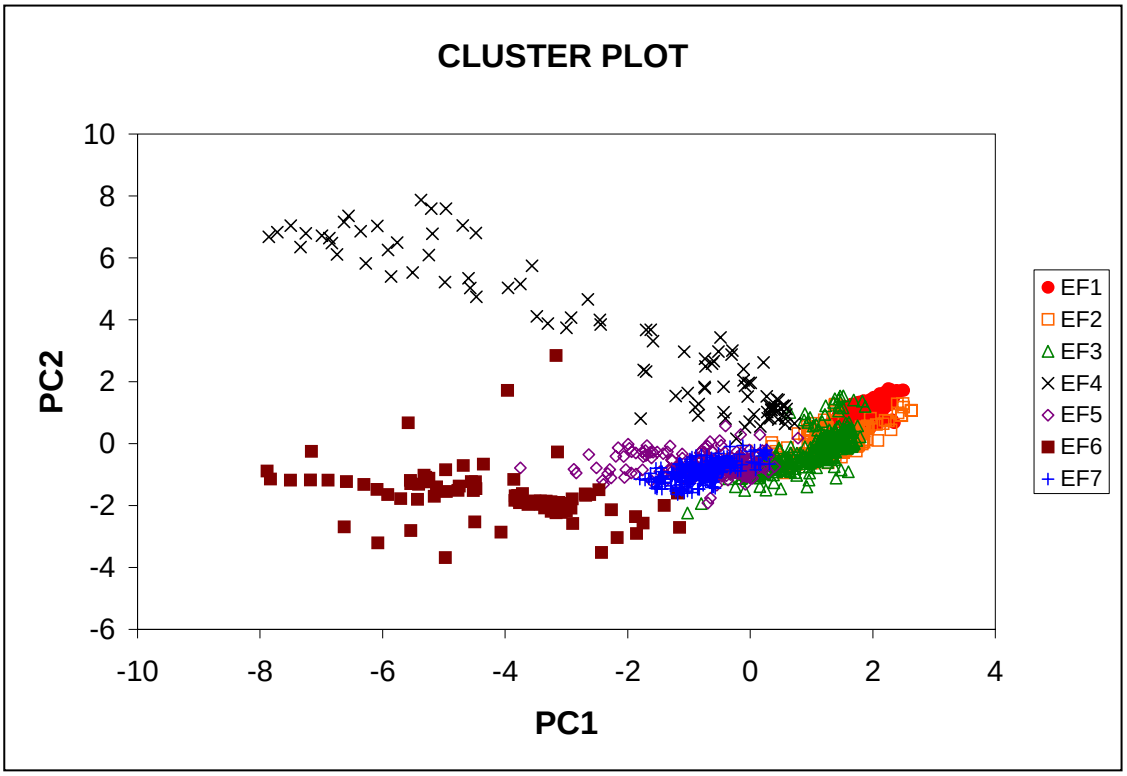

Fig. 2-16 – Distribution of electrofacies data plotted on the first two principal components of well logs.

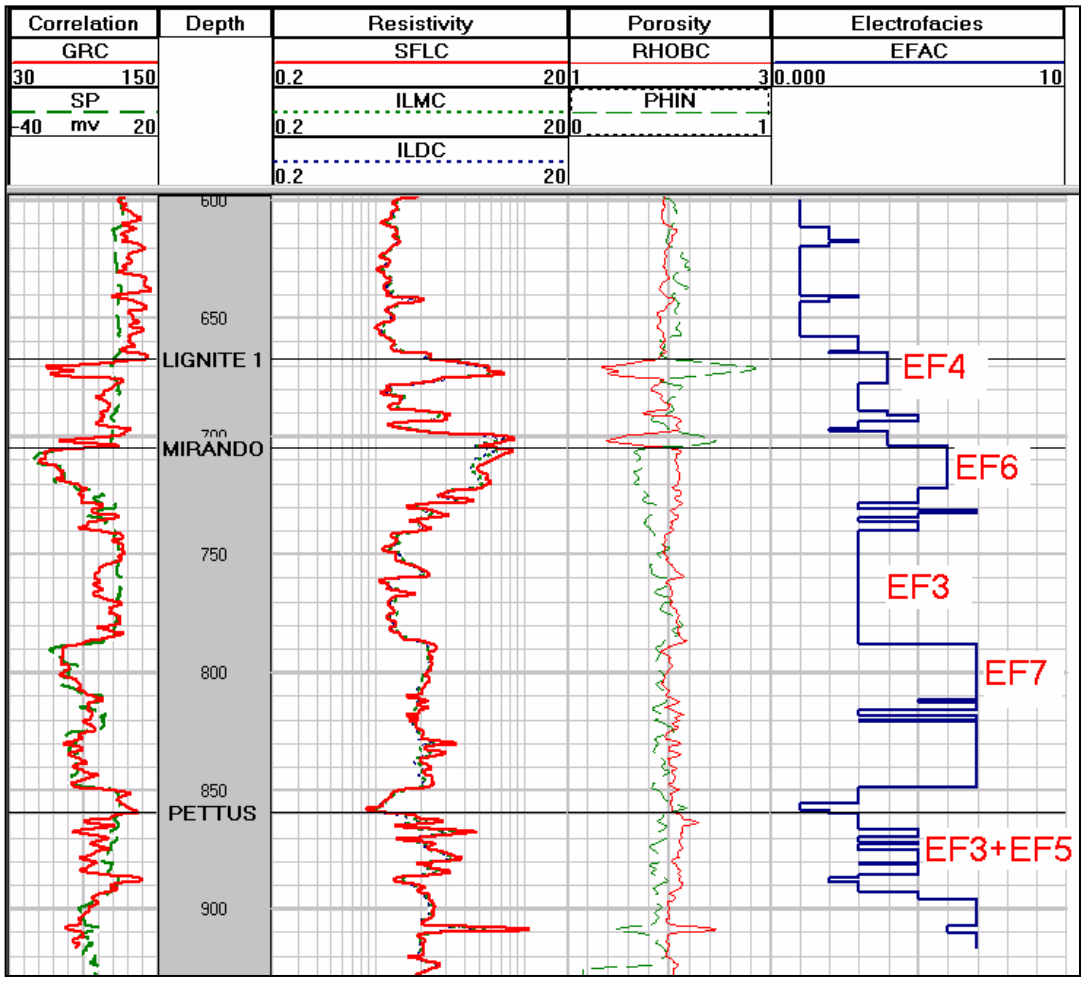

Fig. 2-17 – Electrofacies for the Jacob field.

CHAPTER III

PETROPHYSICAL ANALYSIS

3.1 Introduction

The objective of this section is to determine three basic parameters for later use in the determination of reserves: shale content, effective porosity and water saturation. The analysis will be concentrated only in the stratigraphic column of interest determined in the preceding section (from top lignite to Pettus base).

Log analysis plays an important role in the determination of rock quality. In conjunction with core description and well test, the log analysis forms the foundation to an integrated study[11].

The interpretation of electrical logs allows us to determine the shaliness of the subsurface formations, the porosity of the rocks (total and effective) as well as the water saturation. To reach that objective it is required to have basic log curves, such as: GR or SP, resistivity (shallow, medium and deep), porosity (neutron porosity, density, acoustic).

Table 3-1 summarizes the wireline logs recorded in wells in the Jacob field. Only four logs, out of a total of thirteen, have the logs required to determine the water saturation (117A, 118A, 121A, 122A). For the rest of the wells only the shaliness will be determined.

3.2 Processing logs

3.2.1 Environment corrections

A logging tool is usually designed to function best in a certain environment. The use of the tool in an appreciably different environment results in a low-quality log. Data obtained in an actual measurement environment must be corrected before use in the interpretation equations[11].

Only in two wells it was possible to correct the log readings due to the environment. In the rest of the well logs there was lack of data (no information about mud and filtrate resistivity, no caliper log).

These two wells were: 121-A and 122-A, in which the logs corrected were: gamma ray, resistivity and density. Those logs were corrected for borehole size and mud density.

Moderate changes were made in the GR log, in resistivity logs as well as in density logs the corrections were also very small.

TABLE 3-1 – DESCRIPTION OF WELLS WITH LOGS AVAILABLE

Well (*)	Logging date	Logged Interval		Status after completion	Log Curves
		Top	Bottom		
48-A OH	09/10/1946	44	958	PRODUCER	SP, RES
7-W CSD	06/22/1955	500	814	PRODUCER	GR, NEUT
8-W CSD	06/29/1955	690	917.5	PRODUCER	GR, NEUT
1-C OH	03/09/1960	100	1676	DRY	SP, RES 16", 64", 18'8"
65-A OH	02/08/1963	85	2020	DRY	SP, RES-SN, RES-LN, RES-18'8"LAT
25-W OH	03/04/1963	80	1781	DRY	SP, RES-SN, RES-LN, RES-18'8"LAT
52-A CSD	10/16/1989	700	961	PRODUCER	GR, NEUT
117-A OH	01/18/1990	100	898	PRODUCER	SP, GR, RES, NEUT
118-A OH	10/15/1990	100	998	PRODUCER	SP, GR, LN, SN, RES, NEUT
120-A OH	07/01/1997	33	954	PRODUCER	GR, SP, RES, RES-SN
119-A OH	07/08/1997	35	949.7	PRODUCER	GR, SP, RES, RES-SN
122-A OH	09/04/2002	0	1019	PRODUCER	GR, SP, SFLR, ILM, ILD, PHIN, RHOB
121-A OH	10/16/2002	73	956	PRODUCER	GR, SP, SFLR, ILM, ILD, PHIN, RHOB

(*) OH: Open Hole, CSD: Cased Hole

Logs Description

SP: Spontaneus Potential
GR: Gamma Ray
NEUT: Neutron
RES: Resistivity
RES-SN: Resistivity Short Normal
RES-LN: Resistivity Long Normal
RES-LAT: Resistivity Lateral
SFLR: Spherically Focused Log Resistivity
ILM: Induction Log - Medium
ILD: Induction Log - Deep
NEUT PORO: Neutron Porosity
DEN.PORO: Density Porosity

3.2.2 Log normalization

Well log normalization is the process of identifying and removing systematic error from well log data in order that a quantitative analysis of such data can accurately be made. Given the current diversity of well logging tools and tool vintages combined with the push to apply advanced formation evaluation processing and interpreting algorithms in batch mode, proper well log normalization has never been more significant.

A big problem that we faced during the log analysis was the unit conversion. Old logs were recorded in different units that were different from the new ones.

We used a method called Multi-Well Normalization[12]:

GR and SP adjustment: a linear adjustment was done using the following equation (Shier, 1991):

$$V_{norm} = V_{Rlow} + \left(V_{RHigh} - V_{Rlow}\right)\left(\frac{V_{raw} - V_{low}}{V_{high} - V_{low}}\right) \quad \text{(3.1)}$$

Where:

V_{norm}: Normalized data value

V_{raw}: Raw data value

V_{Rlow}: Field low normalization value

V_{Rhigh}: Field high normalization value

V_{low}: Well's lithological low value

V_{high}: Well's lithological high value

Because of the little data available, we took the log data from wells 121A and 122A as the "type" curves representing correct log responses. The other curves were corrected based on this type of curves.

The log normalization process can be done for a single depth interval or for an entire curve's length. I selected our length interval of interest from the first lignite above the Mirando sand down to the end of the Pettus shaly sand.

Shier (1991) suggested another equation for normalizing old neutron logs recorded in counts per second. This equation converts a scale that is linear with respect to counts per second (cps) to one that is linear with respect to porosity:

$$Log(\phi_{norm}) = \left[\frac{NEU_{cps}\left[Log(\phi_{Rhigh}) - Log(\phi_{Rlow})\right] + NEU_{cpshigh}Log(\phi_{Rlow}) - NEU_{cpslow}Log(\phi_{Rhigh})}{NEU_{cpshigh} - NEU_{cpslow}} \right] \quad \text{..... (3.2)}$$

Where:

ϕ_{norm}: Normalized neutron porosity in percent porosity

NEU_{cps}: Raw neutron porosity in counts per second

ϕ_{Rhigh}: Field value of high porosity lithology in percent porosity

ϕ_{Rlow}: Field value of low porosity lithology in percent porosity

$NEU_{cpshigh}$: High porosity lithology value for the well in counts per second

NEU_{cpslow}: Low porosity lithology value for the well in counts per second

3.3 Determination of the matrix density

The porosity derived from the density log is calculated as follows:

$$\phi_D = \frac{\rho_{ma} - \rho_b}{\rho_{ma} - \rho_{fl}} \quad \text{..... (3.3)}$$

Where:

ρ_{ma}: matrix density (gr/cm^3)

ρ_b: bulk density – recorded from log (gr/cm^3)

ρ_{fl}: density of the fluid (gr/cm^3)

In the analysis of clean formations (i.e. no shales present in the rock structure), the known values of matrix density are usually assumed. For example for sandstones, 2.65 gr/cm^{3}is usually assumed. The shaly character of the formations analyzed in this research was pointed out. The first calculations of porosity derived from density logs showed high values of porosity; this might be an indication of an erroneous value used as matrix density.

In order to determine the true matrix density I followed the Hingle-Pickett interplay approach[11]

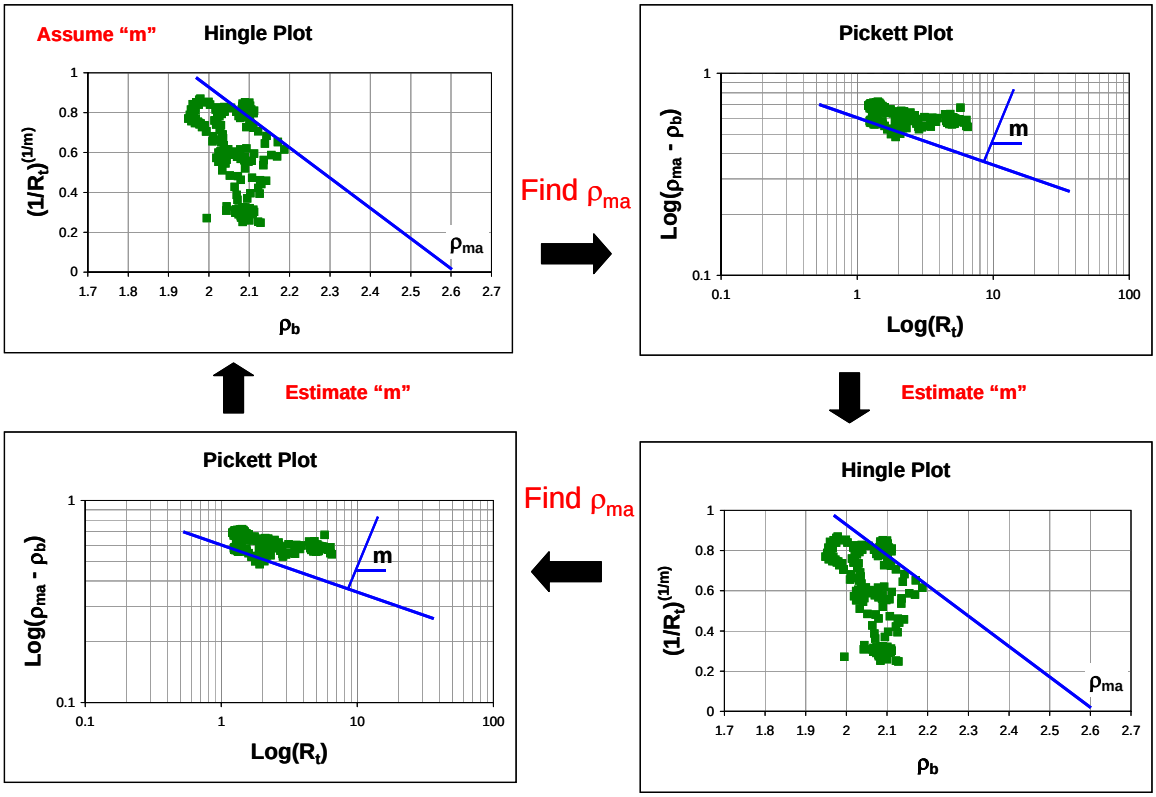

Fig. 3-1 – Interplay of Hingle and Pickett cross plots - Well 121A.

In this approach a value of the Archie's cementation exponent "m" was assumed and the matrix density was calculated from Hingle Plot. With this value the Pickett plot was used and the estimation of "m" value was obtained again. This iterative process is done until a convergence is obtained. This process is graphically explained in **Fig. 3-1**.

For well 121A the matrix density was estimated in 2.68 gr/cm^3 and the porosity exponent "m" in 1.36. And for well 122A the matrix density was estimated in 2.67 gr/cm^3 and the porosity exponent "m" in 1.34. These values are in close agreement with those reported by literature as typical values for shaly sands. These values were later used in the calculation of water saturation.

3.4 Generation of a shale model

In order to understand the shaly character of the pay zone in the Jacob field, it was used the approach given by Heslop (2002) [13].

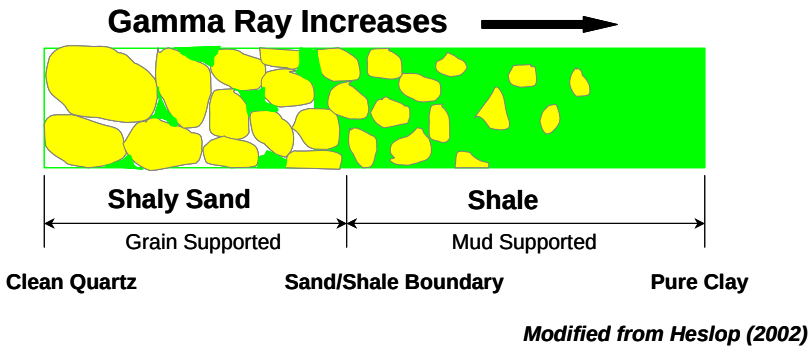

Fig 3-2. Sand/shale continuum.

Consider a reservoir continuum from clean sand to pure clay. Such a continuum is illustrated in **Fig. 3-2**. Moving from left (clean sand) to right (pure clay) the clay volume is increased until all of the available pore space has been filled. Up to this point the reservoir is grain supported. Moving further to the right, the addition of clay displaces sand grains. The formation is now mud supported with sand grains as inclusions. The boundary between grain supported and mud supported is the sand/shale boundary.

In this example we are describing a dispersed clay within a sand matrix. There are two other forms of shale existence in shaly sands: laminated and structural. A laminated shale looks like a shale or a very shaly sand. Structural shales will function as sand grains, and will appear much like a sand except on the gamma ray log.

The gamma ray log is the most common shale volume indicator. This log responds to the changes in natural gamma radiation emitted by the formation.

The neutron log is measuring the hydrogen population of the formation. Therefore, it records a nearly constant response through sands and increases in shales. **Fig. 3-3** shows the Neutron versus Gamma Ray Cross-Plot of well 122A. Notice that the Pettus sand is highlighted and the points lie in the shaly sand zone. Since the population

of hydrogen is nearly the same in water, oil, and wet clay, the neutron log cannot distinguish between them.

In the shale portion of the shaly sand, the quartz fraction is not in grain-to-grain contact and the clays form the matrix. The hydrogen population is therefore no longer controlled by the pore distribution. The neutron log measures increased hydrogen as the clay volume increases.

Fig. 3-4 shows the Gamma Ray versus Bulk density Cross-Plot for well 122A. It can be appreciated that as sand becomes increasingly shalier, fluids in the intergranular pore spaces are displaced by clay, and the bulk density increases as the gamma ray level increases. In shale, the bulk density remains nearly constant since an increase in the clay volume displaces quartz, which has a similar density.

In **Fig. 3-5** a Cross-plot of Bulk density versus Neutron porosity is presented. The combined responses of the neutron and density logs clearly distinguish between sand and shales. On a cross-plot of neutron versus density three points can be defined: the quartz point which is at 0% porosity on a neutron sandstone scale, and the quartz grain density (which is usually taken to be 2.65 gm/cc); the water point defined by the neutron and density responses to formation water (typically 100% porosity and 1.0 gm/cc); and the shale point determined by the neutron and density shale responses selected from the previous cross-plots. The clean sand line connects the quartz point and the water point. The shale line joins the quartz point and passes through the shale point.

Fig. 3-6 shows the cross-plot of Gamma Ray versus deep resistivity. The resistivity response for shales of common depositional environment is generally constant. It is quite common to observe shales with varying clay contents, as identified by the gamma ray log, which have a constant resistivity response as seen in Fig. 3-6. Hydrocarbon sands are identified in the right leg of the triangle of Fig. 3-6; the coarse part of the Mirando sand lies in this region. The blue dots, which represent Pettus formation, lie mostly in the shaly zone and few of them lie in the hydrocarbon zone. Therefore, this analysis shows the low hydrocarbon potential found in wells 121A and 122A in the Jacob field.

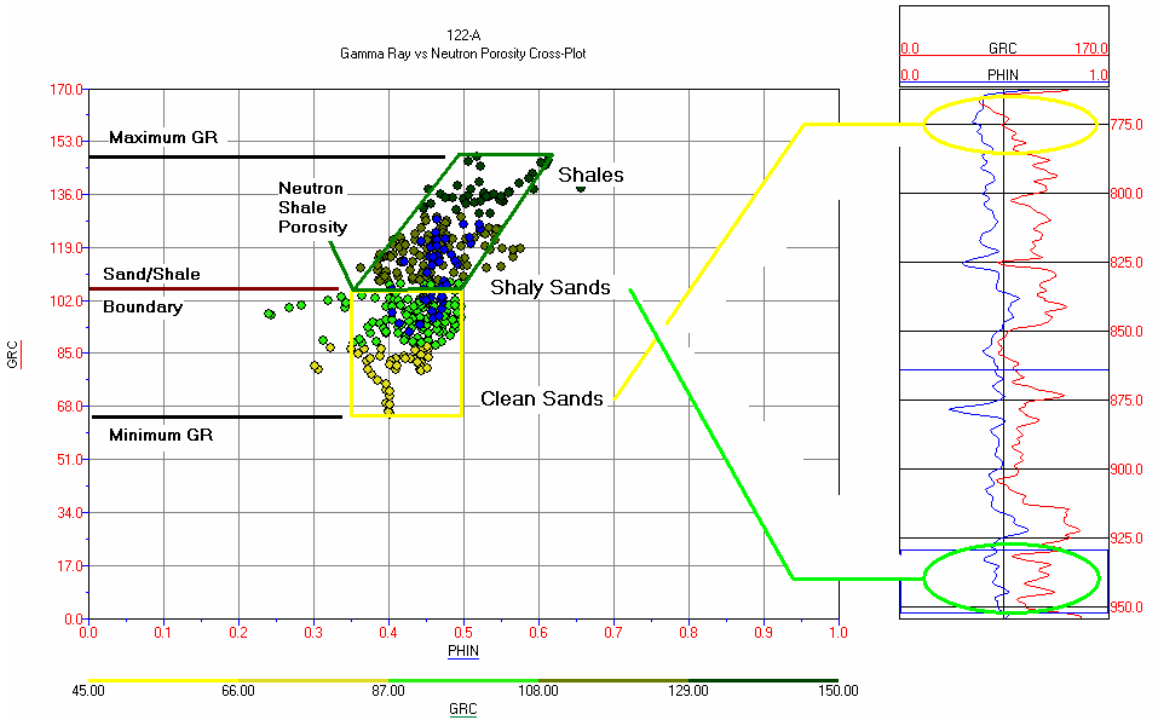

Fig. 3-3 - Gamma ray versus neutron porosity cross-plot for well 122A.

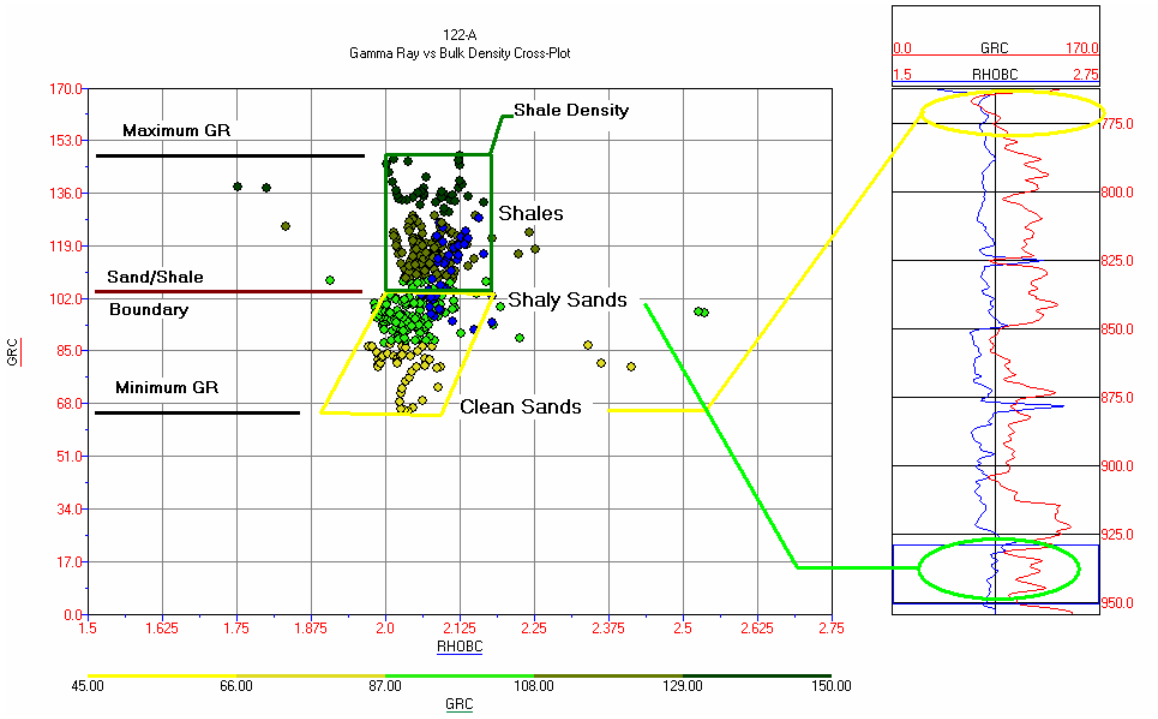

Fig. 3-4 - Gamma ray versus bulk density cross-plot for well 122A.

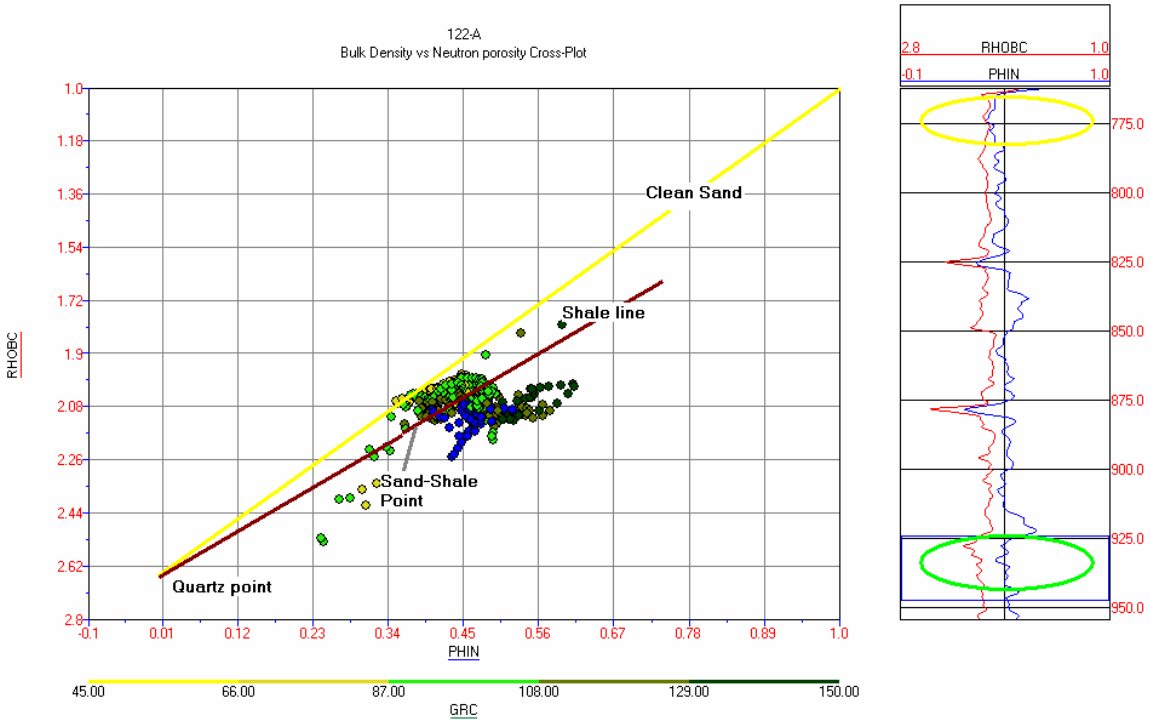

Fig. 3-5 - Bulk density versus neutron porosity cross-plot for Well 122A.

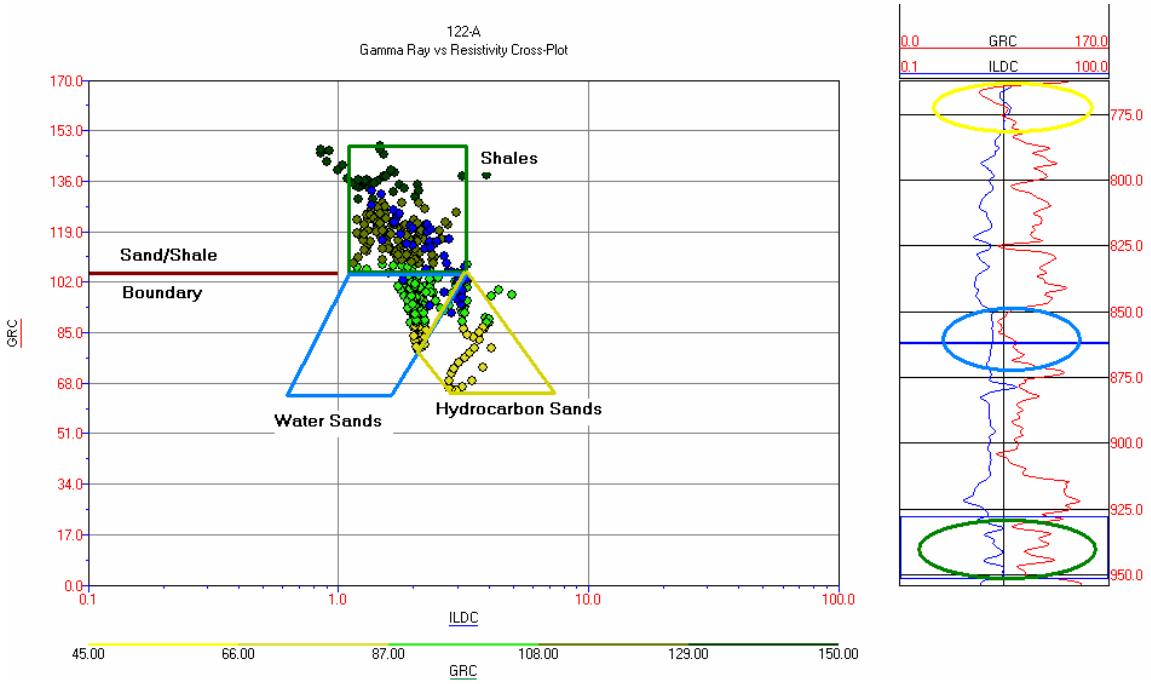

Fig. 3-6 - Gamma ray versus deep resistivity cross-plot for well 122A.

The comparison of responses of the suite of logs allows us to build a shaly sand model that determines the shale content. This shale model will serve mainly on the determination of effective porosity, which impacts directly on the estimation of water saturation.

3.5 Shale content quantification

The first step in shaly sand analysis is to determine the volume of clay, also known as V_{sh} (v-shale). This is a volumetric number and does not take into account such variables as type of clay mineral and distribution.

As it was explained in the previous section, the content of shale in the area of study is significant. From the log analysis of the 13 logs available we investigate the shaliness through the Jacob field.

The shaliness was determined mainly from the analysis of the Gamma Ray (GR) and/or Potential Spontaneous (SP) and Neutron/Density porosity where available (121A and 122A).

Eqs. 3.4 and **3.5** were used to determine the shaliness from GR and SP logs respectively.

$$V_{sh} = \frac{GR - GR_{cl}}{GR_{sh} - GR_{cl}} \quad \text{..... (3.4)}$$

Where:

V_{sh}: Shale content (fraction)

GR: GR value for the depth of evaluation (API units)

GR_{cl}: GR value for clean sandstone (API units)

GR_{sh}: GR value for shale (API units)

$$V_{sh} = \frac{SP - SP_{cl}}{SP_{sh} - SP_{cl}} \quad \text{..... (3.5)}$$

Where:

SP: SP value for the depth of evaluation (Millivolts)

$SPcl$: SP value for clean sandstone (Millivolts)

$SPsh$: SP value for shale (Millivolts)

$$V_{sh} = \frac{\rho - \rho_M + \phi_N(\rho_M - \rho_{fl})}{\rho_{sh} - \rho_M + HI_{sh}(\rho_M - \rho_{fl})} \quad \text{(3.6)}$$

Where:

ρ: Density value at the depth of evaluation (gr/cm3)

ρ_M: Matrix density, determined in previous section (gr/cm3)

ϕ_N: Neutron porosity (fraction)

ρ_{fl}: Fluid density (1.0 gr/cm3)

ρ_{sh}: Shale density (gr/cm3)

HI_{sh}: Neutron hydrogen index shale (fraction)

Eq. 3.6 was used to determine the shale content in those logs having density and compensated neutron tool logs.

Bassiouni[11] suggested that the previous equations overestimate the shale volume of shaly sandstones. Empirical relationships were suggested to adjust the shale index. For poorly consolidated shaly sandstones of the tertiary period (like the Pettus), the "Stieber" equation (**Eq. 3.7**) is usually suggested.

$$V_{sh} = \frac{0.5V_{sh}}{1.5 - V_{sh}} \quad \text{(3.7)}$$

3.6 Estimation of effective porosity and water saturation

3.6.1 Effective porosity

The presence of shale complicates the interpretation of the porosity tools' response because of the diverse characteristics of shales and the different responses of each porosity tool to the shale content. On the density porosity log, shales display low to moderate porosity values. On the neutron log, shales display moderate to relatively high porosity values. Note in **Fig. 3-7** that the electrical log of well 121A shows this behavior:

The neutron porosity curve (blue line in the porosity track) is relatively higher than the density porosity curve (green line in the porosity track).

The true porosity, representing the effective pore volume of a shale formation can be estimated from any of the porosity tools by:

$$\phi_{eff} = \phi_a (1 - V_{sh}) \quad \text{(3.8)}$$

Where:

ϕ_{eff}: Effective porosity (fraction)

ϕ_a: Apparent porosity (fraction)

Bassiouni[11] suggests using the density log porosity since this log is less sensible to an incorrect estimation of Vsh. Therefore, in our analysis we have defined the apparent porosity as the one derived from the density derived porosity.

3.6.2 Water saturation

In order to determine the true water saturation in shaly sandstones, the Archie water saturation equation must be modified by a number of different shaly sand equations.

Two equations are usually recommended in shaly sand analysis and I used both to estimate water saturation in the Jacob field.

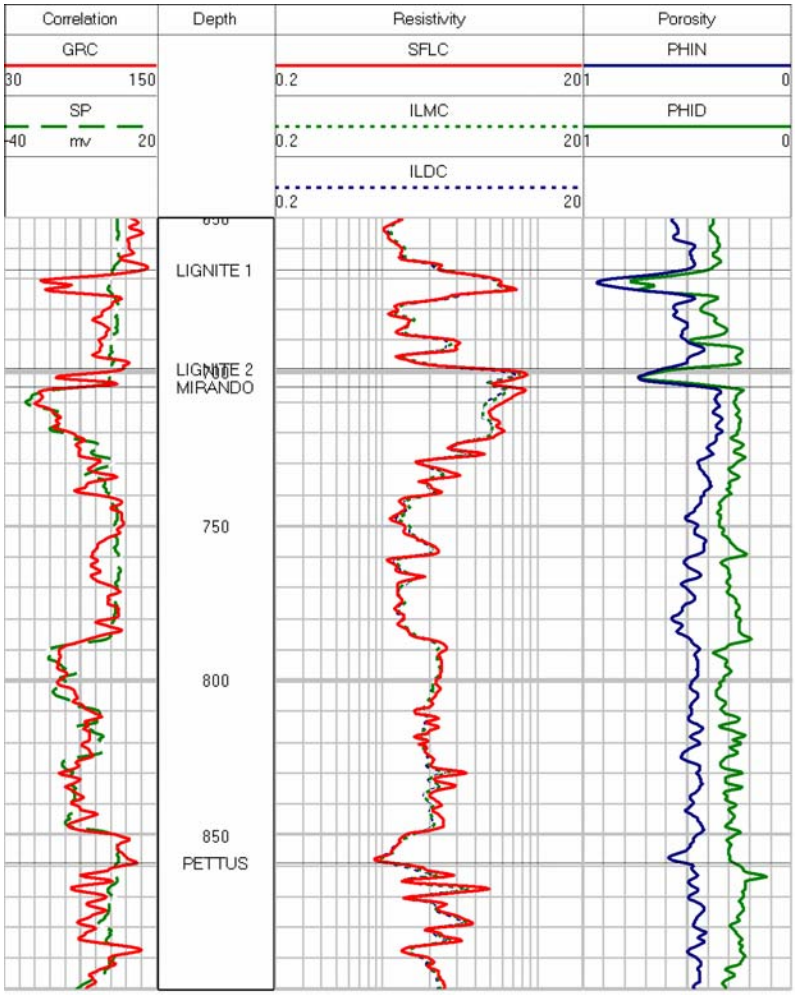

Fig. 3-7 – Log of well 121A previous to interpretation.

Indonesian Model

$$S_w = \frac{\sqrt{1/R_t}}{\frac{V_{sh}^{\,1-0.5V_{sh}}}{\sqrt{R_{sh}}} + \sqrt{\frac{\phi^m}{aR_w}}} \quad \text{..... (3.9)}$$

Where,

R_t: Formation resistivity (ohm-m)

R_{sh}: Shale resistivity (ohm-m)

R_w: Formation water resistivity (ohm-m)

m: Cementation factor

a: Archie "a" constant

Modified Simandoux

$$S_w = \frac{\sqrt{\left[\left(\frac{V_{sh}}{R_{sh}}\right)^2 + 4\frac{\phi_{eff}^m}{aR_w(1-V_{sh})R_t}\right]} - \frac{V_{sh}}{R_{sh}}}{2\frac{\phi_{eff}^m}{aR_w(1-V_{sh})}} \quad \text{..... (3.10)}$$

The values of "a" and "Rw" were calculated using the Pickett plot in a clean sandstone (Mirando) for each well log.

From the log analysis of wells 121A and 122A (**Figs. 3-8** and **3-9**) we can observe that in the pay zone the shale volume averages more than 30% in both wells (121A and 122A). However in the Mirando clean sand the shaliness averages less than 10%. This interpretation strengthens the shale model developed in the previous section.

Note that the pay zone is not very well marked in the SP log, however the GR shows it as a serrate curve. The SP behavior is an indicator of the high shale content of the Pettus sand and makes it difficult to identify it in those wells having only SP log recorded.

Note the close match between the log derived effective porosity and the core derived porosity. This match would indicate the correct interpretation of the shaliness of the formations. In Fig. 3.7 the Neutron/Density derived porosities overestimated the porosity values (30-40%), however the correct interpretation resulted in acceptable values (20-30%).

The Pettus sand has a characteristic low resistivity (2-3 ohm-m) compared to the clean Mirando sand and to the upper shaly sand. In all the interval of interest the deep, medium and shallow resistivities are almost overlayed. It seems to be a complete wet interval with no indication of presence of oil since the shallow resistivity is higher that

the deep resistivity. However the production tests in the Pettus sand in wells 121A and 122A, indicated the presence of oil and gas and few water rates.

The log derived water saturation for the pay zone averages 60% and 50% in 121A and 122A respectively. The two models used (**Eqs. 3.9**, and **3.10**) are in close agreement with each other, but lower with respect to the core derived water saturation. The production tests of these two wells did not indicate too much water production in surface. Therefore the high water saturation would be mostly bond or immobile water.

In order to differentiate between the bond and mobile water the Waxman and Smits' Model can be used. Unfortunately it requires the knowledge of cation exchange capacity (CEC), which is a time consuming experiment and is not available for the Jacob wells.

Figs. 3-10 and **3-11** show the logs interpreted for wells 117A and 118A. The shale volume was calculated using the GR and SP logs (Eqs.3.5, and 3.6) and adjusted by the Steiber equation (Eq. 3.7). The neutron porosity was converted from counts per seconds to porosity units (fraction) by normalizing the data using Eq. 3.2. The normalized curve (PHIN) was used to estimate the effective porosity that matches to those core derived porosity in the cored zone.

The SP and GR curves behave very similarly to those of 121A and 122A making it easier to identify the formations' tops.

In well 117A the log was recorded up to some depth in the middle of the Pettus sand making the determination of the base of the pay zone unclear (In the pay thickness determination, we assumed the perforated interval to be the pay thickness).

In these two wells the resistivity logs show low values, but higher than those of the previous wells. Again, it is difficult to determine the presence of the Pettus sand just from the resistivity curves. The behavior of resistivity curves is suspicious in well 118A. It might be an error from the digitizing job. In both the cases we have used the long resistivity (RES16 in 117A and LN in 118A) in order to calculate the water saturation.

Water saturation was estimated by using the Indonesian equation (Eq. 3.9), and again the values in the pay zone lie between 50 and 60%.

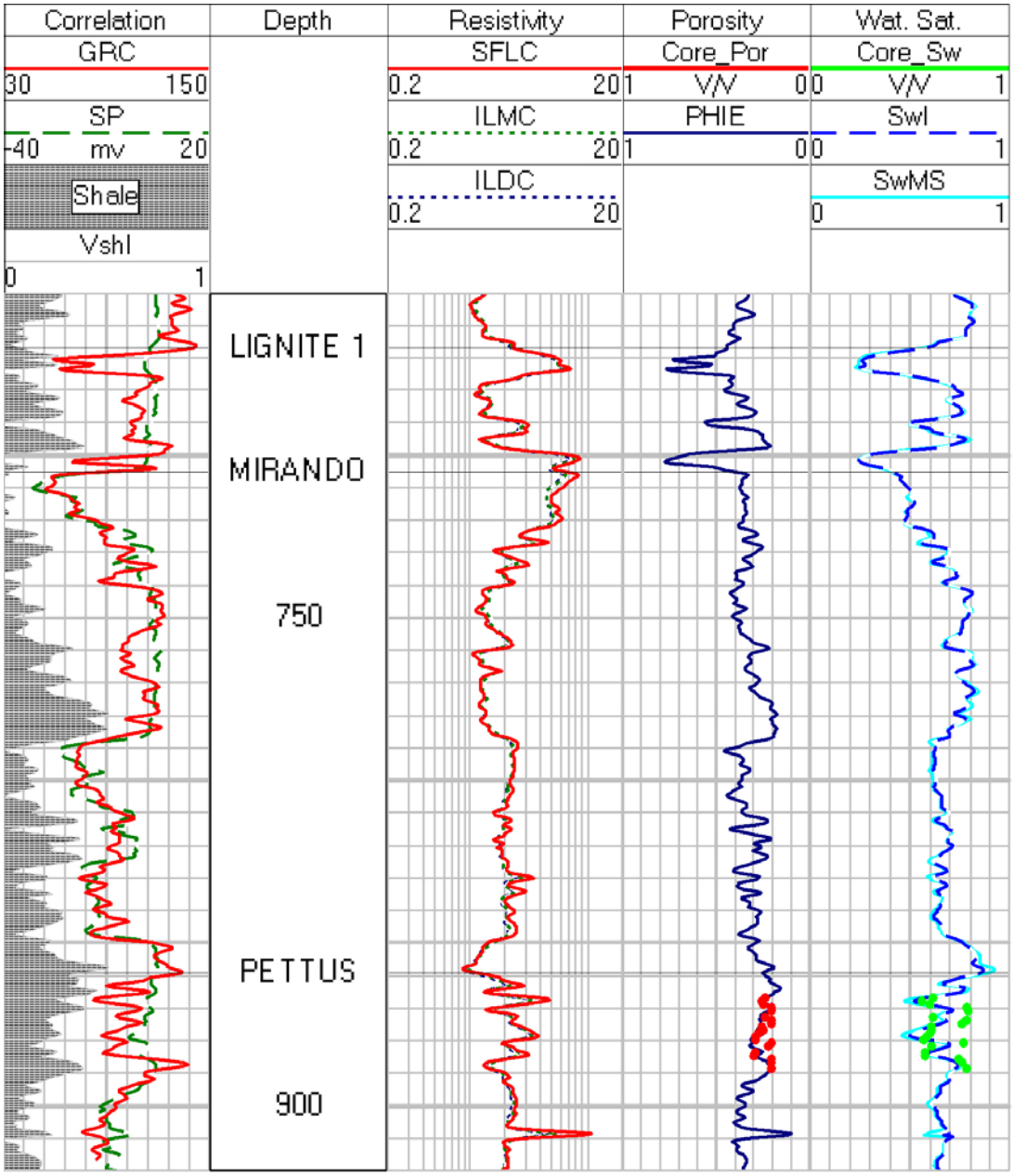

Fig. 3-8 – Interpreted log for well 121A.

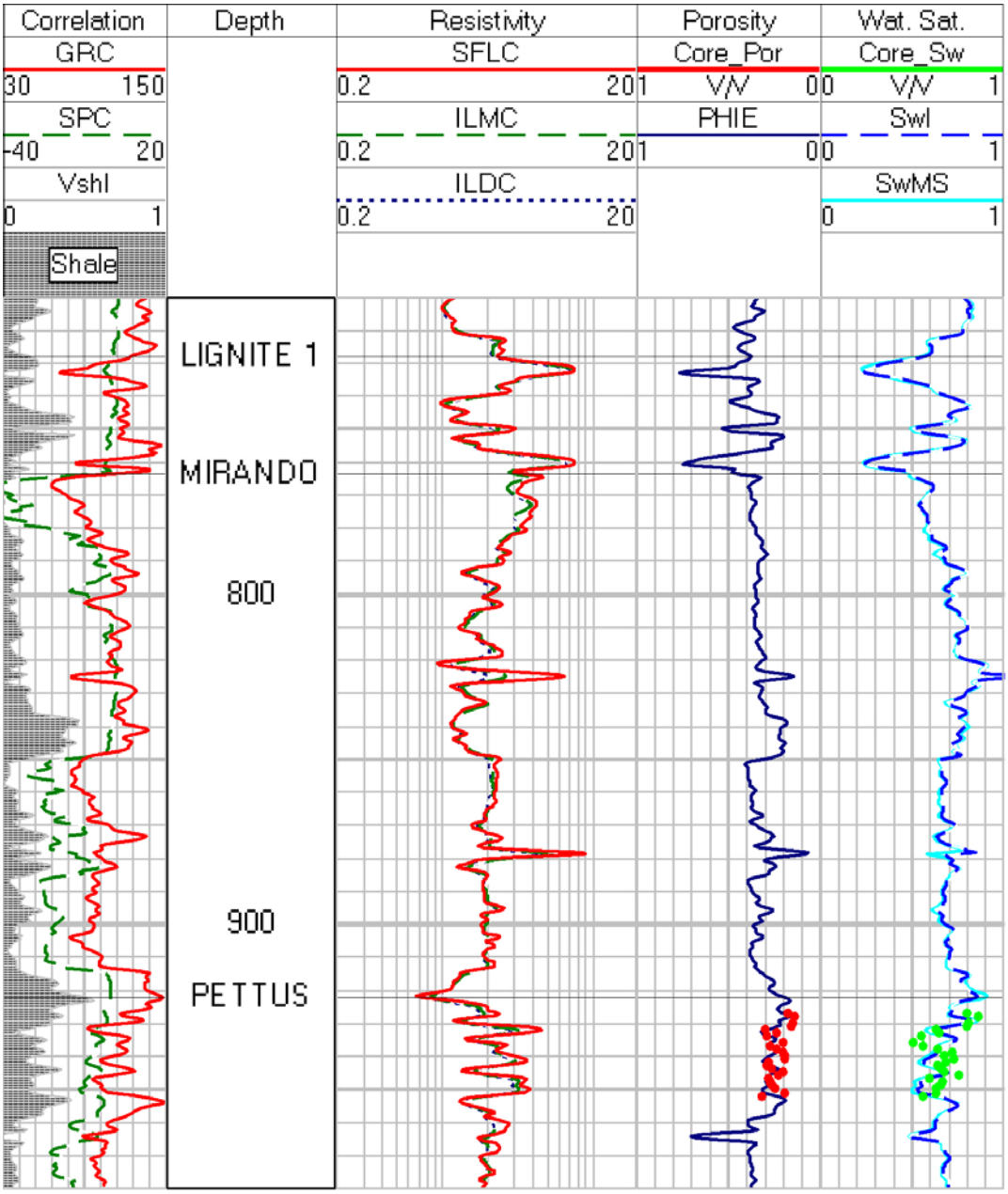

Fig. 3-9 – Interpreted log for well 122A.

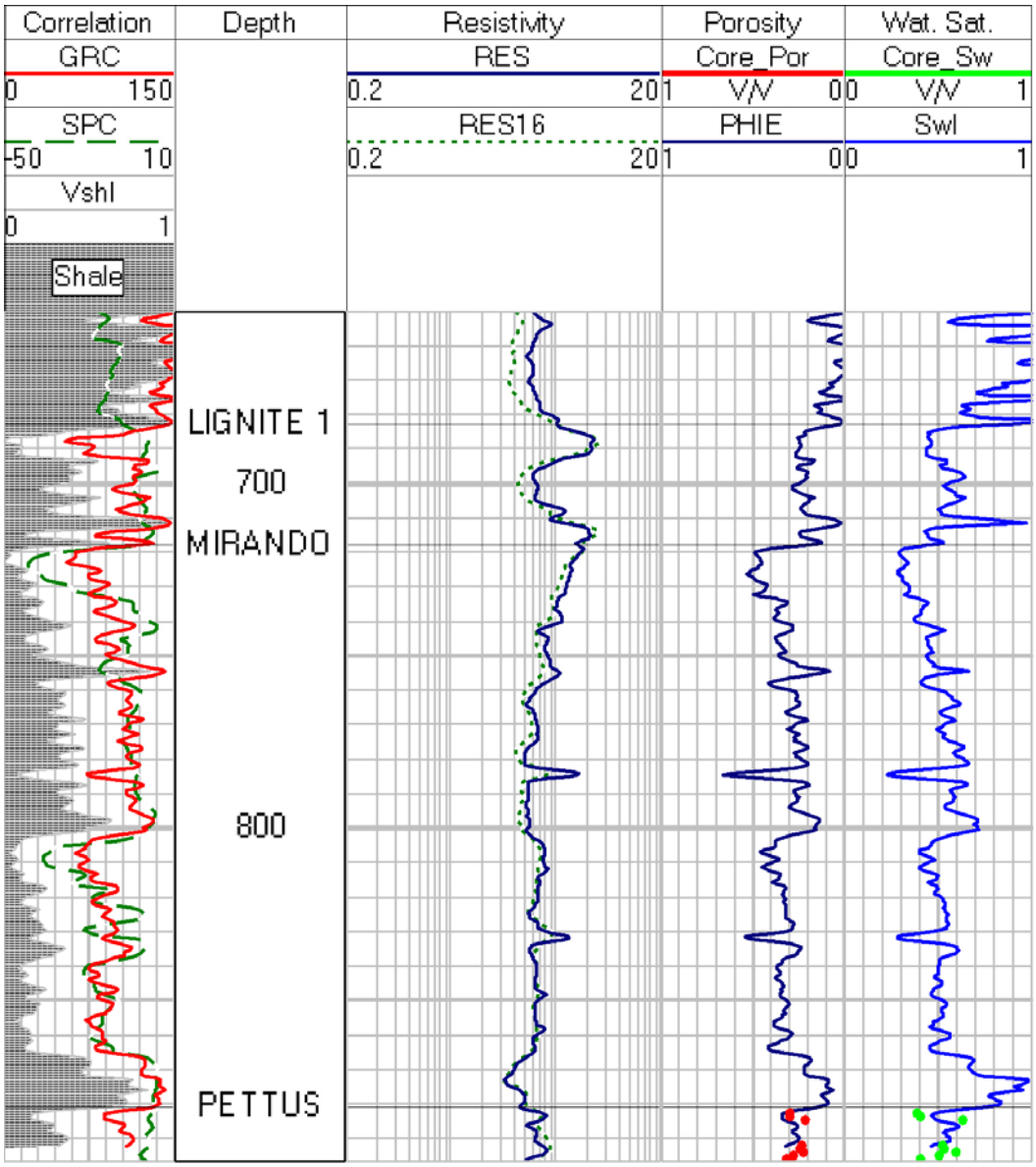

Fig. 3-10 – Interpreted log for well 117A.

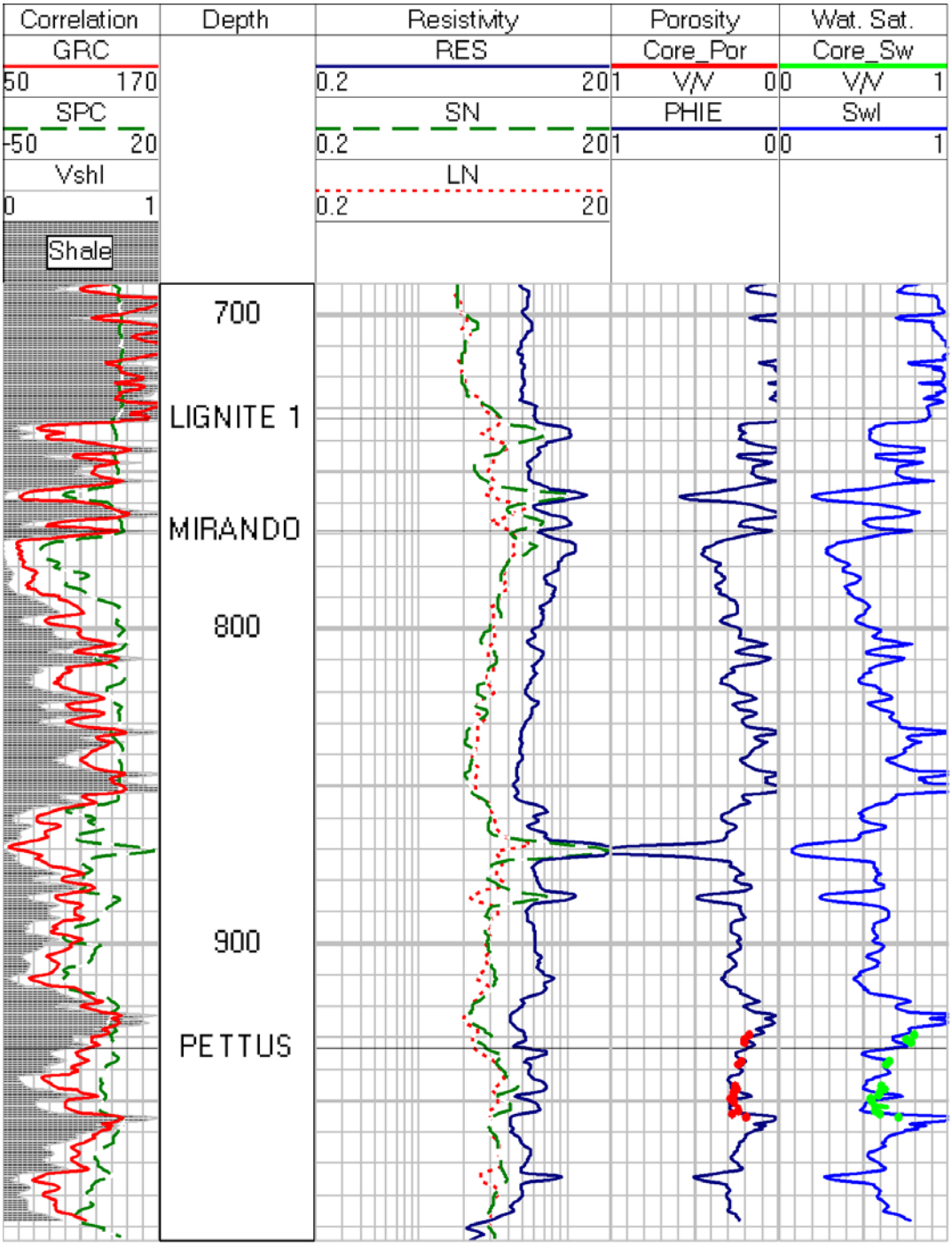

Fig. 3-11 – Interpreted log for well 118A.

Figs. 3-12 and **3-13** show the interpreted logs for wells 119A and 120A. These two wells had only SP, GR and resistivity logs available for any interpretation. Therefore it was only possible to determine the shale content using SP and GR together. Observe that the shale content in the pay zone reaches 30% whereas in the Mirando sand it reaches less than 10%.

The resistivity logs show a gap between the shallow resistivity and the long resistivity (RES), this might be an indication of a salt mud used in the logging process. However, no indication was found of what type of drilling mud was used in logging these two wells. Anyway, the deep resistivity (blue line) shows the usual behavior of the previously analyzed logs: low resistivity values (2-3 ohm-m) in the pay zone.

In **Figs. 3-14** and **3-15** we show the analyzed logs from wells 48A and 65A. The 48A log did not finish logging all the Pettus sand. In these two wells only SP was recorded. In the pay zone of well 65A we appreciate high shale content. This result is in agreement with the production tests performed in this well (it was found water wet). However we have to be aware that the SP tool did not result as a good indicator of shale content especially in shaly sands as outlined above. So the results of quantifying shale content only from SP curve should be arguable in those cases.

In the case of the resistivity curves, they indicate the low values as in the previously analyzed logs in the pay zone.

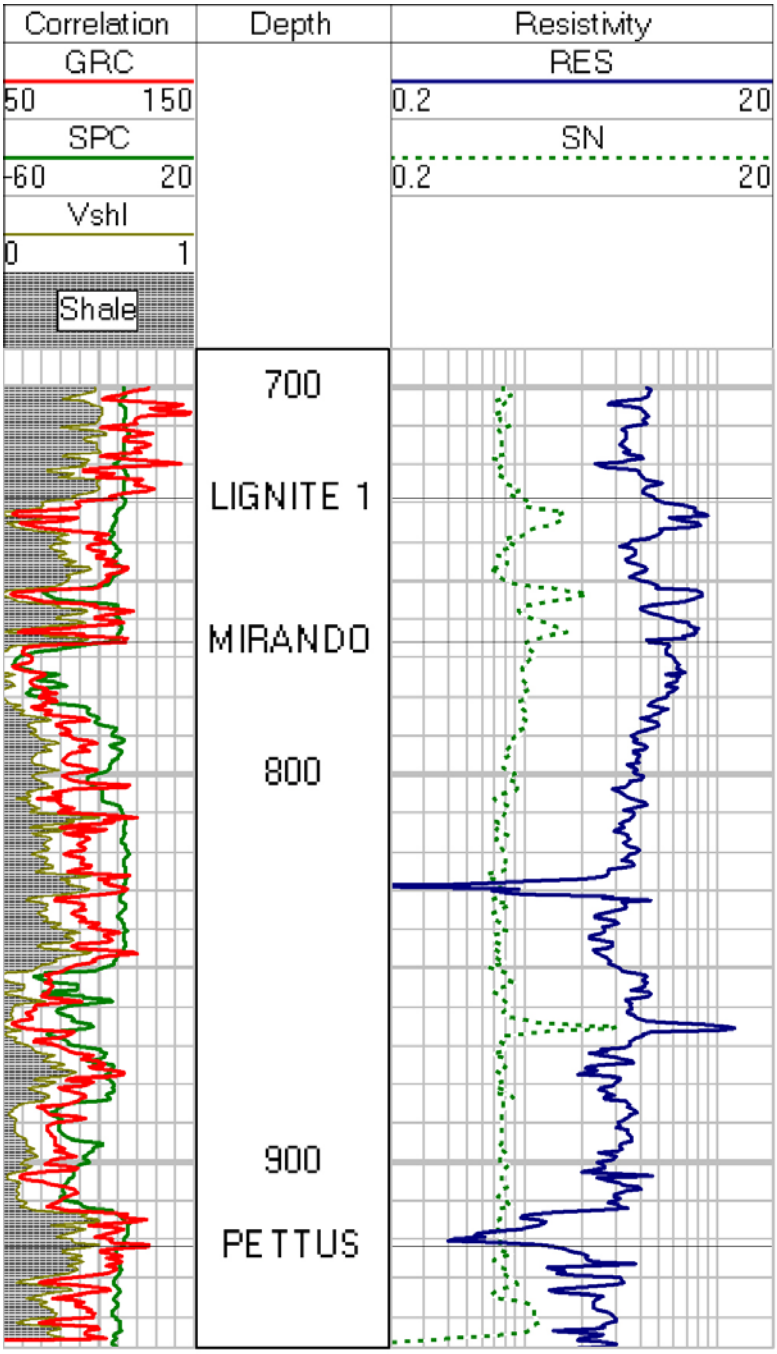

Fig. 3-12 – Interpreted log for well 119A.

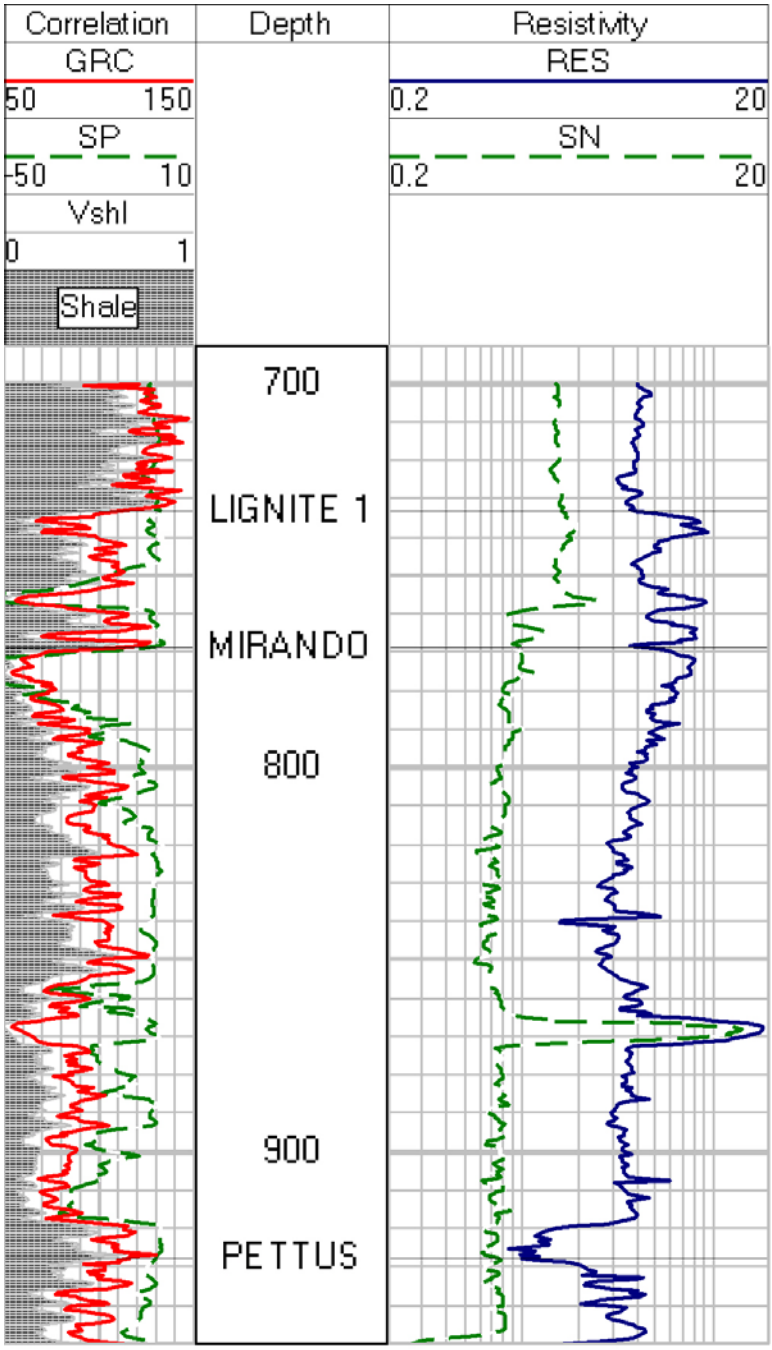

Fig. 3-13 – Interpreted log for well 120A.

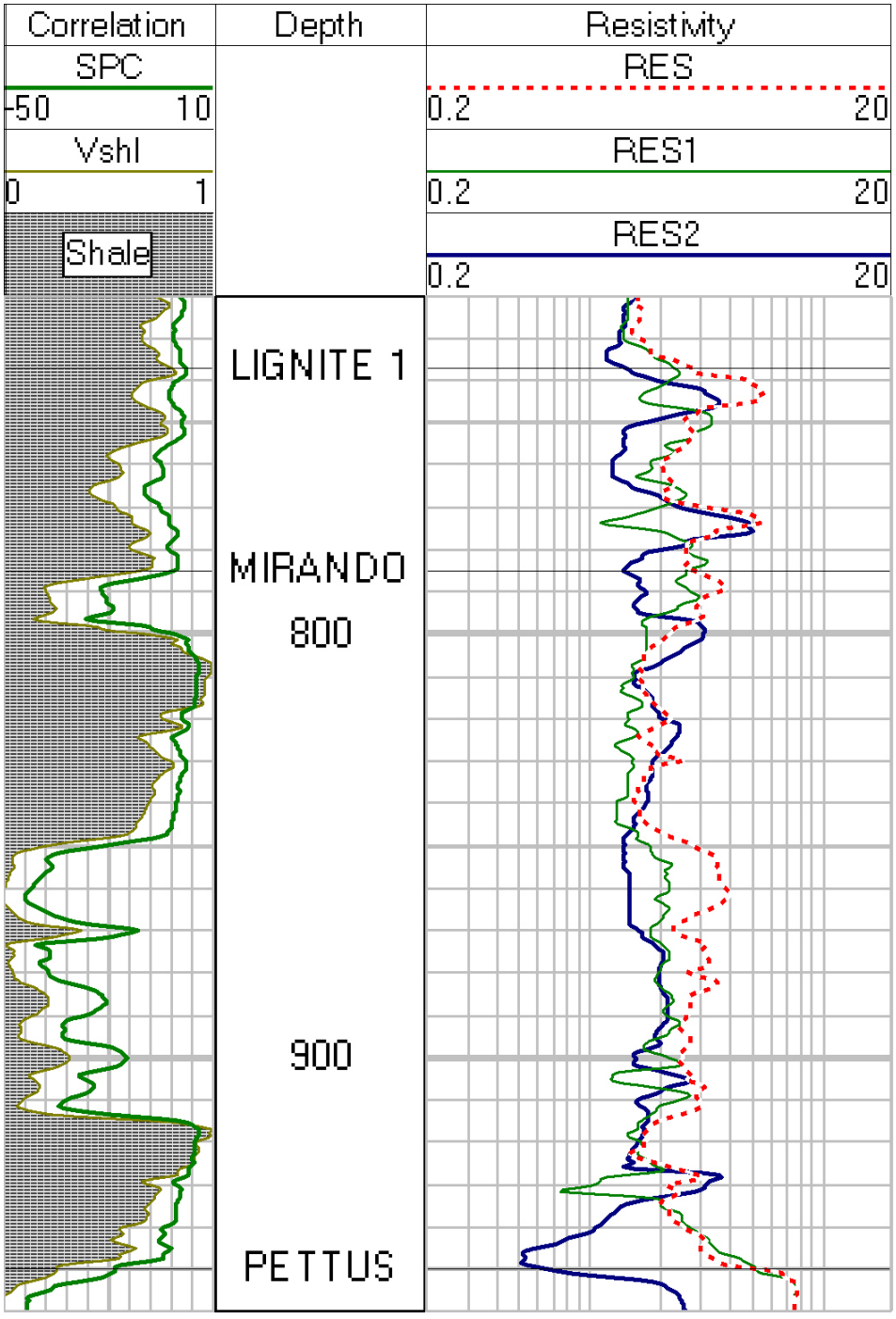

Fig. 3-14 – Interpreted log for well 48A.

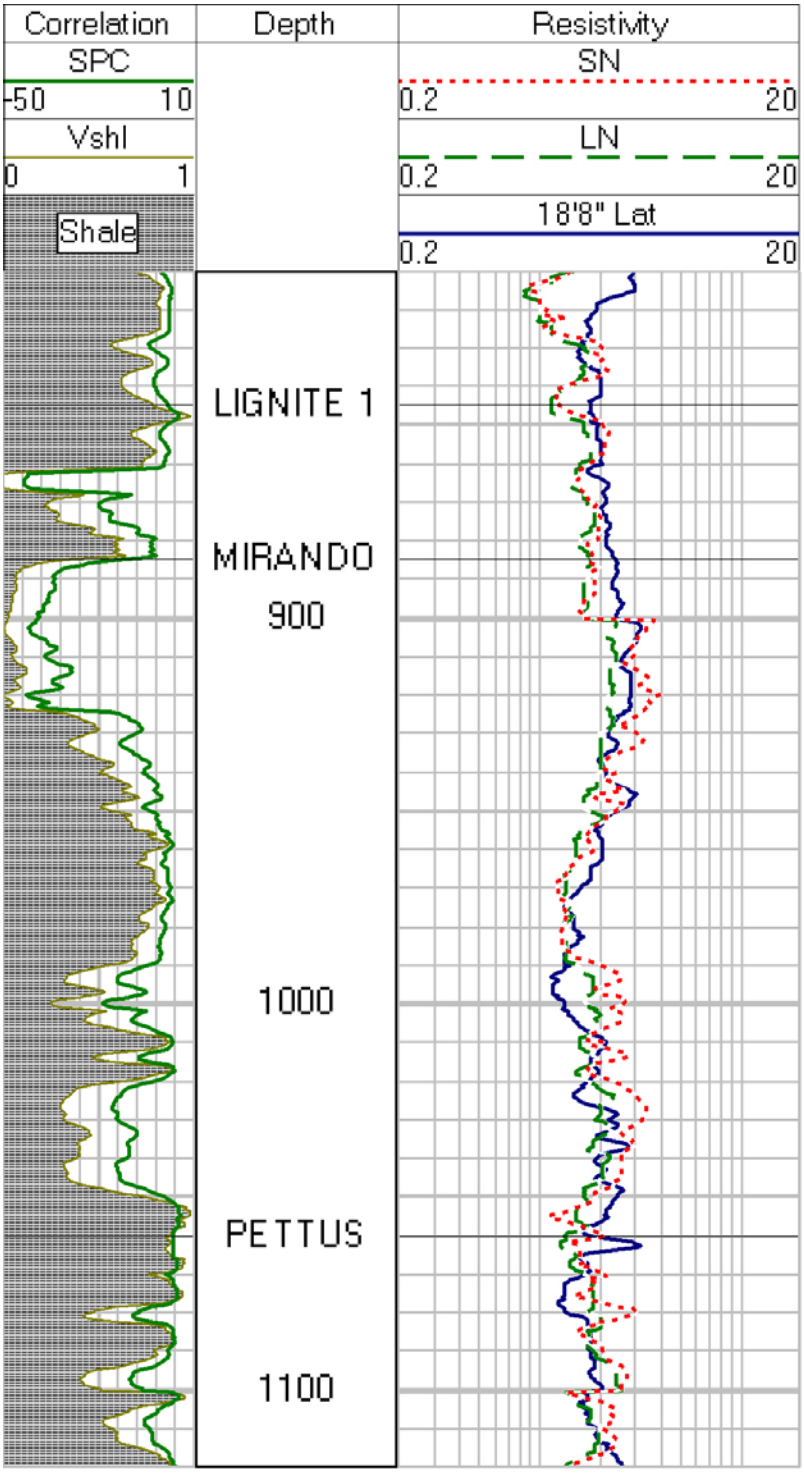

Fig. 3-15 – Interpreted log for well 65A.

Figs. 3-16 and **3-17** show the interpreted logs from wells 1C and 25W. Like in the previous cases only SP and resistivity logs were available. Therefore only shale content was possible to estimate. As outlined before the SP curve does not result a good shaliness indicator for shaly formations. Thus, the shale content values in the Mirando sand are reliable. In the Pettus sand the shale content would be overestimated.

According to production records, tests in well 1C showed oil traces in the Pettus sand. And in well 25W showed water wet.

Figs. 3-18, 3-19 and **3-20** show the analysis for the last 3 wells with logs available: 52A, 7W and 8W. In these wells GR was recorded. Since GR is a good indicator of shaliness, a better estimation was possible. Along the 3 wells, the estimation of shale content in the Pettus sand is around 30%. And all the wells resulted in producers when testing for hydrocarbon production.

In the 3 wells neutron tools were run and recorded in counts per second. In order to convert those readings in porosity units we used the normalization process. Once the neutron porosity was normalized, the effective porosity was estimated; however it was not possible to compare it with any core data. In well 52A there was a cored interval but deeper to the end of the logged interval. In wells 7W and 8W there was no cored interval.

The 4 wells with water saturation calculations are located very close to each other. Therefore if we want to show an areal distribution of the fluids with only these 4 wells would be meaningless. Therefore in a later section we use the water saturations obtained from core analyses data to better define the distribution of fluids within the reservoir.

On the other hand, the availability of shale content calculation in all the wells becomes a point in favor in the reservoir description analysis. We will use all the logs interpreted to build a geological model using geostatistical methods.

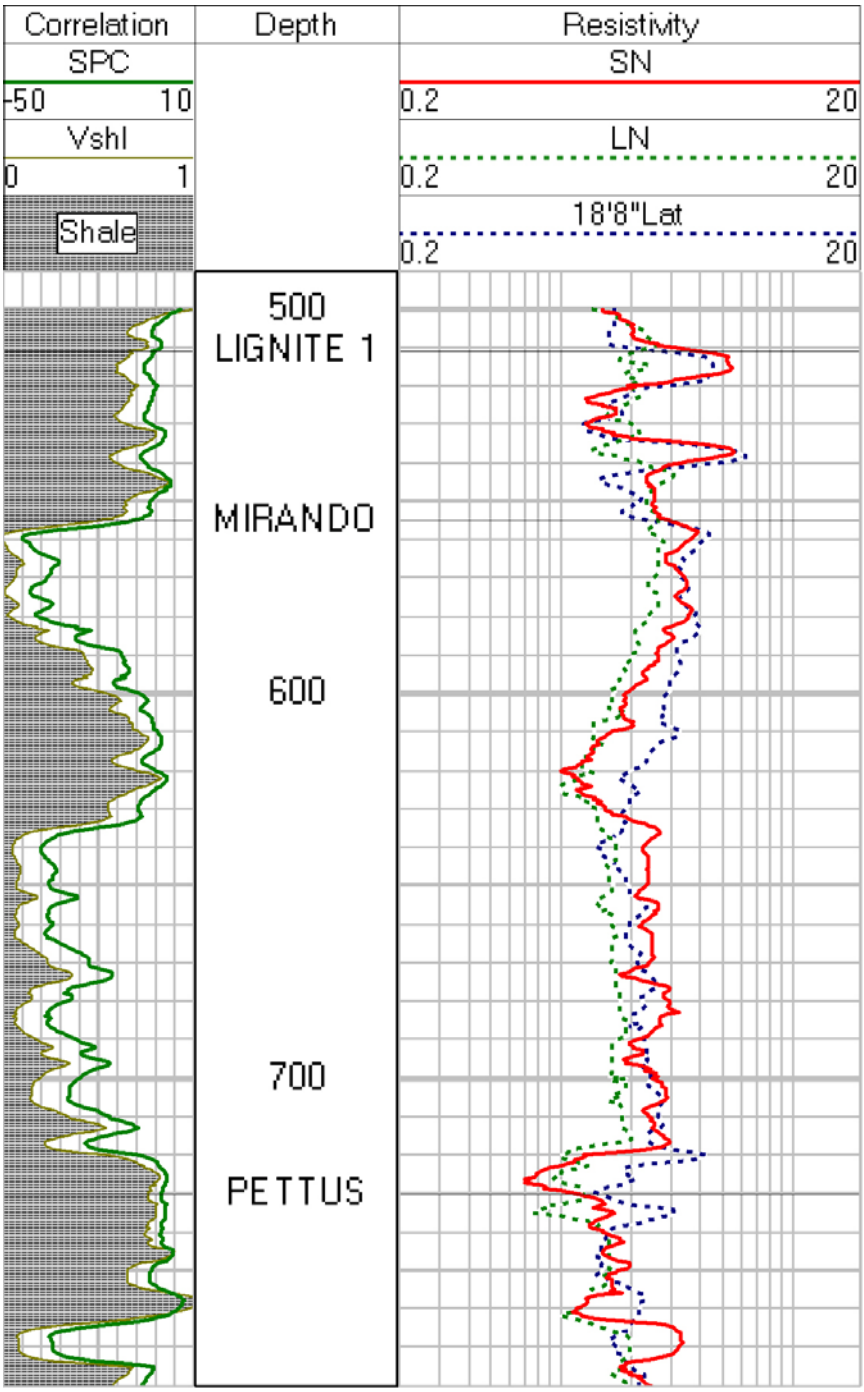

Fig. 3-16 – Interpreted log for well 1C.

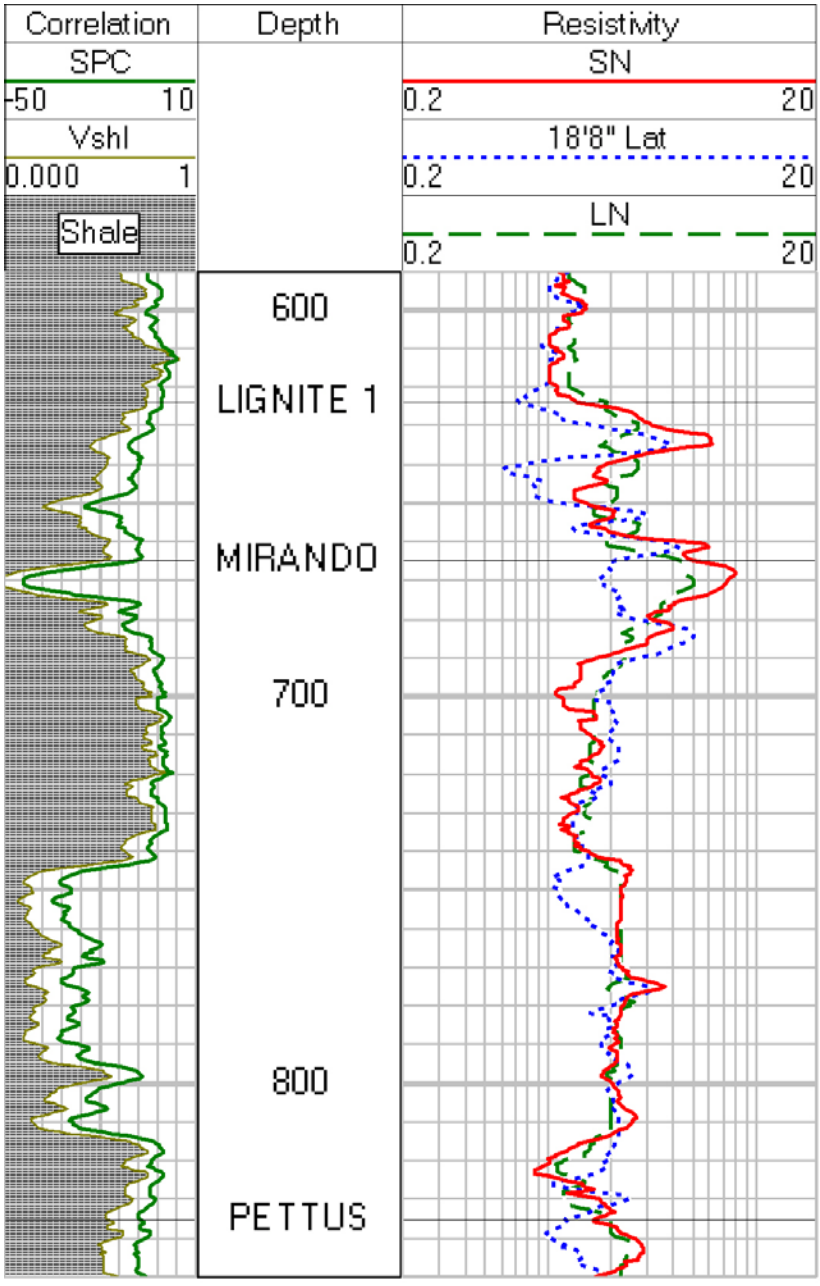

Fig. 3-17 – Interpreted log for well 25W.

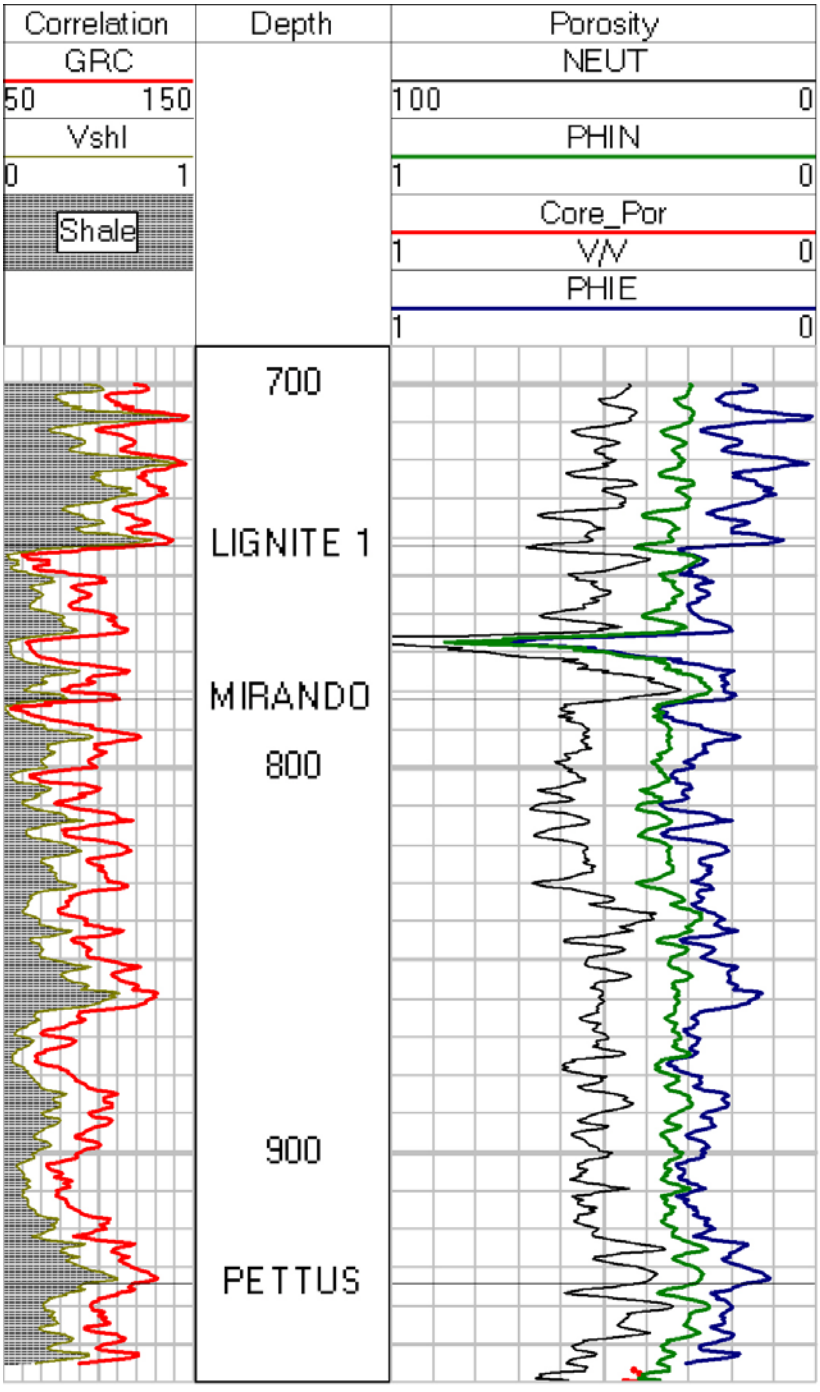

Fig. 3-18 – Interpreted log for well 52A.

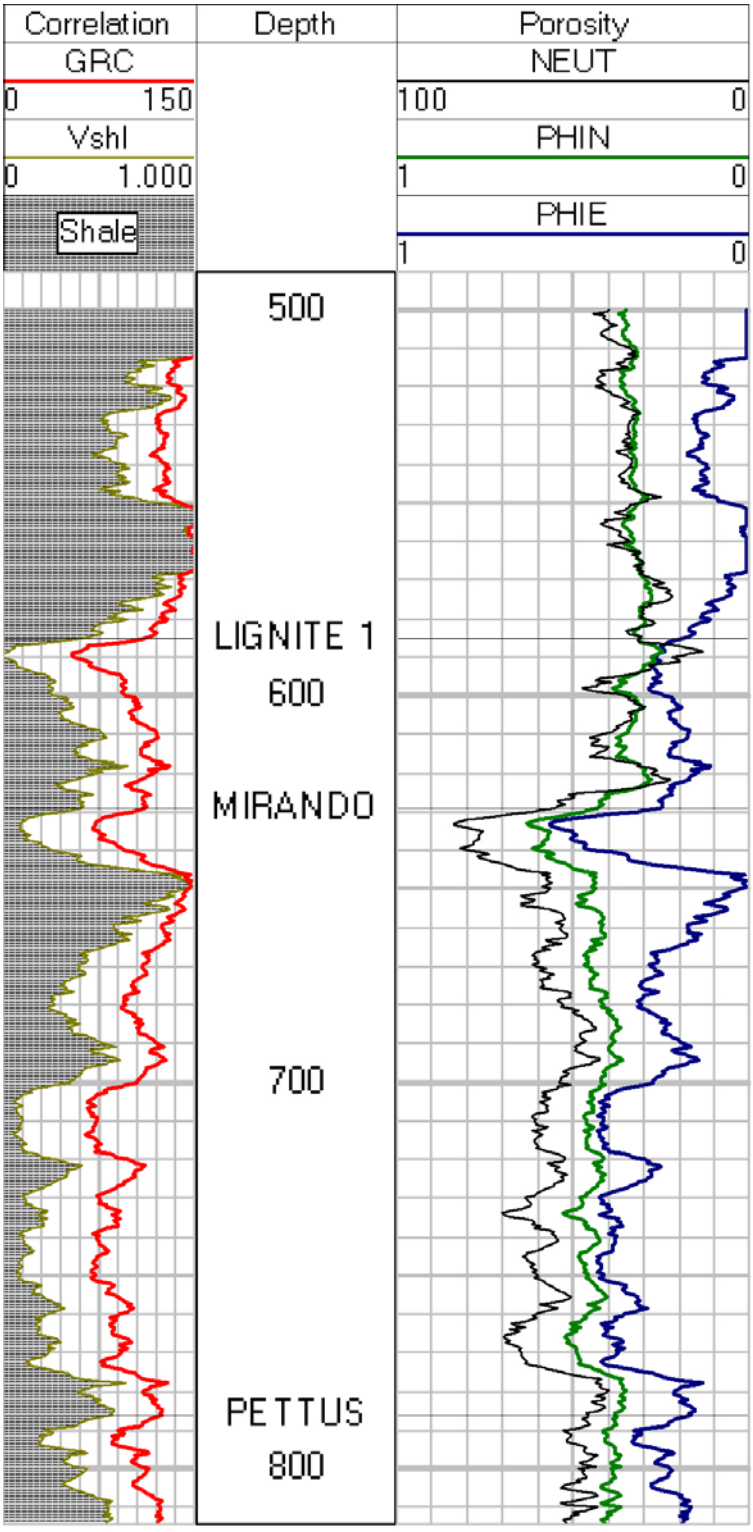

Fig. 3-19 – Interpreted log for well 7W.

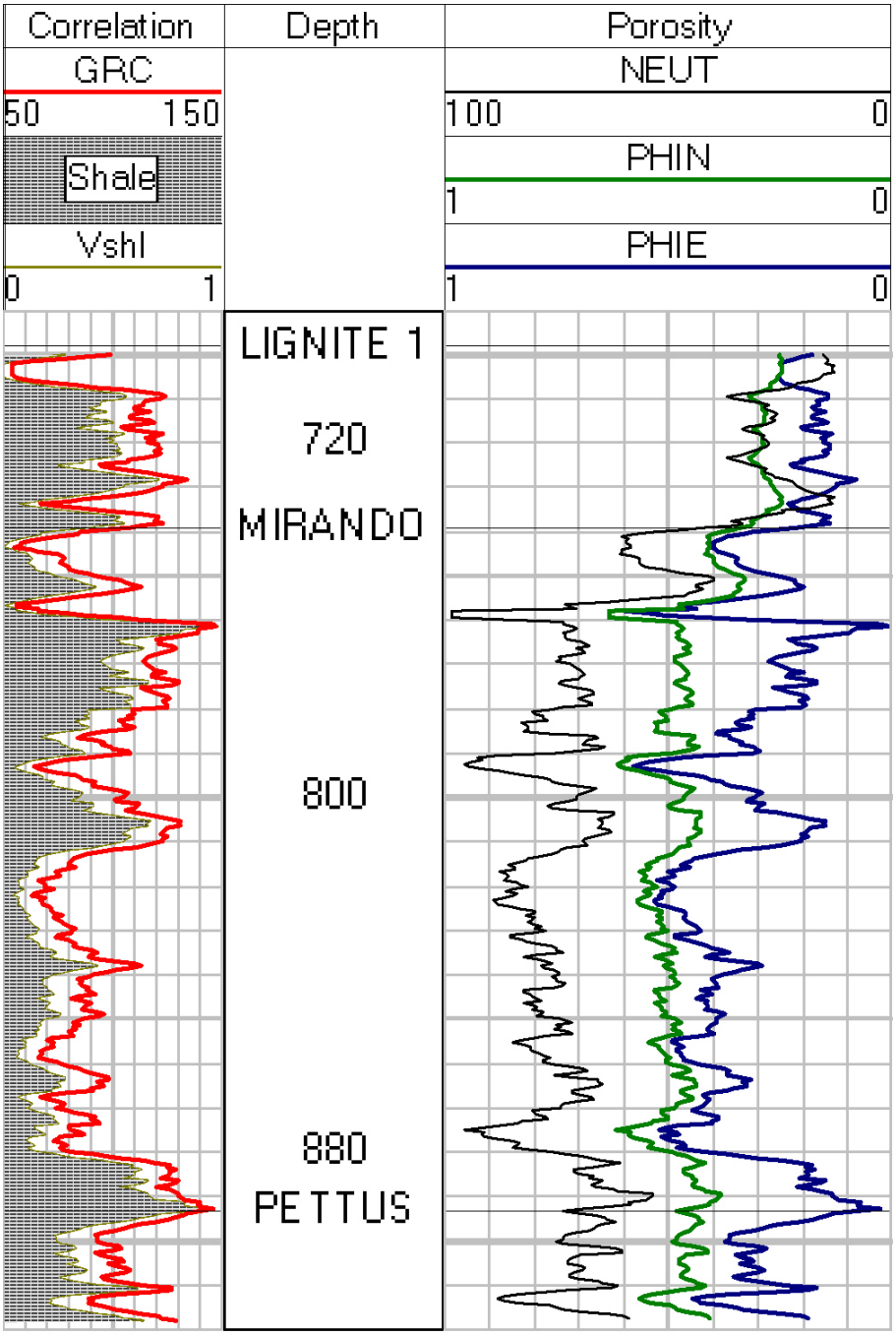

Fig. 3-20 – Interpreted log for well 8W.

CHAPTER IV

RESERVOIR ANISOTROPY

The main objective for this section is to determine the degree of anisotropy of the reservoir in a vertical and areal sense. So patterns of distributions can be identified and integrate them with the geological settings for the formations under study.

Two sources of data were used: core analyses data and shale content derived from the petrophysical analysis section.

4.1 Introduction

In the presence of limited information, any reservoir description involves the use of statistics. Geostatistics takes advantage of the fact that, in many natural phenomena, variable values measured close to each other are similar. As the distance between the measured values increases, the similarity between the two measurements decreases. On the basis of this similarity, geostatistics captures the spatial relationship through certain correlation functions[14].

Geostatistical procedures were used basically in two aspects: interpolation and extrapolation of values of reservoir variables at unsampled locations, so contour maps can be created from the estimated values; spatial-distribution analysis that provides the quantitative relationship describing the spatial variability of a reservoir property (porosity and permeability), including the distance over which a given variable is related as well as how that variable is spatially related to other variables.

4.2 Analysis of core data

The stratigraphic interval that was cored in all the wells corresponds to that of the Pettus formation. In most the wells the interval cored covered both pay and no pay thickness.

Two types of analyses were found in the files of the Jacob wells: Whole core and Sidewall core analyses. Whole core analysis examines the complete length of full-diameter core in the interval being tested and affords the maximum possible sample size. Sidewall core analysis is performed on cores recovered by any of the sidewall coring

techniques (percussion and rotary). Analysis is limited to basic tests for permeability, porosity, and residual fluid saturation.

The accuracy of core porosity measurements is claimed to be within half a porosity unit (0.5%). Those methods requiring that the core be cleaned and dried are subject to error if the core contains hydrated clay material. Retorting such a sample may drive off water of hydration and thus the porosity measured may be larger than effective porosity.

In our case we have to be aware that due to the unconsolidated nature of the sediments there are particular problems in determining porosity and permeability. According to Matax et.al.[15] the permeability measurements are more sensitive to the porosity measurements when handling unconsolidated sands. By doing several experiments Matax et.al.[15] concluded that unconsolidated media is very sensitive to the change of overburden pressure, therefore the core measurements at surface conditions would reflect lower values of petrophysical properties than the actual ones in the reservoir. However since the pay reservoir in the Jacob field is located at shallow depths (less than 1000') we do not expect much difference in the petrophysical properties due to the change of overburden pressure.

For unconsolidated media there are recommended techniques in analyzing cores at the lab in order to get reliable measurements. Monicard[16] suggested using the "fluids summation" method for determining petrophysical properties from whole core and sidewall core samples from unconsolidated samples. This method works excellent when handling fresh core samples. For the determination of saturations, the "Retort method of fluid summation" is suggested. In Monicard's book this method is recognized as of high degree of precision but not ranges of precision were given. According to our records the cores obtained from the Jacob wells were analyzed using the methodology outlined above.

The use of core porosities in reserve calculation should be tempered by considering the size of the core in relation to the size of the reservoir. In addition, a core

plug is very small, and core plug porosities may be higher or lower than whole core porosities if the core has some heterogeneity.

We had access to 25 core and 4 sidewall-core analysis data. In all the wells cored, the interval of interest was that of the pay zone. The main data reported was porosity, vertical and horizontal permeability, oil and water saturation. Some of the cores had a fair to poor description somehow useless to the development of geologic facies.

Table 4-1 summarizes the mean values of core data for each of the wells having core data. For the core analyses, porosity, permeability (horizontal and vertical), water and oil saturation were determined. For the sidewall core analyses, porosity, permeability (horizontal), water and oil saturation were determined.

For this section I used the porosity and permeability data only. The oil and water saturation data is left for a later section in which an analysis of the fluids distribution from core data and water cut is performed.

4.2.1 Vertical anisotropy

The simplest way to analyze sample data is by doing basic statistics. The histogram plot helps to determine the type of distribution that the data follows, if any.
I have investigated the heterogeneity behavior of the cored wells in the Jacob field. By plotting the distribution of porosity and permeability (horizontal and vertical) we can say that there is no unique behavior, as it is shown in **Figs. 4-1 through 4-5**.

In terms of porosity (**Figs. 4-1** and **4-2**) only in few wells the porosity data tend to follow a normal distribution, like for example 51A, 118A, 122A, and 13W. Some wells did not have enough data to determine even a trend, such as 63A, 64A, and 11W.

TABLE 4-1 – CORE AND SIDEWALL-CORE DATA

CORE ANALYSIS

Well	Analysis Date	Interval cored (ft)	Horizontal Permeability (md)	Vertical Permeability (md)	Porosity (%)	Oil Saturation (%)	Water Saturation (%)
2-A	05/03/1948	962.7 - 969.2	1365	1110	41	38	35
49-A	01/14/1948	1028.0 - 1032.5	248		42	7	74
50-A	02/17/1948	992.5 - 1002.5	1795	1566	41	35	41
51-A	03/12/1948	991.5 - 1000.4	1894	2218	40	27	50
52-A	04/26/1948	957.0 - 966.7	2090	1930	43	35	39
53-A	05/15/1948	961.2 - 965.2	2197	1772	38	36	40
54-A	08/30/1948	967.5 - 970.5	3085		37	46	41
55-A	09/08/1948	957.5 - 983.5	441		39	24	55
63-A	06/20/1960		2092	1562	40	38	60
64-A	07/06/1962	982.5 - 986.5	4456	3273	36	24	69
118-A	10/16/1990	929.5 - 955.5	82		25	19	59
4-W	01/22/1957	873.0 - 885.5	439		32	31	53
10-W	01/22/1957	882.5 - 897.5	988		36	21	65
11-W	02/06/1957	895.5 - 902	1768		40	15	79
12-W	12/20/1958	906.5 - 915.5	363		35	11	74
13-W	08/16/1959	704.5 - 891.5	1507		35	22	61
19-W	01/09/1962	881.5 - 891.5	1389	1083	38	25	59
21-W	03/16/1962	913.5 - 919.0	648	315	35	16	74
22-W	01/31/1962	886.5 - 896	1059	684	38	23	73
25-W	02/28/1963	844.0 - 848	1489	535	36	6	71
33-B	04/19/1957	995.5 - 1007.5	2289	1266	40	6	87
34-B	04/30/1957	1011.5 - 1032.5	727	438	39	6	83
30-B	01/29/1957	993 - 1001.75	697		30	22	68
31-B	02/07/1957	984.2 - 994.7	964	581	40	15	70
3-C	02/22/1962	810	2635	818	37	8	52

SIDEWALL CORE ANALYSIS

Well	Analysis Date	Interval Cored (ft)	Permeability (md)		Porosity (%)	Oil Saturation (%)	Water Saturation (%)
121-A	10/17/02	867 - 889	110		26	18	60
122-A	9/5/02	927 - 952	63		28	15	62
117-A	1/18/90	883 - 896	228		27	21	46
119-A	7/8/97	931 - 942	80		24	15	54

What calls our attention is the high porosity values observed in some wells. Values as high as 48% were recorded in wells 50A and 52A. We might be suspicious of this data, since we know that the maximum porosity in a packing arrangement of perfect spheres is 47.6%. Since the core analyses were performed back in 1948 (see Table 4-1) the credibility of the method used in determining the porosity is arguable.

In terms of horizontal permeability (**Figs. 4-3** and **4-4**) because of the high variability of the data I have plotted the natural logarithm of the data. An excellent example of lognormal distribution is that of well 2A, which shows clearly a normal distribution of natural logarithm of permeability. Some other wells that tend to follow a normal distribution are 118A, 4W, and 10W. Again the same wells mentioned above did not have enough data to establish a pattern.

Only few wells had vertical permeability analysis (**Fig. 4-5**) Of those, wells 2A, and 52A show a tendency to a normal distribution. Wells 53A, 63A, 64A did not have enough data to establish anything about their behavior. Well 33B even having 9 data points shows a linear distribution.

A common indicator of heterogeneity is the vertical to horizontal permeability factor. In reservoir engineering this factor is usually assumed to be 0.1. It determines the preference of the fluids to flow whether in the horizontal or vertical direction. In the Jacob field, this factor is high (see **Fig. 4-6**). A minimum value of 0.327 was calculated for well 64A. It shows the preference of the fluids to flow in the horizontal direction rather than in the vertical direction. A maximum value of 0.992 was estimated in well 63A. It shows that this area could be of danger to water encroachment because of the same preference of the fluids to flow in the vertical or horizontal direction.

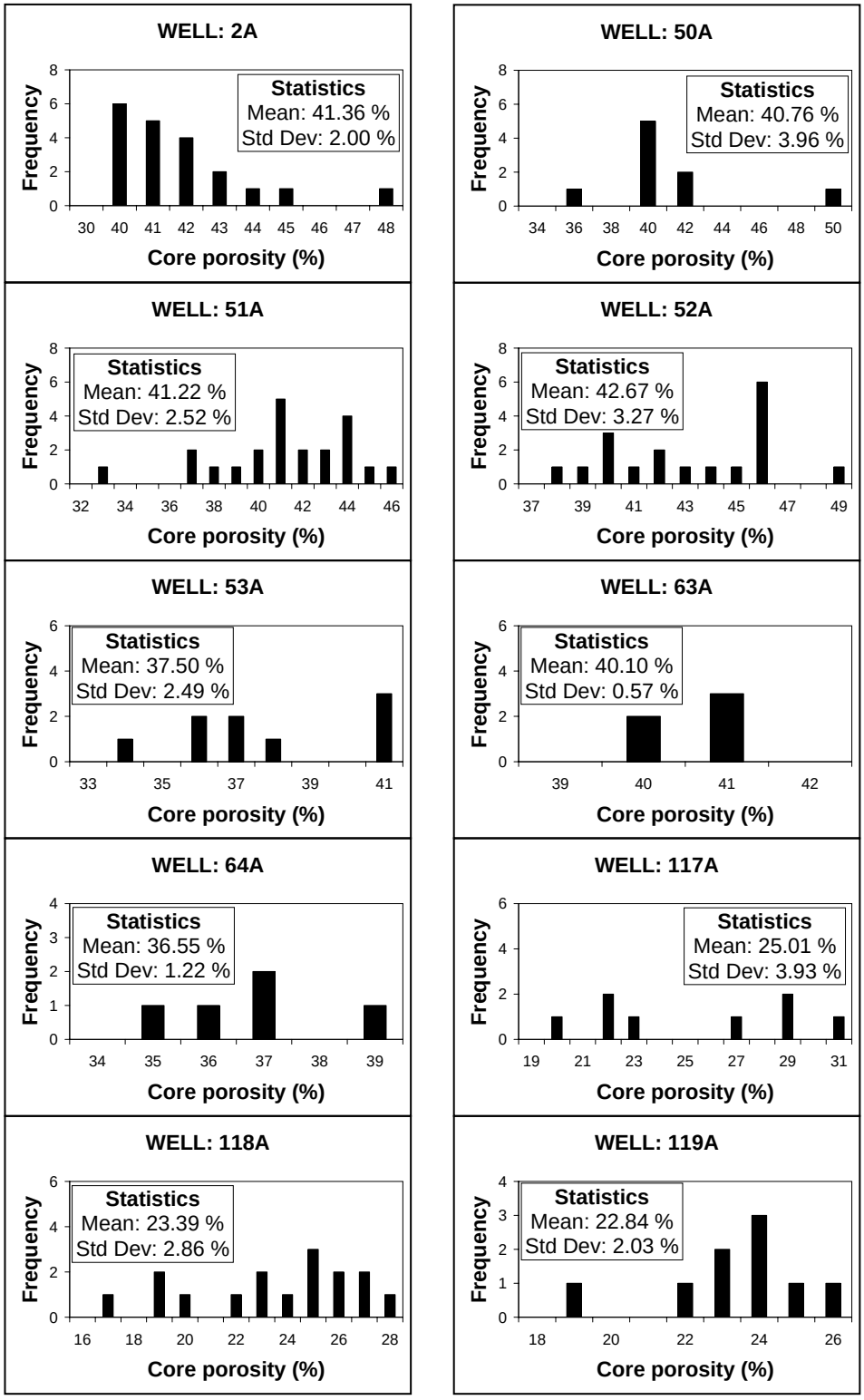

Fig. 4-1 – Histogram plots of core porosity (1st part).

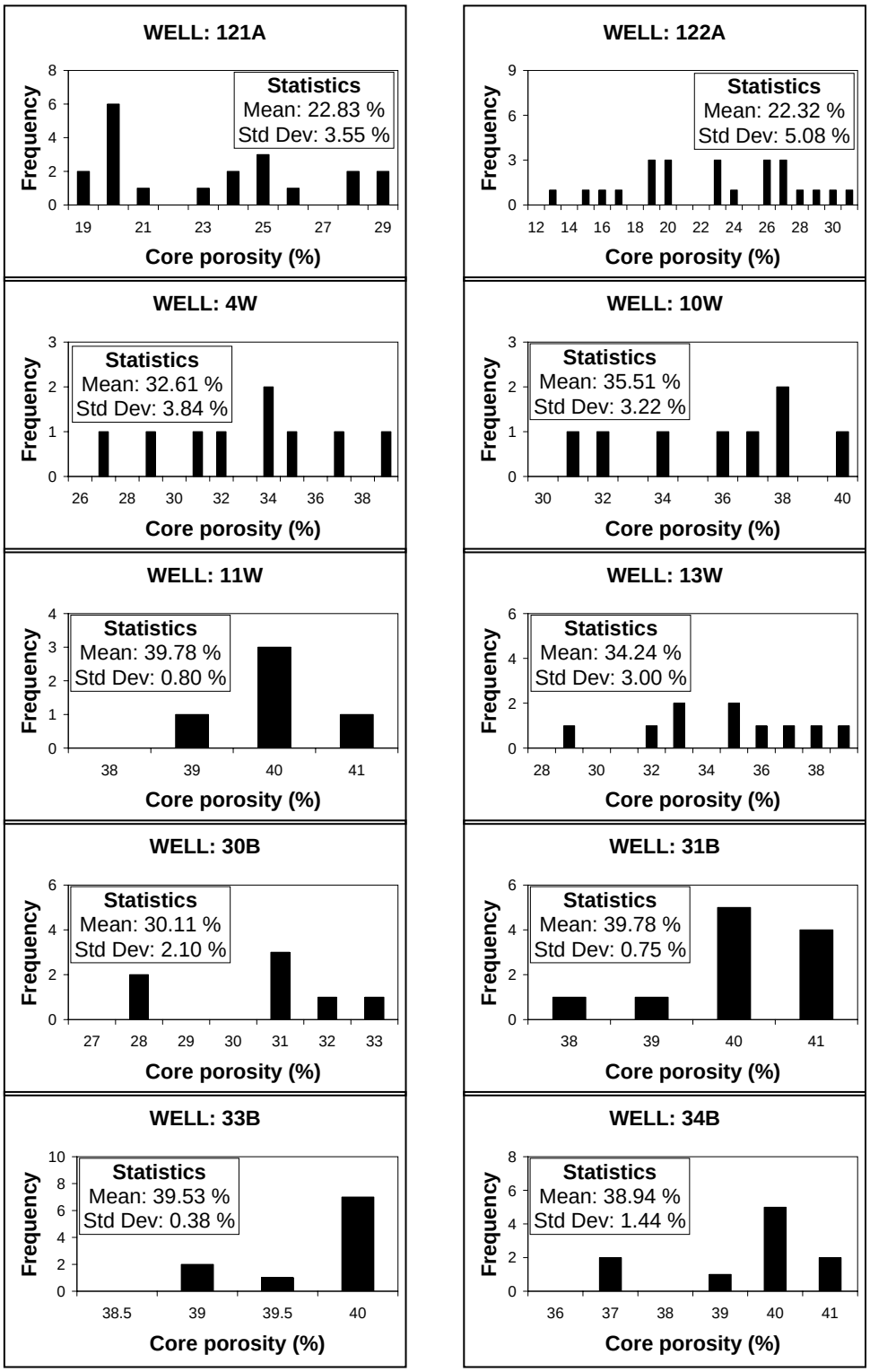

Fig. 4-2 – Histogram plots of core porosity (2nd part).

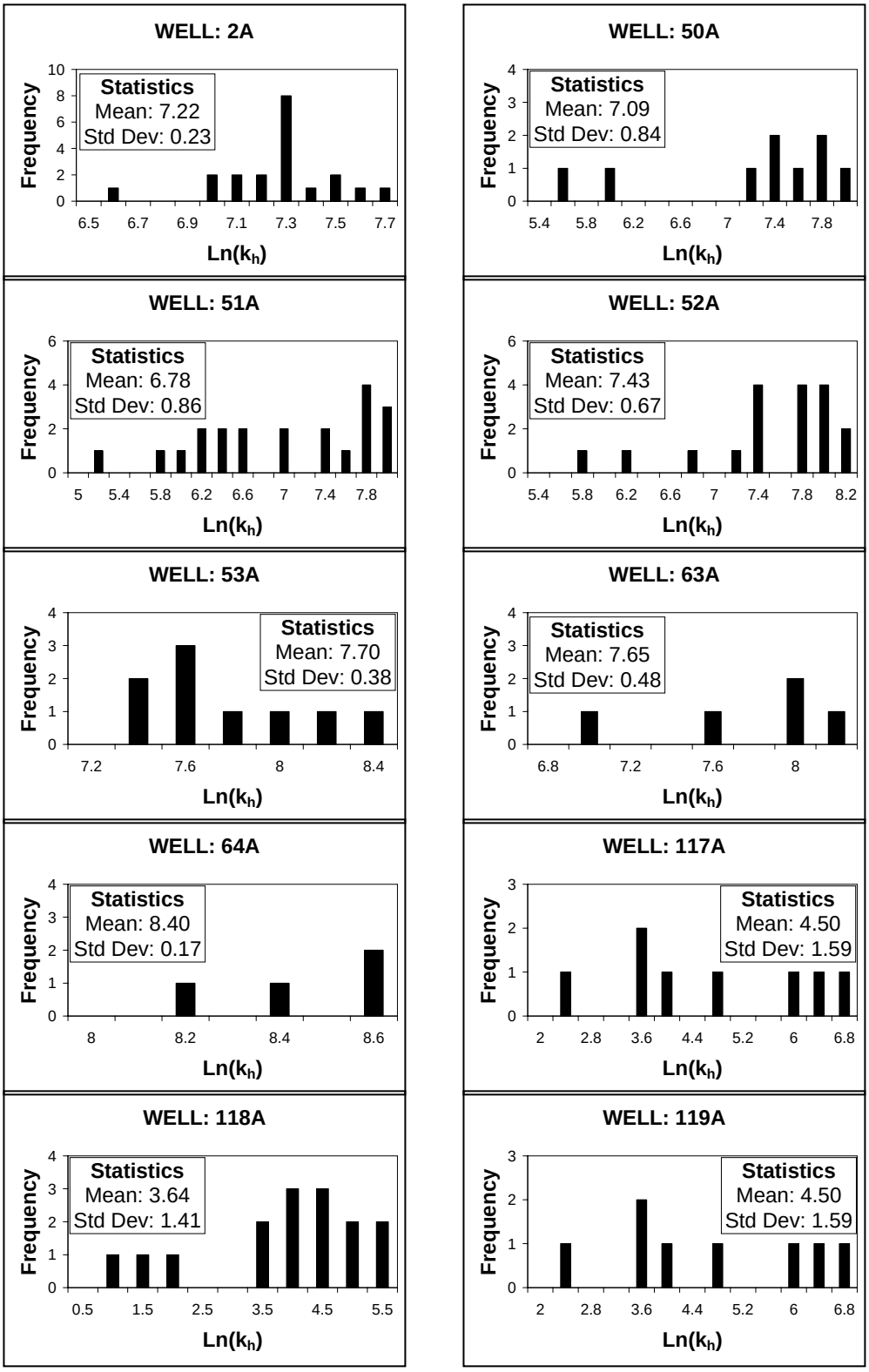

Fig. 4-3 – Histogram plots of horizontal permeability (1st part).

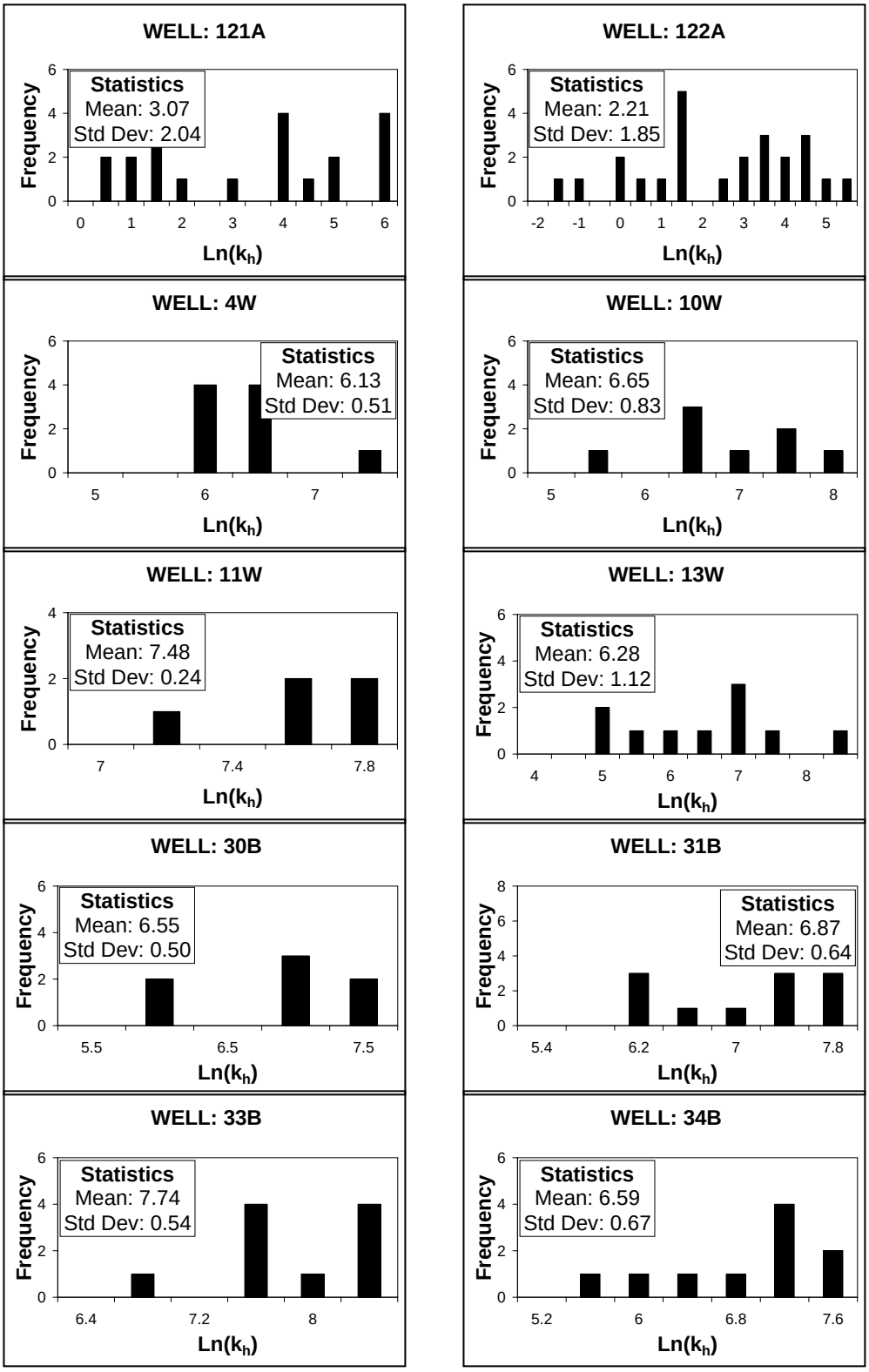

Fig. 4-4 – Histogram plots of horizontal permeability (2nd part).

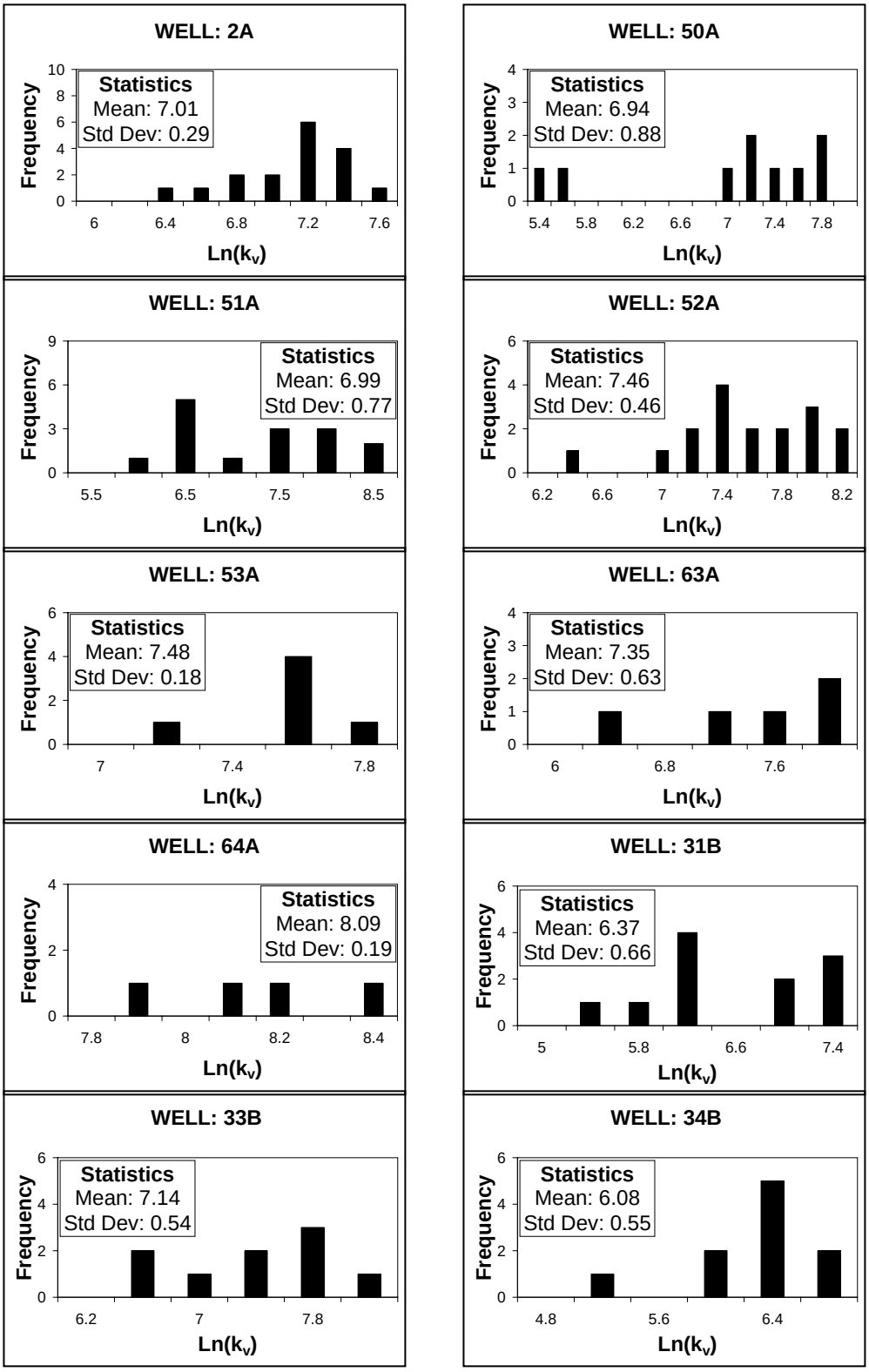

Fig. 4-5 – Histogram plots of vertical permeability.

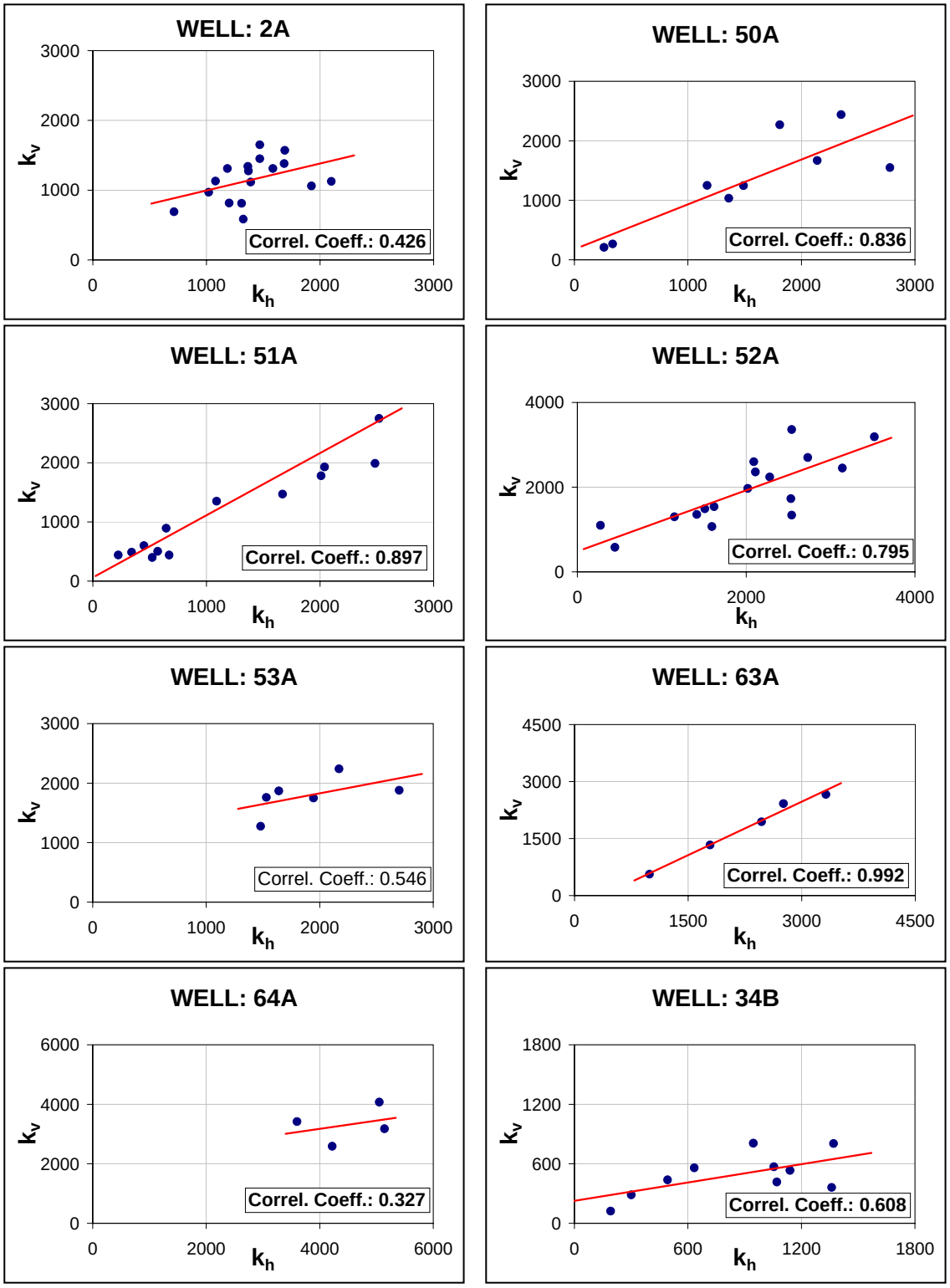

Fig. 4-6 – Vertical to horizontal permeability correlation.

Permeability to porosity optimal correlation

Very often in reservoir engineering we are interested in the simultaneous behavior of two random variables. More importantly, we want to know the pattern of dependence relating one variable to another. Knowledge of this pattern of dependence will be critical if we are interested in predicting the spatial behavior of one variable (permeability) from the known behavior of another variable (porosity).

The bivariate (two variables) equivalent of a histogram is called a scattergram. In a scattergram, each data pair is plotted as a point. To investigate the relationship of the data plotted, a "best fit" line is established and the goodness of fit is indicated by the correlation coefficient between the two variables.

In **Figs. 4-7 through 4-9** it is shown the optimal correlations of the scattergrams of permeability (horizontal) versus porosity for the area of study.

The simplest type of this kind of relationship is a linear one (k_h vs ϕ). However, in using a linear relationship, the correlation coefficient was not optimal for any of the wells (**Table 4-2**).

Literature[14] suggests plotting the natural logarithm of permeability versus porosity ($Ln(k_h)$ vs ϕ). In doing so 5 wells reached a very good correlation coefficient (117A, 118A, 119A, 121A and 122A).

Sometimes neither method reaches an acceptable correlation coefficient. Geostatistical methods suggest transforming the data into normally distributed. This is achieved by transforming the data into a new set of data with zero mean and variance of "1". Only in two wells we got the maximum correlation coefficient in comparison to the other methods used. These wells were 64A and 33B. In the plots corresponding to wells 64A and 33B (Figs. 4-7 and 4-9) the x-axis correspond to the normal score transform of porosity (NST(ϕ)) and the y-axis to the normal score transform of permeability (NST(k)). The normal score transform (NST) is the transformation of the data into a new variable with zero mean and variance of "1".

The previous methods explained are known as parametric regression. In a parametric regression, a priori assumption of the relationship between the two variables

is imposed. The counterpart of the parametric regression is the non-parametric regression. In a nonparametric approach no previous model is imposed and the best correlation coefficient is expected.

TABLE 4-2 – OPTIMAL CORRELATION FOR PERMEABILITY-POROSITY

Well	k_h vs ϕ	Ln(k_h) vs ϕ	NST(k_h) vs NST(ϕ)	Tr(k_h) vs Tr(ϕ)
2A	-0.019	-0.021	0.014	**0.348**
50A	0.278	0.242	0.068	**0.684**
51A	-0.600	-0.578	-0.589	**0.820**
52A	-0.110	-0.028	-0.185	**0.750**
53A	0.527	0.492	0.548	**0.573**
63A	0.288	0.254	0.223	**0.311**
64A	-0.009	-0.026	**0.151**	0.009
117A	0.906	**0.982**	--	--
118A	0.885	**0.958**	--	--
119A	0.892	**0.988**	--	--
121A	0.871	**0.975**	--	--
122A	0.806	**0.959**	--	--
30B	-0.552	-0.517	-0.546	**0.639**
31B	-0.230	-0.284	-0.451	**0.877**
33B	0.249	0.233	**0.453**	0.371
34B	0.250	0.241	0.341	**0.585**
4W	0.432	0.414	0.345	**0.561**
10W	0.688	0.777	0.765	**0.839**
11W	0.221	0.209	0.340	**0.416**
13W	0.174	-0.028	0.070	**0.263**

I used the approach given by Xue et al.[17] to get the optimal correlation for our core data. In Table 4-2 the nonparametric approach is represented by the relationship of Tr(kh) vs Tr(f). “Tr” meaning transformed data. In the scattergrams of Figs. 4-7 to 4-9 the same symbology was used. Note that for 14 out of 20 wells analyzed, this methodology gave the highest correlation coefficient (Table 4-2).

Table 4-2 summarizes the correlation coefficients obtained using all of the approaches mentioned above and the maximum correlation coefficients obtained are highlighted.

It is interesting to outline the high correlation coefficients obtained in wells 117A, 118A, 119A, 121A and 122A. Even a linear regression gives high values. We recall that these wells are close neighbors. Having this degree of correlation means that there is a strong relationship between permeability and porosity in this area. As we analyzed in the log analysis section the log derived effective porosity and the core porosity matched very well. Therefore for future wells to be drilled in areas surrounding the mentioned wells it would not be necessary to core and the relationships developed could be used with a high degree of confidence.

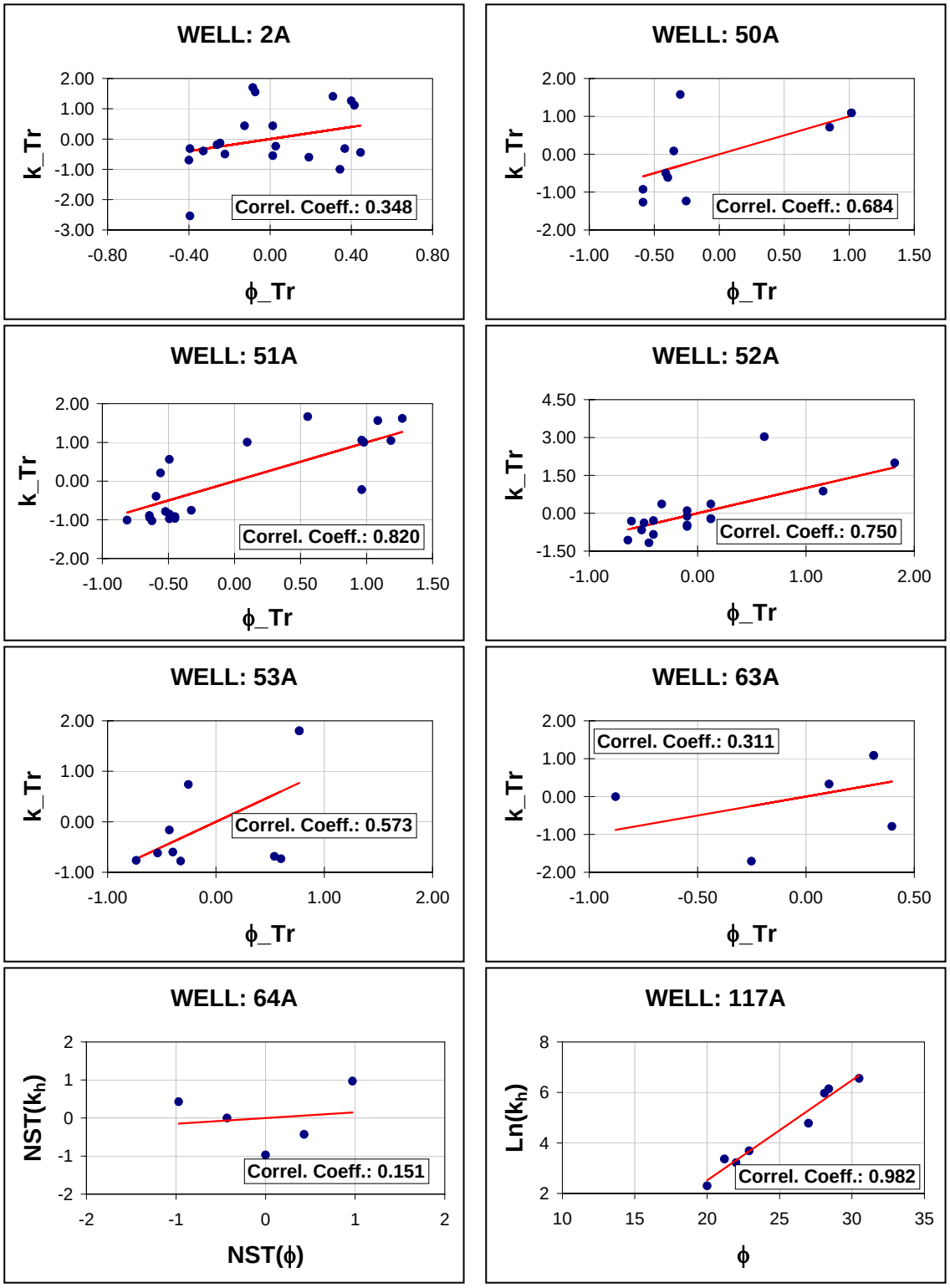

Fig. 4-7 – Horizontal permeability to porosity optimal correlation (1st part).

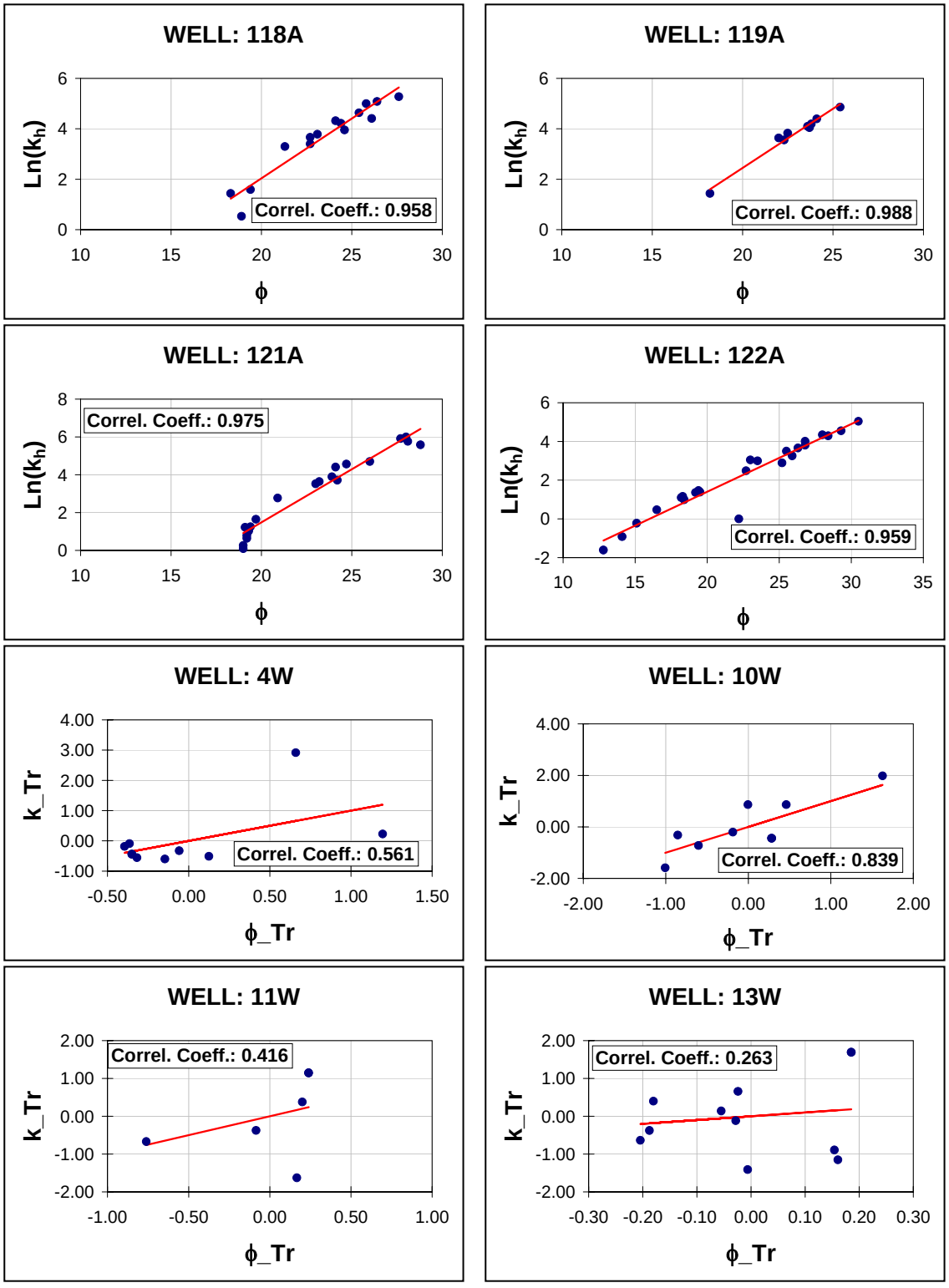

Fig. 4-8 – Horizontal permeability to porosity optimal correlation (2nd part).

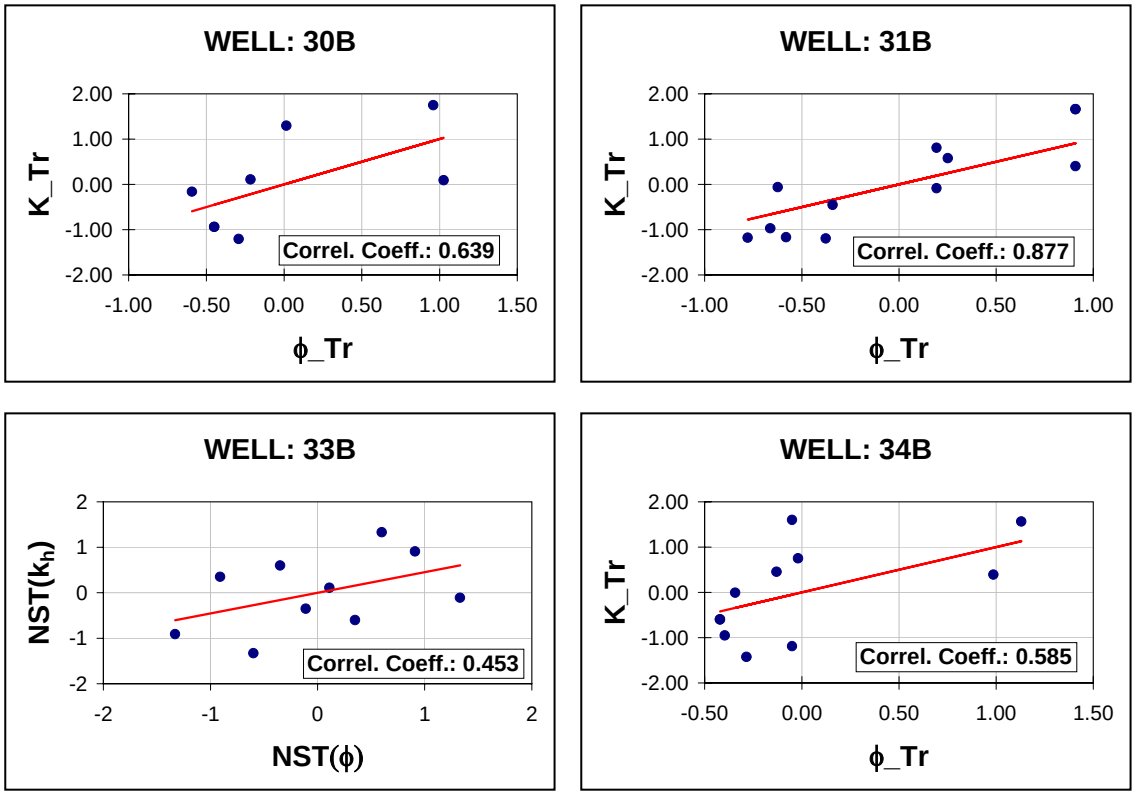

Fig. 4-9 – Horizontal permeability to porosity optimal correlation (3rd part).

4.2.2 Areal anisotropy

Reservoir heterogeneity is defined as a variation in reservoir properties as a function of space. Ideally, if reservoirs were homogeneous, measuring a reservoir property at any location would allow a full description of the reservoir. However as we noticed in the previous analysis there is a lot of difference in values of porosity, for example, in the Jacob field. For a proper reservoir description, the variation in porosity and permeability as a function of spatial location is studied.

In this sense, the variogram is the most widely used tool to investigate and model spatial variability of petrophysical properties. Furthermore, the variogram reflects our understanding of the geometry and continuity of reservoir properties.

As is defined by Gringarten and Deutsch[18] the variogram is a measure of variability; it increases as samples become more dissimilar.

$$2\gamma(h) = E\left\{[Y(u) - Y(u+h)]^2\right\} \quad \text{..... (4.1)}$$

Where,

$2\gamma(h)$: Variogram

$Y(u)$: Random variable

h : Distance

E : Expectation

In pure mathematical rigor, the variogram is the expected squared difference between two data values separated by a distance vector h, as defined by **Eq. 4.1**.

Variogram modeling for core porosity

Fig. 4-10 shows the variogram plots for porosity in different directions. The intention of plotting the data in different directions is to establish the direction towards which the data tend to be more correlated. By “data correlated” we mean that the data follow a certain trend. For example the data points (Fig. 4-10) tend to follow an exponential behavior in the 120º direction. However, in the other directions the relationship of the data is lost very close to the axis origin.

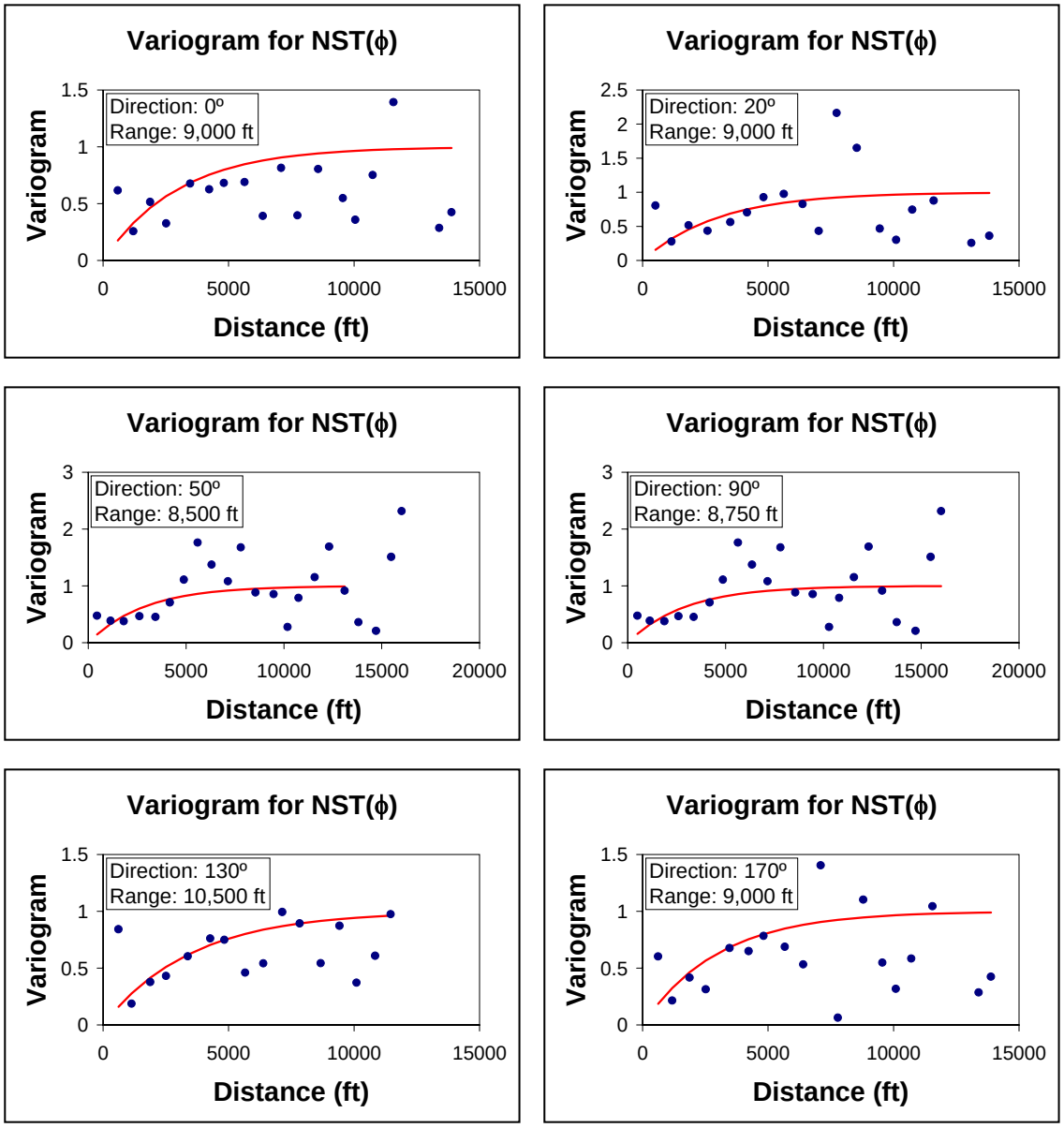

Fig. 4-10 – Variogram analysis for porosity data.

The data points in the plots shown in Fig. 4.10 are called experimental variograms. For modeling purposes the data is fitted to certain known models (continues lines in plots). In this case I have fitted the data with an "exponential model" since the data tend to follow that kind of behavior.

As it was observed in Fig. 4-10 the porosity data show different ranges of correlation depending upon which direction is chosen. However, all the variogram models reach the same "sill" (1.0). This type of behavior is called geometric anisotropy[14]. When we plot the different ranges modeled with respect to the direction of the variogram, we obtain the "Ellipse of anisotropy[14]." **Fig. 4-11** shows the Ellipse of anisotropy in which we can observe the direction towards which the data tend to be more correlated (major range highlighted with the green line) and the direction towards which the data tend to be less correlated (minor range highlighted with the blue line).

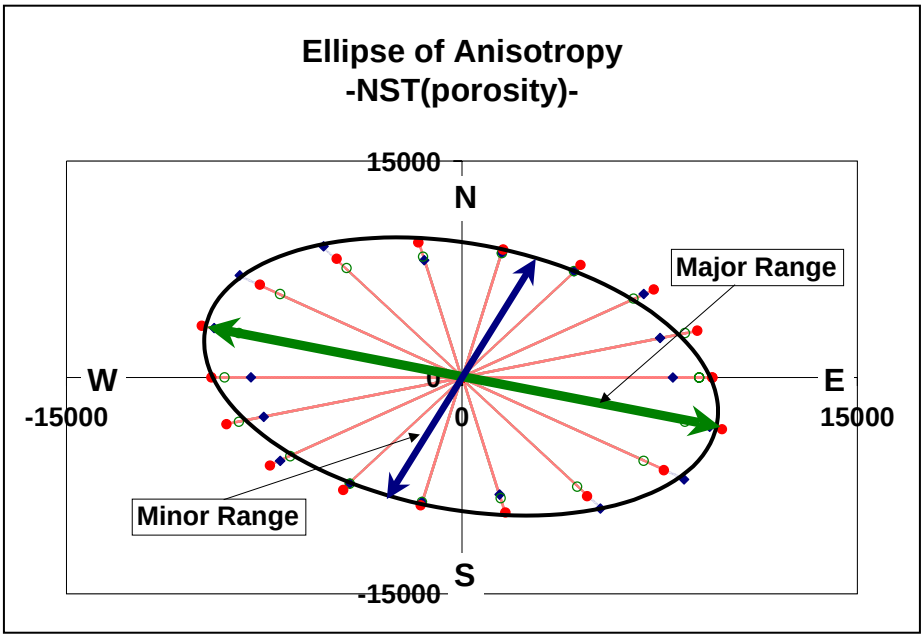

- Anisotropy
  - Major angle: N70ºW
  - Minor angle: N20ºE
  - Major Range: 10500 ft
  - Minor Range: 8800 ft
  - Variogram Model:
    - Exponential

Fig. 4-11 – Ellipse of anisotropy for core porosity data.

Therefore, from this analysis we can say that the direction of more homogeneity is N70ºW and the direction of more heterogeneity is N20ºE.

Variogram modeling for core permeability

The same procedure as explained above was used in the variogram modeling for the permeability data.

The variograms obtained for horizontal permeability data show a slightly different behavior from those of the porosity. From the variograms shown in **Fig. 4-12** the one obtained at the direction of 150º shows a better correlation than the other variograms calculated at 0º, 40º, 90º, 130º, and 170º. In this case a spherical model was used to fit the experimental variograms.

The Ellipse of anisotropy (**Fig. 4-13**) shows that the major range is pointing towards N50ºW direction and the minor range is pointing towards N40ºE. It means that the data is more correlated in the direction of the major range and less correlated in the direction of the minor range.

Comparing the two ellipses of anisotropy (porosity and permeability) we notice that the ranges are bigger for the case of porosity relative to the case of permeability. Since the permeability is directly related to the flow of fluids, therefore it better represent the anisotropy of the reservoir.

Even though in this analysis both ellipses of anisotropy showed the same direction of homogeneity (direction of major range) it would not necessary be like that. In our case happened both ellipses happened to follow the same direction mainly due to the high relationship existing between porosity and permeability as demonstrated in the preceding section.

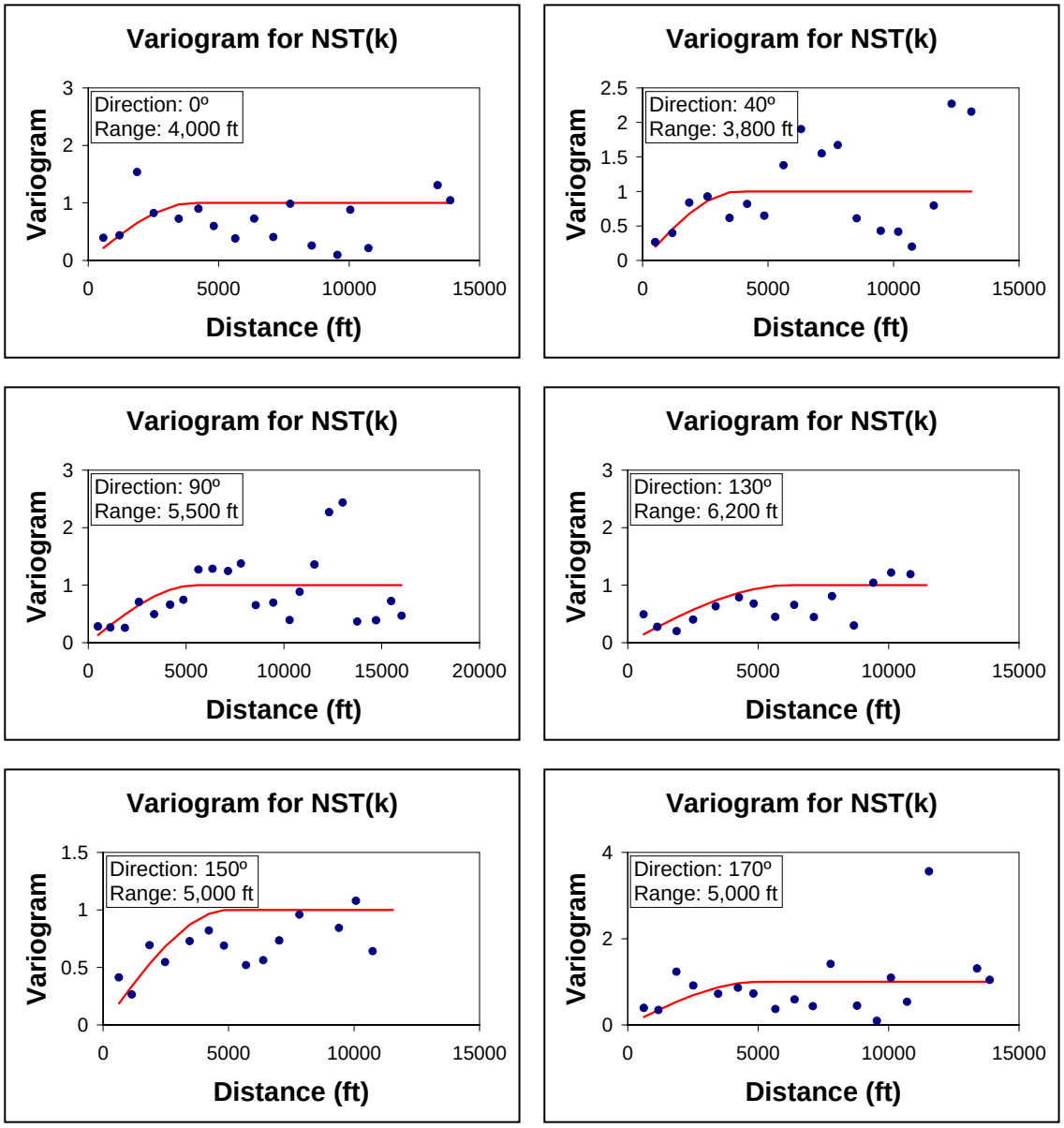

Fig. 4-12 – Variogram analysis for horizontal permeability.

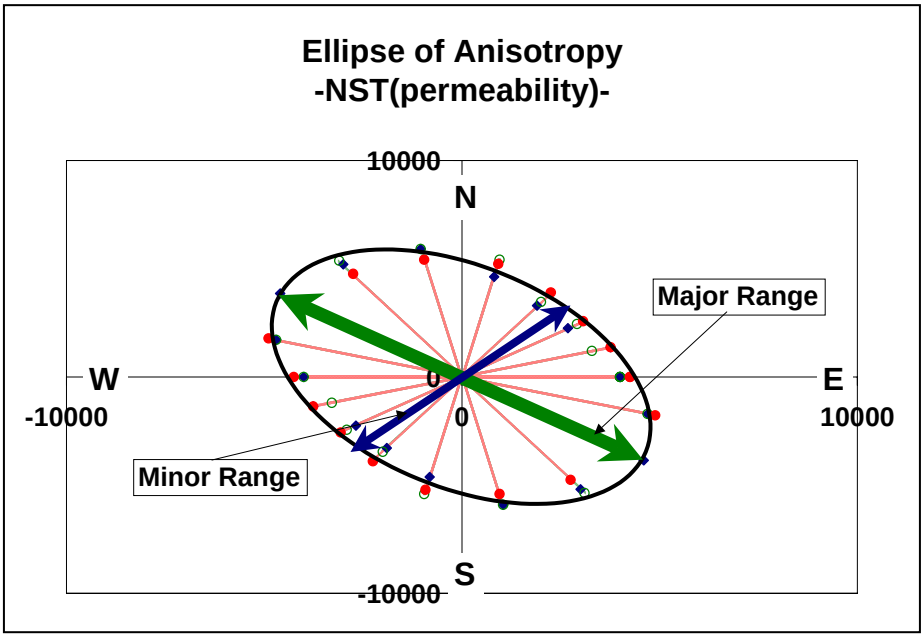

- Anisotropy
  - –Major angle: N50ºW
  - –Minor angle: N40ºE
  - –Major Range: 6000 ft
  - –Minor Range: 3800 ft
  - –Variogram Model:
    - Spherical

Fig. 4-13 – Ellipse of anisotropy for horizontal permeability.

4.2.3 Generation of contour maps

The variogram modeling is used in the kriging procedure to generate contour maps. The kriging technique is a geostatistical tool that uses a linear estimation procedure to estimate a value at unsampled locations. In principle, the technique assumes that the value at the unsampled location is estimated by[14]:

$$z^* = \sum_{i=1}^{n} \lambda_i z_i \quad \text{..... (4.2)}$$

Where,

z^*: the estimated value

z_i: the value at a known location

λ_i: kriging weights.

In simple words, the estimated value is a weighted average of the neighboring values. The goal in the estimation procedure, is to calculate the weights assigned to the individual neighboring points. These weights depend on the spatial relationship between the unsampled location and the neighboring values, as well as the relationship among the neighboring values. These relationships are obtained from the modeling of the variogram.

In this study I have built the contour maps for core data: porosity and horizontal permeability. Also the contour maps for pay thickness were included.

I have used the variogram models of the previous section: exponential for porosity and spherical for permeability. In building the contour map for thickness I have used both variogram models in order to show the difference that might be encountered in using either model.

An alternative methodology to the kriging technique is the Inverse Distance method. In this method no variogram is used. The purpose of making these maps was to demonstrate the importance of using the variogram modeling.

Fig. 4-14 shows the contour maps for core porosity using the inverse distance method and the Kriging technique. Observe that the main difference in both maps is the smoothness of the contours. The zones of low porosities are the yellow areas and the

zones of high porosity values are those corresponding to the green color. As it is observed in Fig. 4-14 the green areas are the predominant ones. It means that the pay zone has mostly high porosity values.

Fig. 4-15 shows the contour maps built for permeability using the same techniques as in the porosity case. The type of variogram used in generating the Kriging surfaces was the spherical model. The use of the spherical model for modeling permeability is usually suggested because it reflects the anisotropy of the reservoir better.

In the permeability case, the difference between the estimation of the contours is more significant than in the porosity case. This is because of the difference in the distribution of the data: the porosity distribution is more normally distributed whereas the permeability follows a log-normal distribution and the presence of high permeability channels and low permeability barriers can be better modeled.

In the permeability contour maps we can observe the presence of a zone of very high permeability towards the east part of the reservoir. Another zone of very low permeability is present towards the south part of the reservoir.

Something that we need to clarify in this section is that we used the mean values of the actual data in order to show a pattern in an areal sense. However “averaging” the data might be dangerous since some clues of heterogeneity, especially in the vertical sense, might be lost. In section 4.4 we will talk about spatial patterns and the “average” method will be overcome.

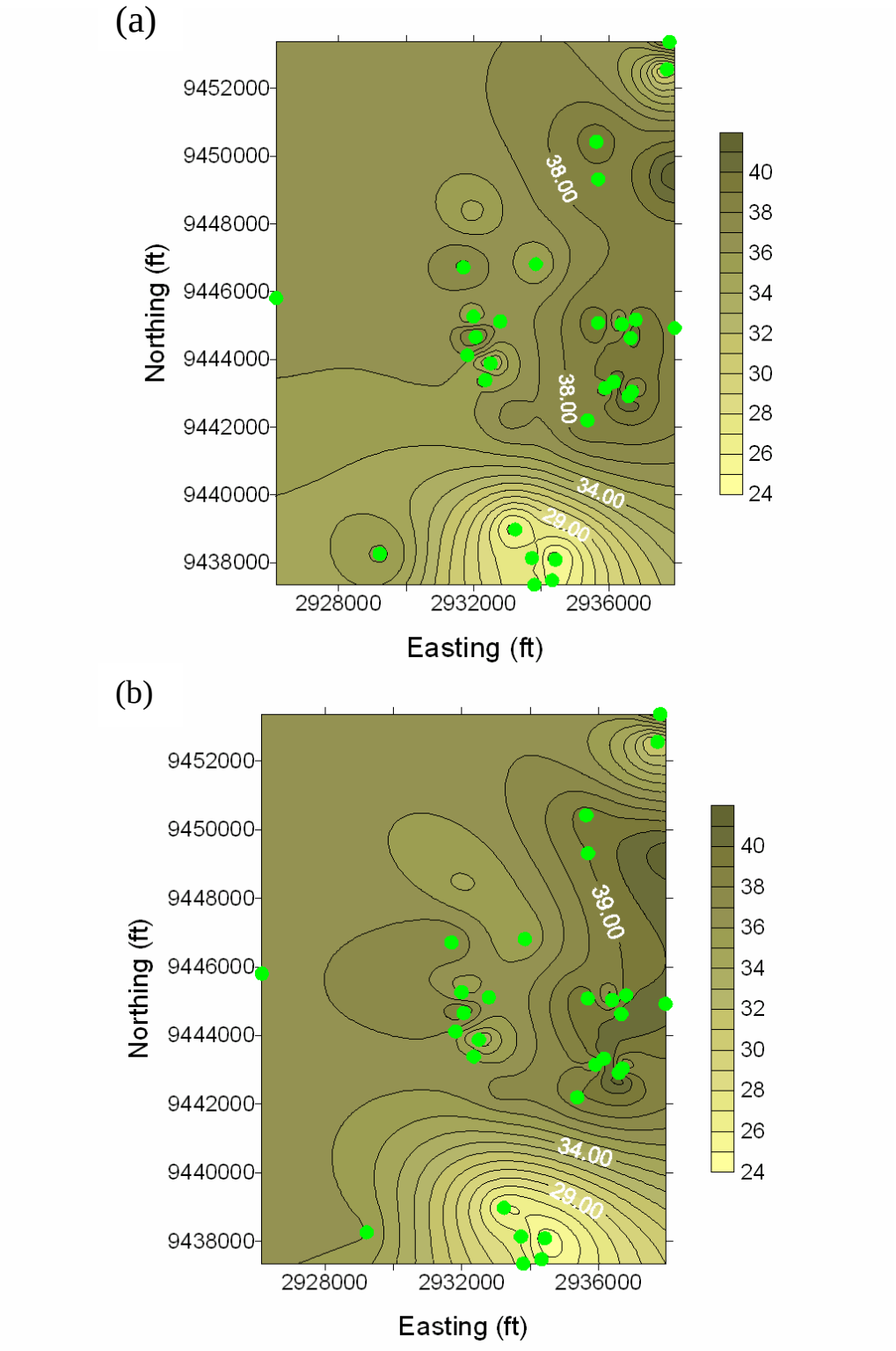

Fig. 4-14 – Porosity contour maps for Pettus formation generated using (a) inverse distance, (b) Kriging.

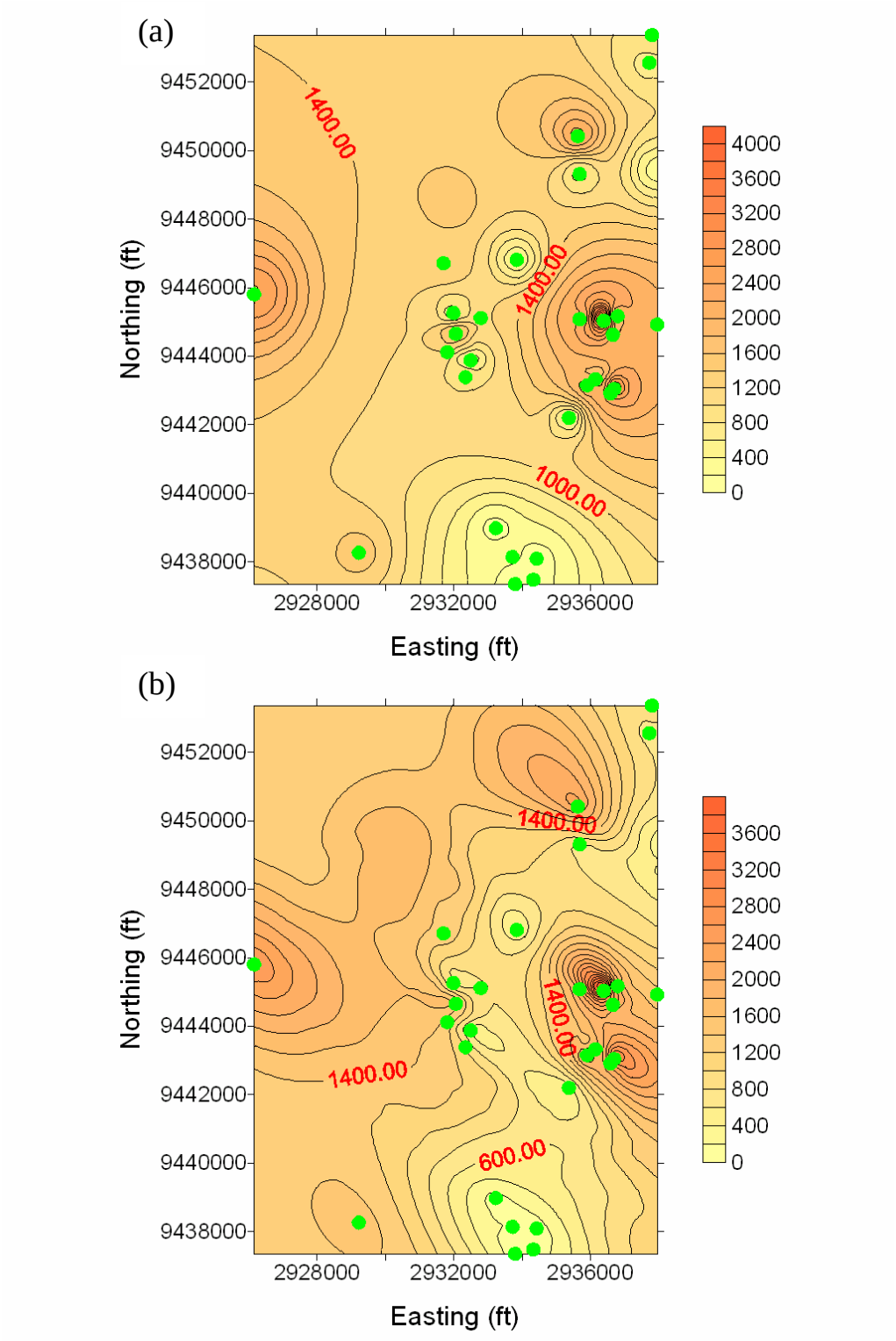

Fig. 4-15 – Permeability contour maps for Pettus formation generated using (a) inverse distance, (b) Kriging.

Isopach maps

Using the Kriging technique the contour maps for the gross and net thickness for the Pettus sand were developed.

First it was needed to integrate data from log analysis, core and cuttings drilling description.

In terms of total thickness (gross), the most reliable data was that derived from log analysis (13 wells). A little less reliable data was that from core analysis (not all the wells were cored the entire pay section). And the least reliable data was that obtained from the cuttings drilling description, due to the lack of precise description. All data used accounted for 77 wells with gross thickness data to build the contour map showed in **Fig. 4-16**. The average value of gross thickness was estimated to be 20 ft with a range of variance from 7 to 30 ft. The variogram model used for the gross thickness contour map was the exponential one. When doing the variogram analysis we found that the data was more correlated towards the northwest direction. This behavior can be appreciated in Fig. 4-16.

Previous to building a net thickness map, first it was necessary to define a criterion to define the pay interval.

For the case of those wells having only core data, the samples showed oil production for water saturations less than 60% in average. So that value was used as a threshold to define a pay thickness.

For the case of wells having both core data and log analysis (4 wells) the first criteria was the shale content. By comparing the core data and log analysis results we realized that a water saturation of less than 55% in the log matched with oil shows in the cores. And as a consequence of that the shale content corresponding to this values of water saturation was below 30%. Therefore 55% for water saturation and 30% for shale content were the cutoffs in this case.

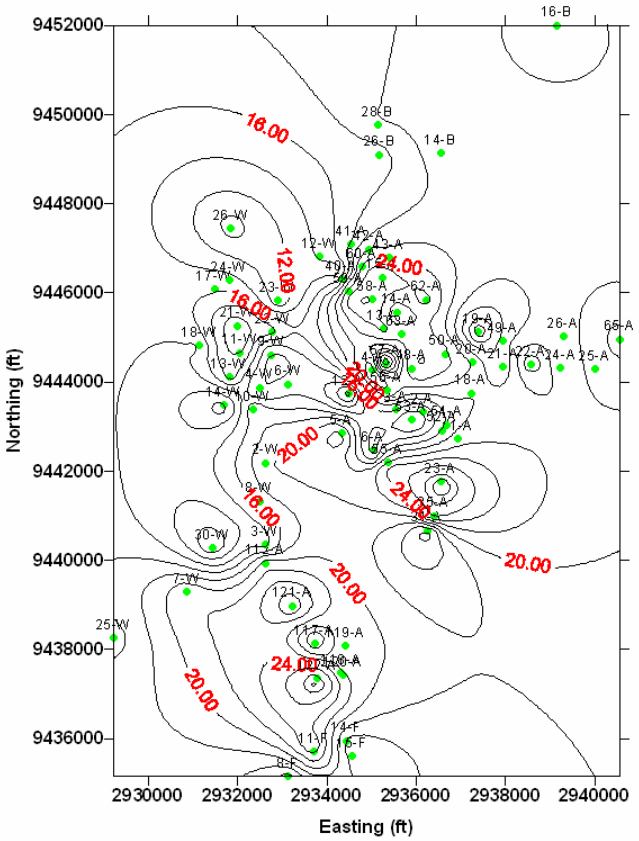

Fig. 4-16 – Isopach map of gross thickness for Pettus sand.

For wells having only well logs we used the shale content as cutoff. That criterion worked very well. For example, for the wells 65A, 1C, and 25W the V-shale values in the Pettus sand were calculated to be higher to 60% or 70%. And the production test for this wells resulted in water wet or few shows of oil.

Fig. 4-17 shows the contour map for the net thickness for Pettus sand. The average value was estimated to be 5 ft, having a maximum value of 15 ft. There are areas of zero pay thickness. Those areas corresponded to wells being water wet. For the areas of 1 ft of pay thickness correspond to wells having only few oil shows. Actually, when determining the pay thickness values we realized that values higher than 3 ft were enough to have an oil production of at least 5 BOPD as initial production.

In Fig. 4-17 we can observe that the thickest part of the reservoir is concentrated in the east central part of the field (darkest area).

For those areas that are outside to the area of interpolation (e.g. the area in the northwest vertex of the map) the data is meaningless because it is a simple extrapolation of the data trend. So do not put too much attention on those areas.

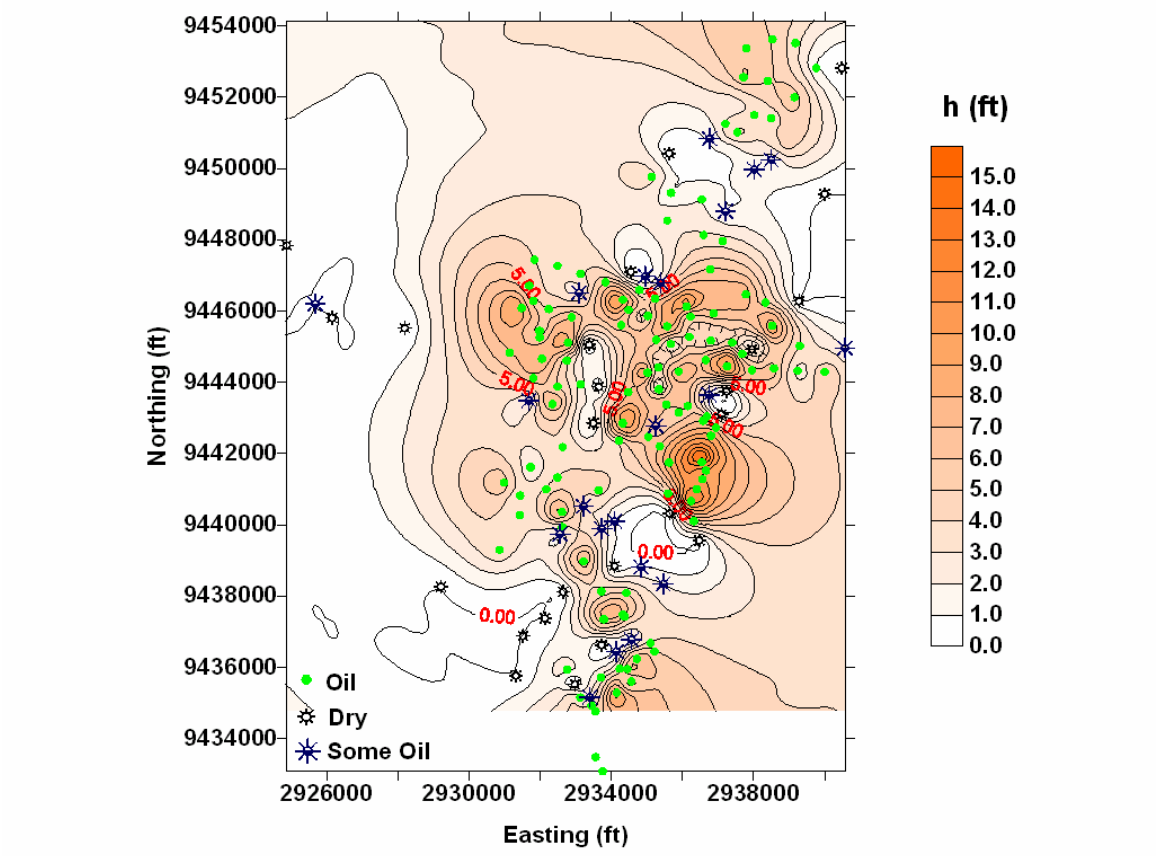

Fig. 4-17 – Isopach map of net thickness for Pettus sand.

4.3 Building a geological 3D model

Up to the last section we have talked of 2D modeling. The cross sections were developed only in two directions in the vertical direction and the core data was analyzed in the vertical and the horizontal direction. Geostatistical methods allow us to build 3D models that help us to better understand the geological settings of the area of study.

In order to build a 3D model, two types of analyses were coupled: the shale content determined from log analysis and the variogram analysis explained in the previous section.

I used the thirteen "v-shale" logs derived from the petrophysical analysis section to build directional variograms in both directions, vertical and areal.

In both vertical and areal directions the variogram model that best fit the experimental variogram was the spherical one, so it is chosen for kriging purposes.
The vertical variogram (**Fig. 4-18**) shows that the range of correlation is 20 ft. It means that in a thickness higher than 20 ft the data looses correlation.

The areal variogram (**Fig. 4-19**) shows that the data is more correlated in the N20ºE direction. This result might confuse the interpretation of the anisotropy developed using core data. However, both interpretations reflect the degree of anisotropy of the reservoir and none of the interpretations is conclusive alone.

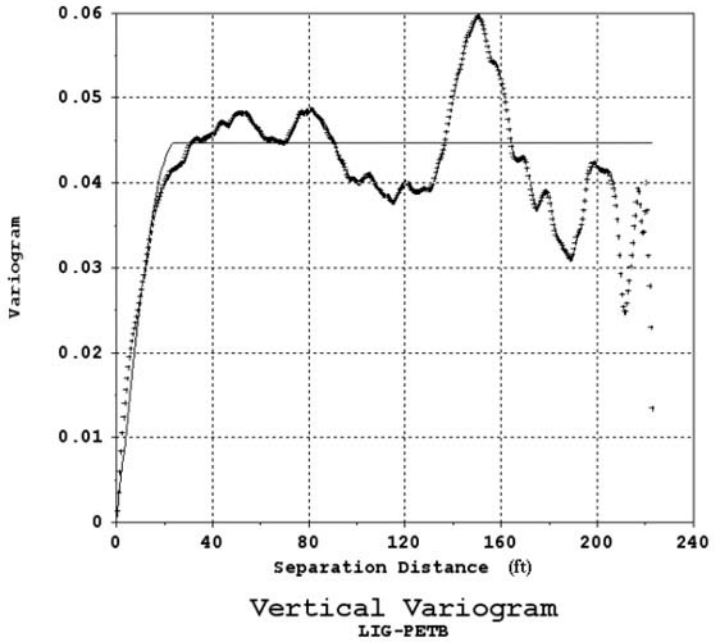

Fig. 4-18 – Vertical variogram for modelling with v-shale derived from log analysis.

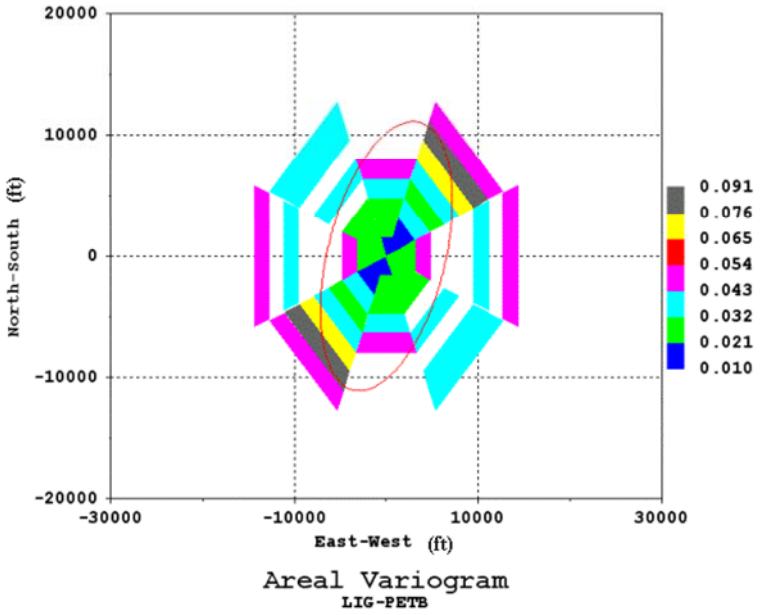

Fig. 4-19 – Areal variogram for modelling with v-shale derived from log analysis.

The 3D model is built on the basis of a grid system. For our model I have selected 18x18x113 grid blocks (18 grids in the north direction, 18 grids in the east direction and 113 grids in the vertical direction). In the vertical direction the model covered the same stratigraphic column used in the cross sections (from top Lignite to base Pettus).

In building a 3D model, the properties are averaged in the grid unit and the contour maps are built using the variogram model already mentioned above.

The 3D model built is shown in **Fig. 4-20**. The areal coverage of the model is 14,800 ft in the east direction and 8,800 ft in the north direction, making a total area of 3,000 acres. Even though this number is similar to the total acreage of the Jacob lease (3100 acres) it does not reflect the same area, since our model is not reflecting the area to the west of 1C and to the north of 48A and to the east of 65A. However, having a model that represents more than 50% of the surface area is of great advantage.

The model clearly shows the monocline structural shape of the formations, dipping from Northwest to East-South.

By making a horizontal cut to the areal distribution we can observe the shaliness distribution along the top and bottom of the Mirando sand (**Fig. 4-21**). The clean character of the Mirando sand is appreciated at the top. However; at the base the shaliness increases more in the Northwest direction. This makes us presume that the thicker part of the Mirando sand can be found in the East-South area of the field (light blue in the right map of Fig. 4-21).

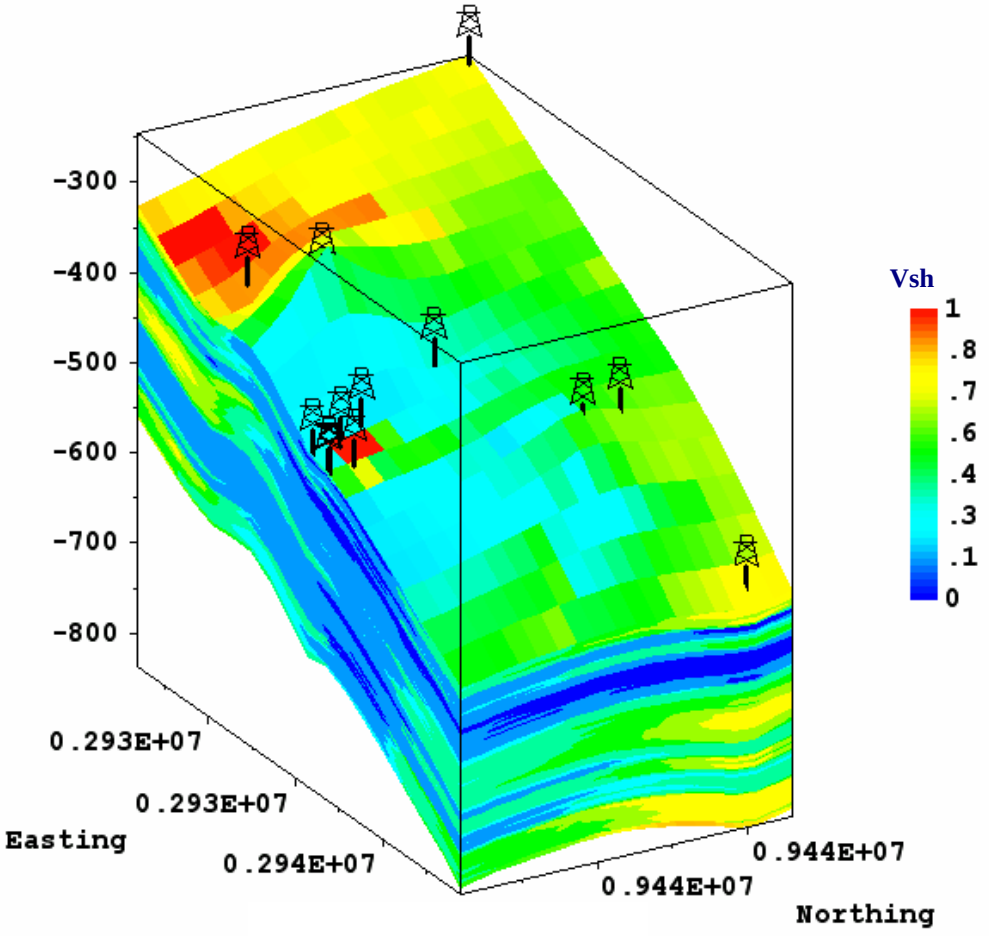

Fig. 4-20 – 3D model built using v-shale data derived from log analysis.

Also by making another cut to our model at the top and base of Pettus sand we can investigate the shaliness distribution of this formation (**Fig. 4-22**). It is observed that

there is not a trend of shaliness as observed in the Mirando sand. This behavior is because of the different environments of deposition. At the top of the Pettus, the shale content is high (30-60%). However, at the base of the Pettus (right map of Fig. 4-22), the formation becomes cleaner, having the cleanest area around wells 52A and 48A. Not having a unique pattern would mean that the type of deposition in the Pettus sand was more probably due to a lagoon as a part of a barrier system: the tidal and wave activity brought big sediments each time it entered to the lagoon but predominantly fine grains are encountered due to a low energy environment.

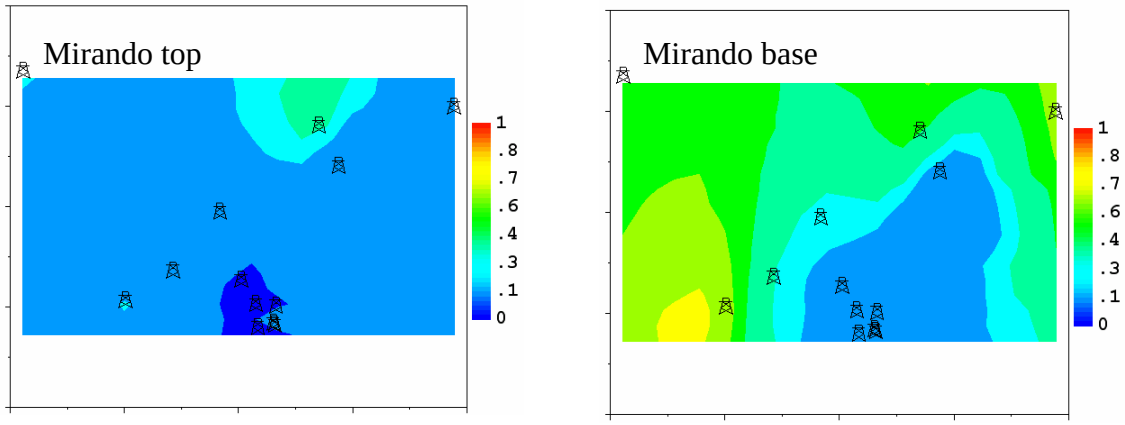

Fig. 4-21 – Areal distribution of shale content in the Mirando top and base.

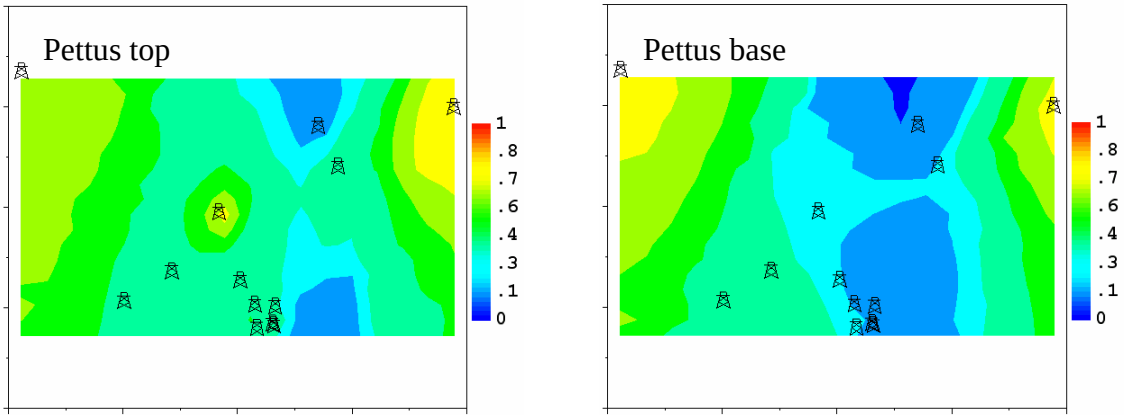

Fig. 4-22 – Areal distribution of shale content in the Pettus top and base.

I have also investigated the vertical distribution of shaliness in our 3D model. **Fig. 4-23** reflects the shale vertical distribution along the North-South direction. The blue areas show the cleaner intervals. The Mirando and Pettus sand is marked. The Mirando thickens towards the North direction. The Pettus shows a higher content of shale towards the west; however, it shows a relatively high degree of shaliness in both maps.

Fig. 4-24 shows the shale vertical distribution along the East west direction. Again towards the East-South direction the Mirando thickens and it gets thinners towards the Northeast direction. The Pettus sand does not show a clear trend of thickening to any direction. The clear conclusion of this analysis is that the Pettus sand shows a relatively high degree of shaliness.

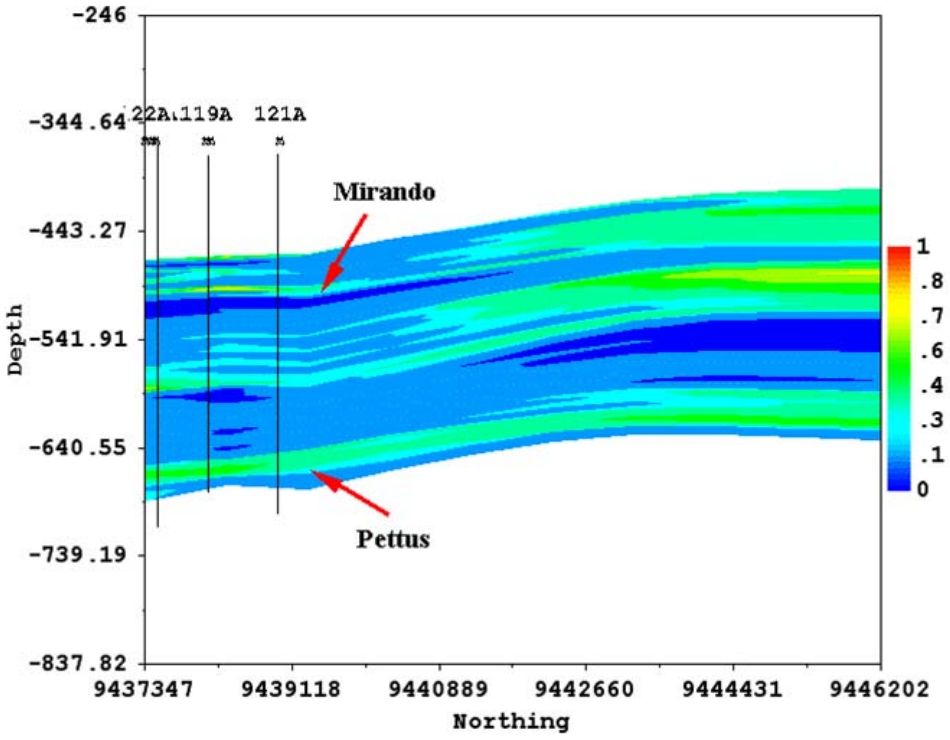

Fig. 4-23 – Structural section of the 3D model in the North-South direction.

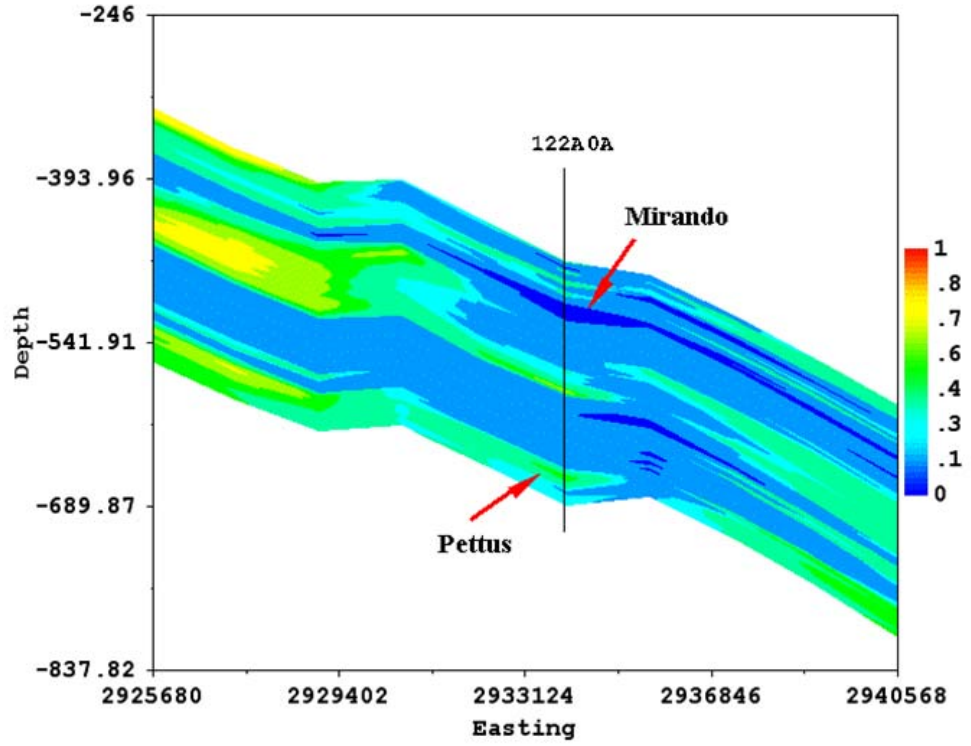

Fig. 4-24 – Structural section of the 3D model in the East-West direction.

In the cross section analysis of well logs it was built a “layer-cake” type of stratigraphy. That type of analysis sometimes does not reflect the real type of geological deposition, not being usually accepted by geologists.

In order to improve our reservoir description, I have selected the same cross sections in our 3D model and a better display of the distribution of the sand bodies is shown (**Figs. 4-25**, and **4-26**).

The cross section along the NW-SE direction (Fig. 4-25) shows the sand distribution along the dip angle.

The cross section along the NE-SW direction (Fig. 4-26) shows the geological body distribution along the strike.

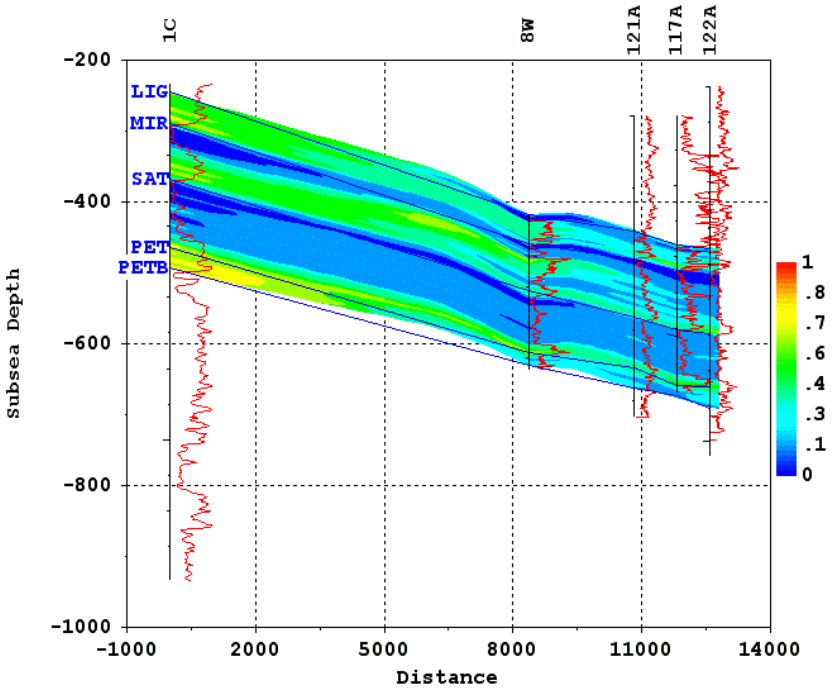

Fig. 4-25 – Structural cross section along NW-SE from 3D model.

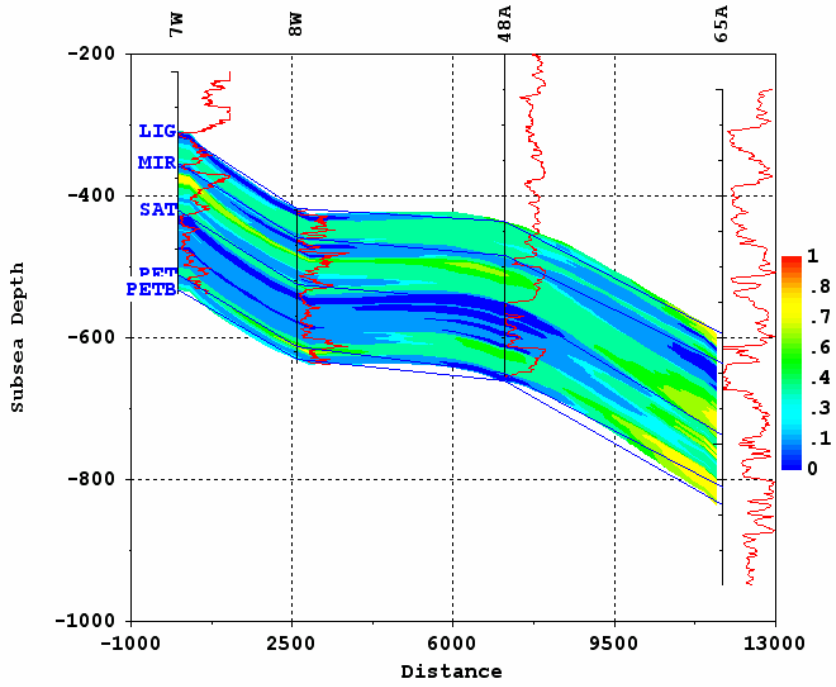

Fig. 4-26 – Structural cross section along NE-SW from 3D model.

4.4 Spatial patterns of porosity and permeability

Using the same approach described in section 4.3, we have integrated gross thickness map with those of porosity and permeability data. In this case we have used all the data available. It means that we did not average the data per well. Instead, we investigated the spatial distribution of actual data.

The grid used was 18*18*23. The idea was to model every foot in the vertical direction and one well per grid block. This model is shown in **Fig. 4-27**. It shows the spatial distribution of porosity in the reservoir. The blue zones represent the lower values and the green zones the higher ones.

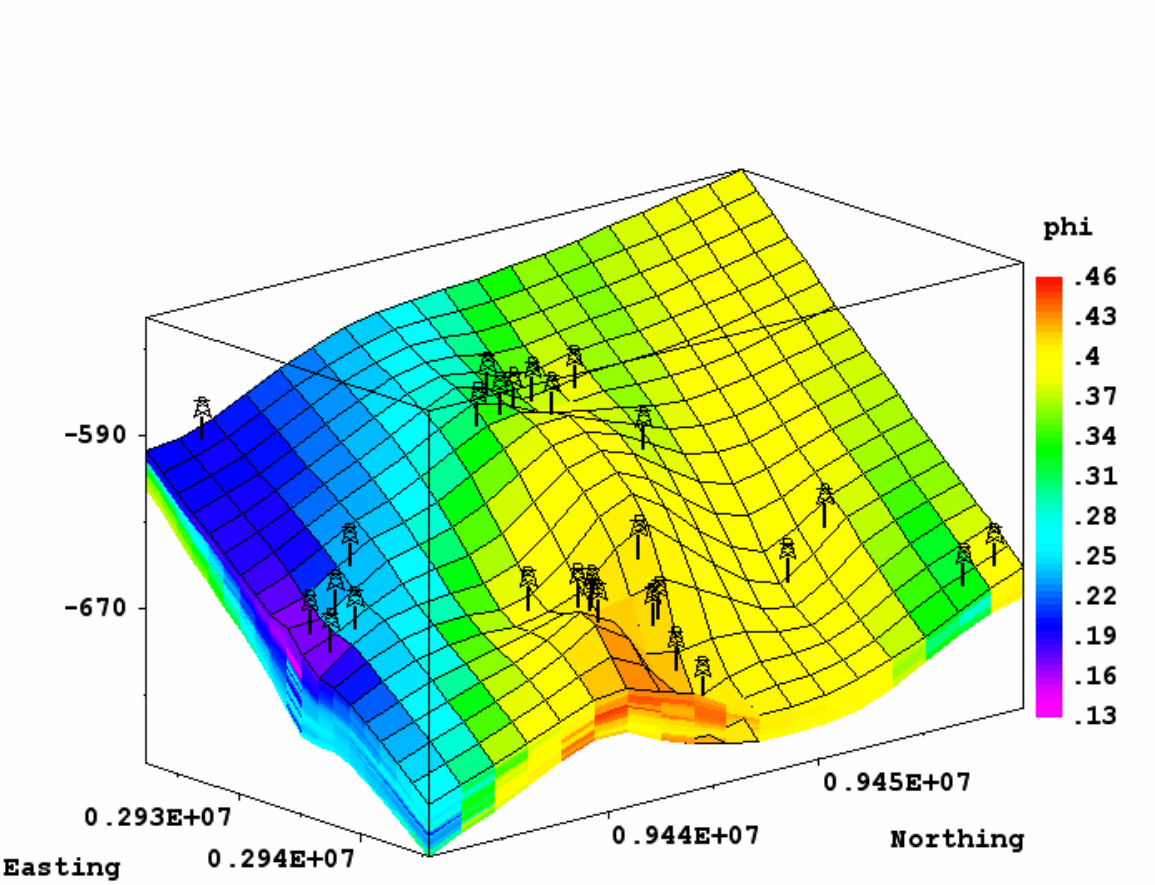

Fig. 4-27- Spatial distribution of core porosity.

We have selected areal sections corresponding to a certain structural depths. **Fig 4-28** shows the areal distribution corresponding to a 6 different depths. Each view represents one foot of Pettus sand in a structural sense. The top view 1 corresponds to the top of the Pettus sand and top view 23 corresponds to the base of Pettus sand. The other views correspond to intermediate depths.

Since not all the wells were cored the same amount of feet, for some wells the values at the well block represent actually an interpolated or extrapolated value. However, having areal patterns every foot of the reservoir might give us interesting observations.

From a quick look to all the grid maps, we observe that the lower values are accordingly concentrated in the southwest part of the reservoir. In the northern part of the structure the values of porosity do not decrease below 0.30. The highest values are concentrated in the east-central part of the grid map labeled as “top view 15” and “top view 20”.

If we look back to our variogram analysis and compare the contour maps (Fig. 4-14) with these new pattern maps we realize that somehow the data tend to follow the same direction of homogeneity: towards north-west. However in this case we can observe that the degree of anisotropy is not the same in all depths.

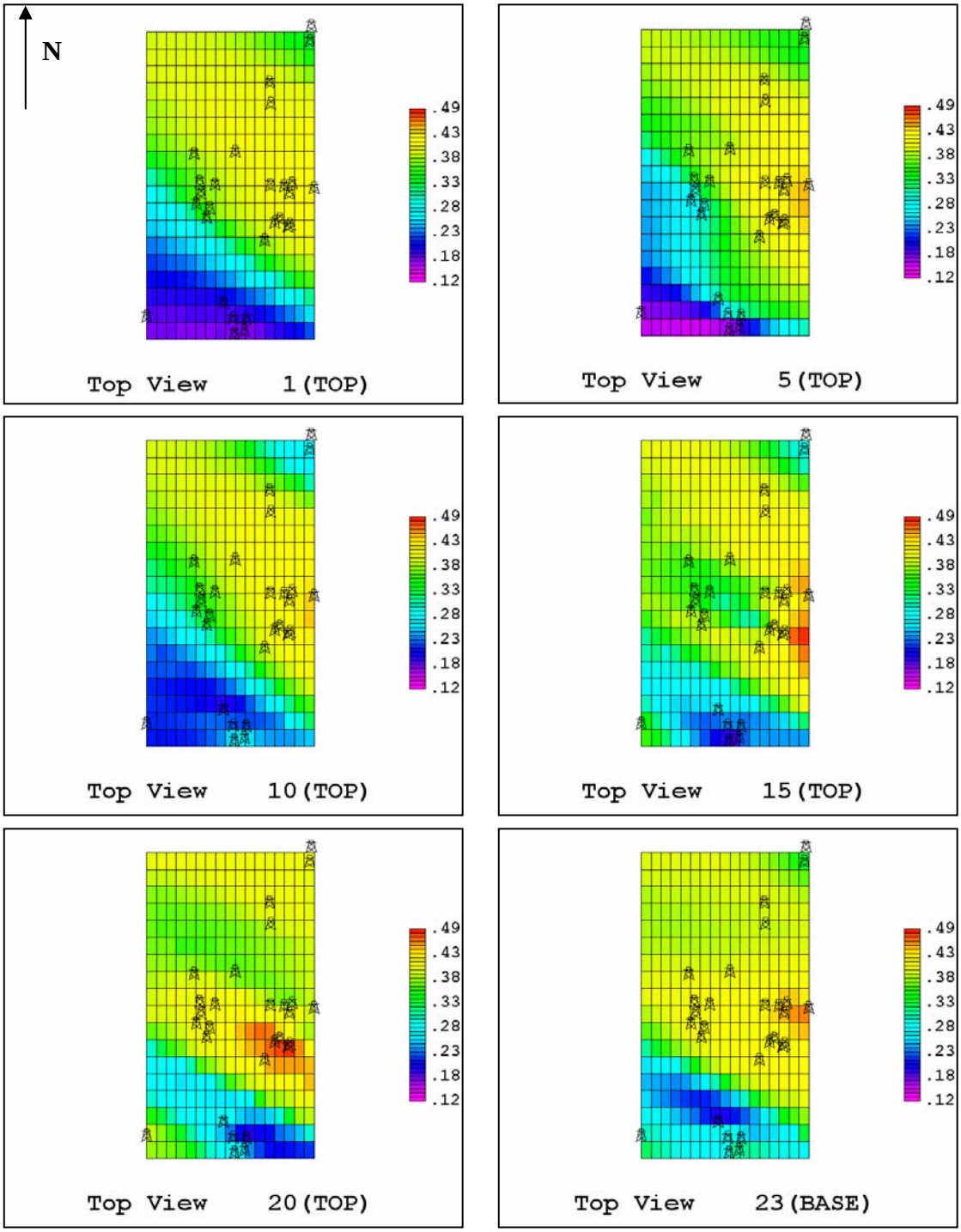

Fig. 4-28 - Areal patterns of core porosity. Each view representing one vertical foot of Pettus sand.

The same approach was used for permeability. The same grid arrangement as in the porosity case was used.

In a previous section we have determined the good correlation existing between porosity and permeability. This can be confirmed in this section. Both spatial distribution of porosity and permeability show the same trend: in the south part of the structure low permeability values and towards the north and the east the higher values.

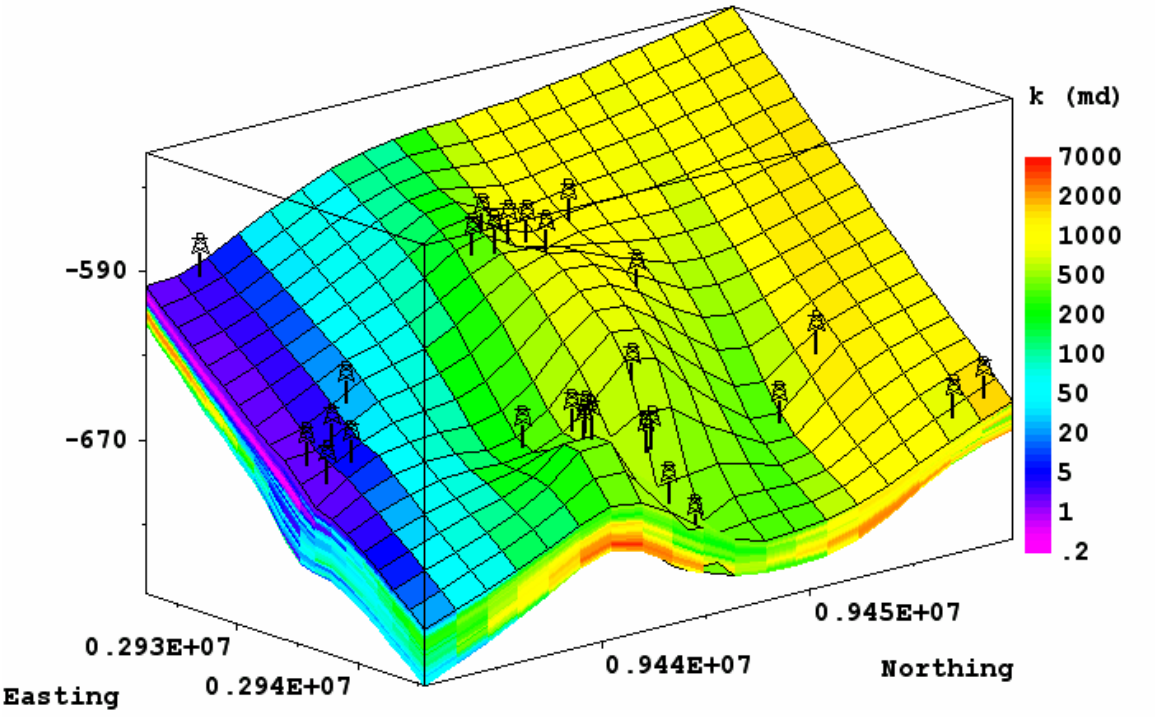

Fig. 4-29 - Spatial distribution of core permeability.

Fig. 4-29 shows the spatial distribution of permeability. There is a clear large variation of the data. The lowest value recorded was as low as 0.3 md and the highest value recorded was as high as 6000 md. Therefore a clear difference of high permeability channels and low permeability barriers will be appreciated in this analysis.

For the grid maps at several depths the same explanation given is valid and correspond to the same depths as in the porosity case. From **Fig. 4-30** observe that permeability give us a better picture of the anisotropy of the reservoir. The difference of colors in the maps show large variations of permeability in small areas. This is better appreciated in Top views 15, 20 and 23. The orange areas represent values around 2000 md. The green areas represent values around 200 md. Therefore the fluid will move easily in the orange areas. Those areas might be of importance in investigating the movement of fluids. In a later section we will confirm this statement when handling with production data.

As in the case of porosity, the low values of permeability are located at the southwest part of the reservoir. This again confirms the high correlation coefficients obtained in a previous section.

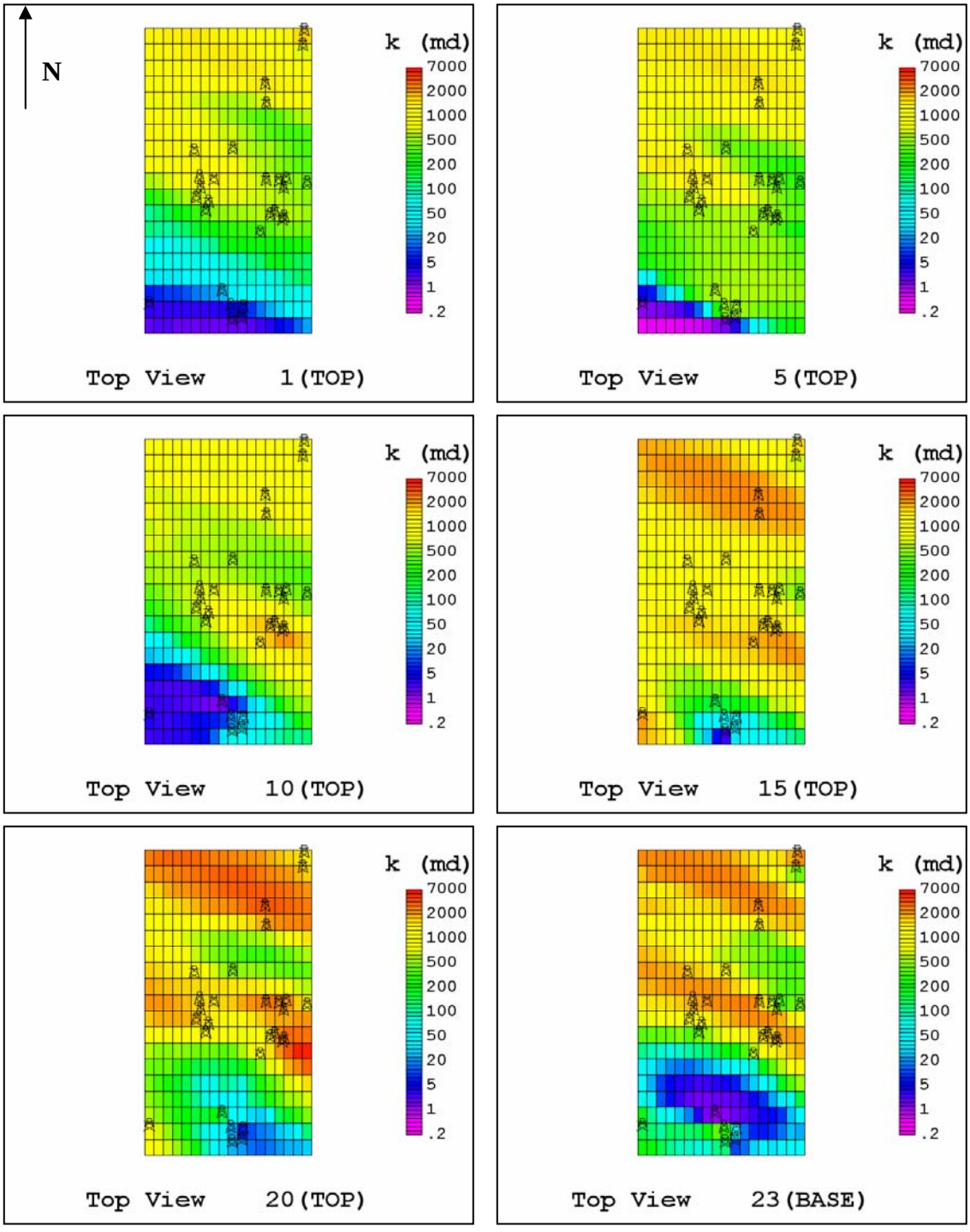

Fig. 4-30 – Areal patterns of core permeability. Each view representing one vertical foot of Pettus sand.

4.5 Uncertainty in modeling

In building a 3D model it was used the Kriging methodology to estimate the v-shale in the unsampled locations. However Kriging itself has some drawbacks that could undermine our analysis of the reservoir. Some of the drawbacks of kriging are:

- Surfaces are generally too smooth and tend to underestimate heterogeneity.
- Kriging surface is deterministic (properties are estimated rather than simulated).

We can say that our previous model was a "picture" of the reservoir. However the model is "as good as the log analyst interpretation." In order to reduce the uncertainty present in our "picture" of the reservoir, geostatistical methods suggest the use of conditional simulation.

Quoting Kelkar and Perez[14]: "The conditional simulation technique is a procedure that simulates various attributes at unsampled locations. The overall goal is to simulate reality rather than to obtain a picture of the reservoir, which minimizes error variance." So, what we intend to get in doing conditional simulation is to present several alternatives to the reservoir model that better represent the different possibilities that we can find in doing a reservoir description.

The sequential simulation methods are kriging-based methods, in which unsampled locations are sequentially visited in random order until all unsampled points are visited. For our data (V-shale) it is more proper to use the so called "sequential indicator simulation (SIS)." [14]

The SIS algorithm allows building alternative, equiprobable, numerical models of reservoir heterogeneities that reflect spatial-connectivity patterns of extreme values and honor data values at their locations.

I have generated three models that reproduce the v-shale values at the sampled well locations (**Fig. 4-31**). However, at the unsampled grids the values change (note the color difference of the top view in the three different models). For example making a comparison of the Pettus top from the three models we observe that we have different trends of v-shale (**Fig. 4-32**).

Therefore, each of the models could represent the reservoir. The only way to define the more likely model is to use them as a priori information in a dynamic data integration and find the model that best represent the dynamic data (i.e. oil rate, water cut, pressure, etc.)

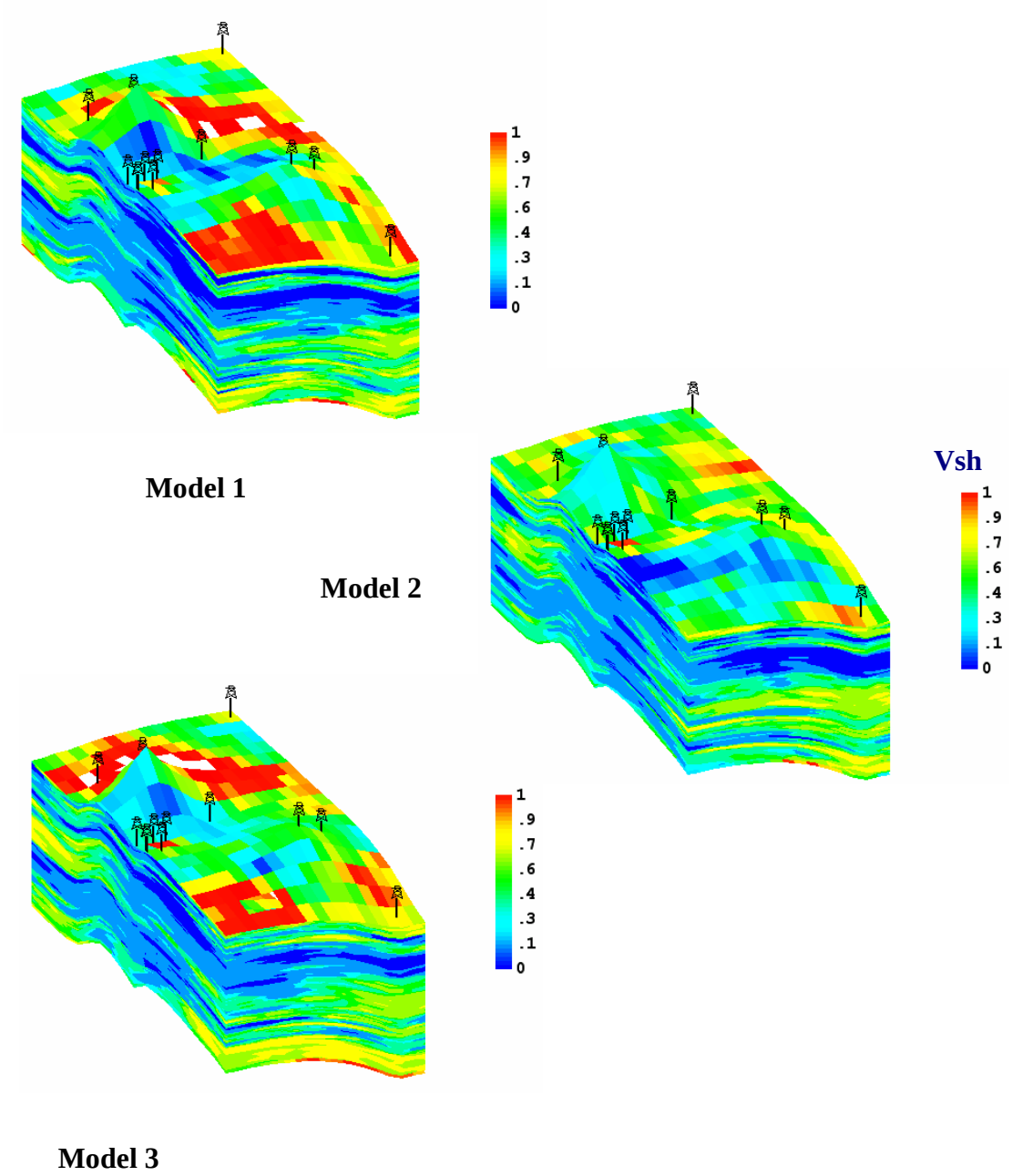

Fig. 4-31 – Realizations of 3D models using sequential indicator simulation.

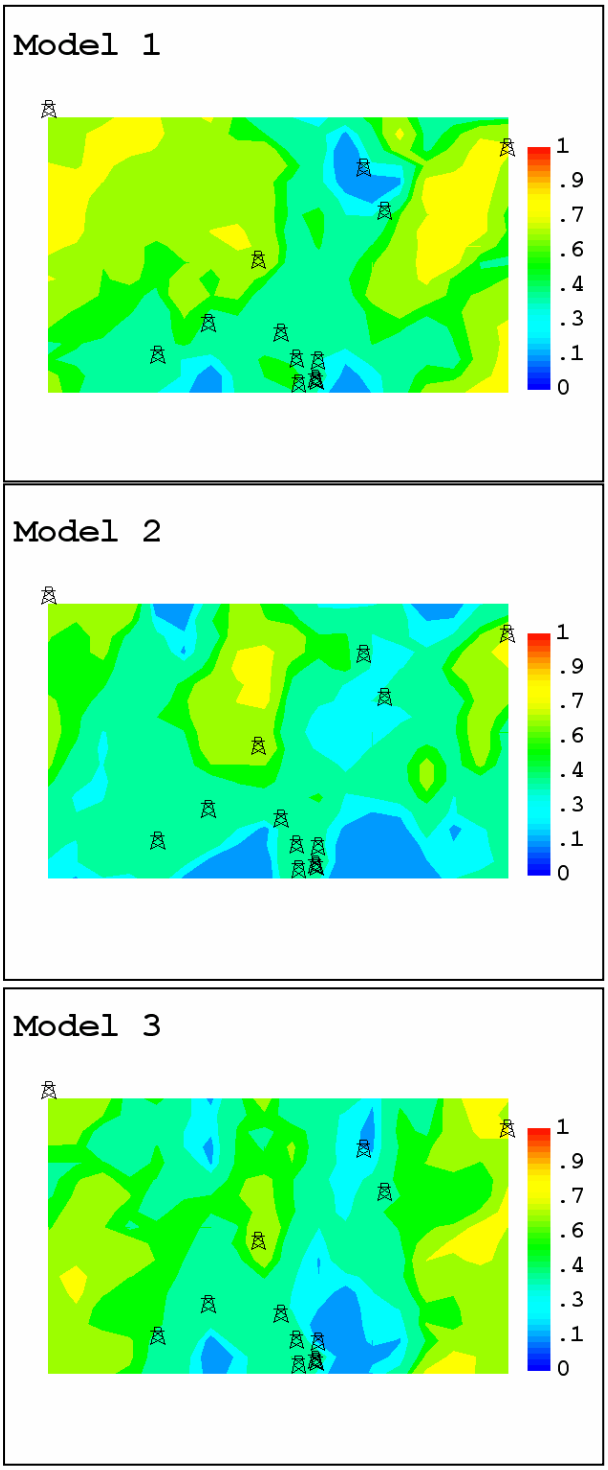

Fig. 4-32 – Areal distribution of v-shale of Pettus top for three different realizations.

CHAPTER V

RESERVES ESTIMATION AND PRODUCTION ANALYSIS

The objectives of this chapter are to estimate the original oil in place, the cumulative production, the remaining reserves and the evaluation of the dynamic data (oil and water rates).

5.1 Reserves estimation

Oil in place is estimated using the standard volumetric equation:

$$OOIP = A * h * \Phi * \frac{(1 - S_w)}{B_o} \quad \text{..... (5.1)}$$

If a single, best estimate value is chosen for each term on the right hand side of the equation, then the resulting single OOIP estimate is called the "Deterministic" value. It contains no information about the range of uncertainty that exists in each of the input parameters. If instead A, h, ϕ, S_w and B_o are each described by a distribution with a mean and a standard deviation, and if it is assumed that the distributions are independent from each other, then the Stochastic Method can be used to estimate the mean and coefficient of variation of the OOIP range.

For the case of the Jacob's pay formation we have used the maps developed in previous sections in order to reduce the level of uncertainty in our results. The value for the area "A" was the one given by the lease limits. For thickness "h" and porosity "f" we have used the corresponding contour maps (Figs. 4-17 and 4-14 respectively). So by integrating those maps we have developed the grid map for pore volume showed in **Fig. 5-1**. For getting this grid map we have subdivided the reservoir into small grid blocks (500 ft * 500 ft) and obtained pore volumes for each grid block. Therefore we have preserved the actual porosity distribution of the field and the pay thickness distribution as well.

As a consequence of doing this calculation, the total pore volume was estimated to be **2.0604 * 10^{8}** ft^{3}. This value will be used to estimate our original oil in place.

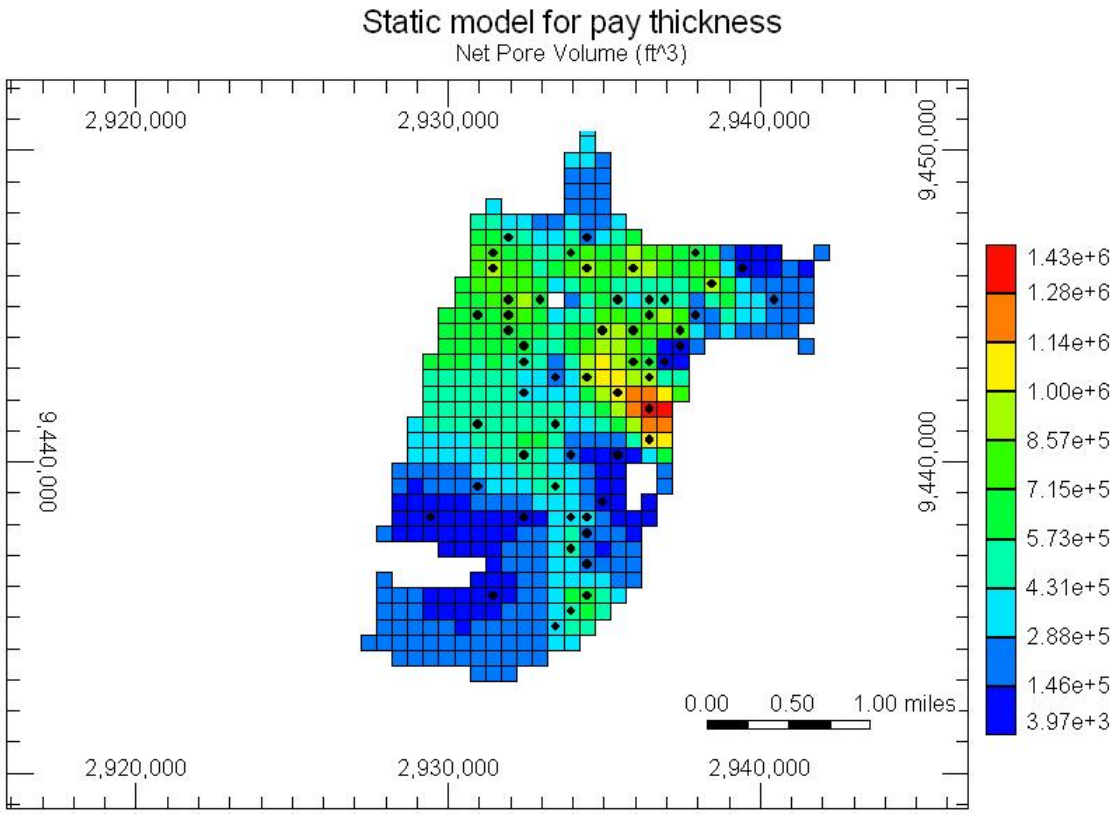

Fig. 5-1 – Net pore volume grid map for pay formation – Pettus sand.

5.1.1 Deterministic

For the deterministic approach each of the variables was determined as follows: Pore volume as described above. For water saturation values I used both means obtained from core data and log analysis. The oil formation volume factor was assumed to be 1.0 STB/bbl (since the reservoir is at a shallow depth this can be a valid assumption).

Table 5-1 summarizes the results obtained using this technique. As it is observed there is a difference of 1.84 MMSTB, which resulted from the different values of water saturation.

TABLE 5-1 – DETERMINATION OF OOIP

Parameter	Value (source)	
Pore volume (ft3)	2.0604 x10^8 (grid map)	
Water saturation (v/v)	0.50 (core mean)	0.55 (log mean)
OOIP (MMSTB)	**18.35** (core)	**16.51** (log)

The main drawback of this approach: it does not reflect the variability of the data in the reservoir. In reservoir engineering it is no longer useful to have a unique estimation. For that reason the stochastic approach must be taken into account.

5.1.2 Stochastic

In the stochastic approach the mathematical model is the same as in the deterministic one (Eq. 5.1); however, the values of the parameters are known in a probabilistic sense. I have used the Monte Carlo simulation that uses random numbers to generate values for the varying and uncertain parameters. And also assumes that all the variables are independent of each other.

The idea of using Monte Carlo simulation is to help to quantify the uncertainty in the Jacob field.

Since we have calculated the pore volume with a very good degree of precision, the only two variables considered in a probabilistic sense were water saturation and formation volume factor.

For the water saturation distribution we have used all the values obtained from core samples and from log analyses. We have plotted a histogram and a probability plot showed in **Fig. 5-2**. As it is observed in the plots, we can assume that the data follows a normal distribution with a mean of 48.7% and a standard deviation of 10.82 %. These values were later used in the montecarlo simulation.

For the formation volume factor we have considered a linear distribution from a minimum of 1.0 to a maximum of 1.1. The reason for doing these is basically because we did not have access to any data corresponding to this parameter. Due to the shallow depths of the reservoir the value that is more likely to be the “true” one is 1.0, but nothing can be true until at least a PVT analysis is done from the fluids produced.

(a)

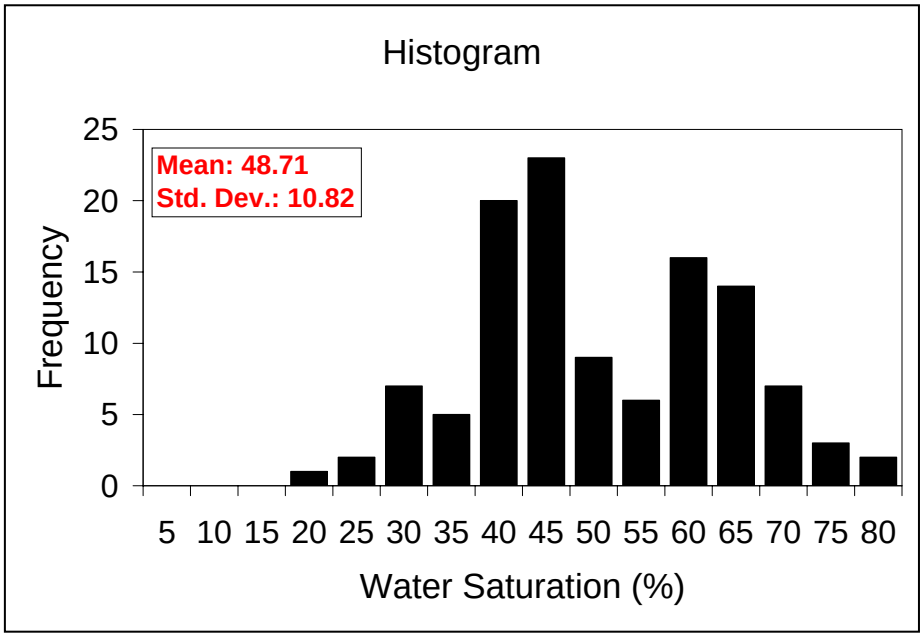

(b)

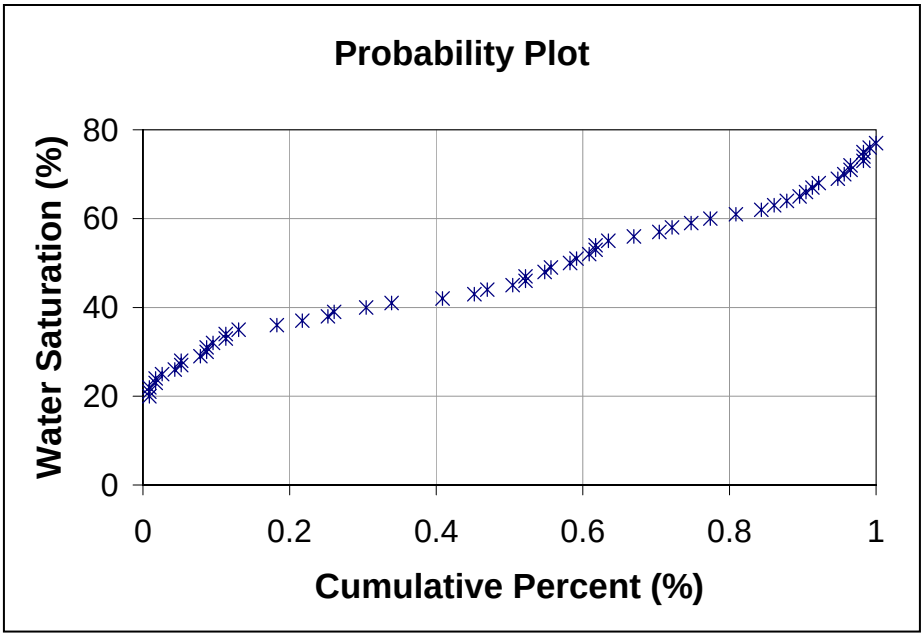

Fig. 5-2 – Water saturation for Pettus sand (a) Histogram, (b) Probability plot.

Fig. 5-3 shows the plot and the results for original oil in place when using the stochastic approach. The goodness of the stochastic approach is the reporting of the range of confidence, which is the range of expectation of getting the results. It is more probable that the original oil in place would be 18.12 MMSTB with a range of confidence of 13.4 MMSTB (90% probability) to 22.7 MMSTB (10% probability)

If we compare the more probable value from this approach (18.12 MMSTB) with the ones calculated using the deterministic approach (18.35 and 16.51 MMSTB) we can see that there is a close agreement in the results. Therefore, since the result obtained from the stochastic approach is somehow in the middle of the other ones we will report 18.12 MMSTB as the estimated original oil in place for the pay zone of Jacob field.

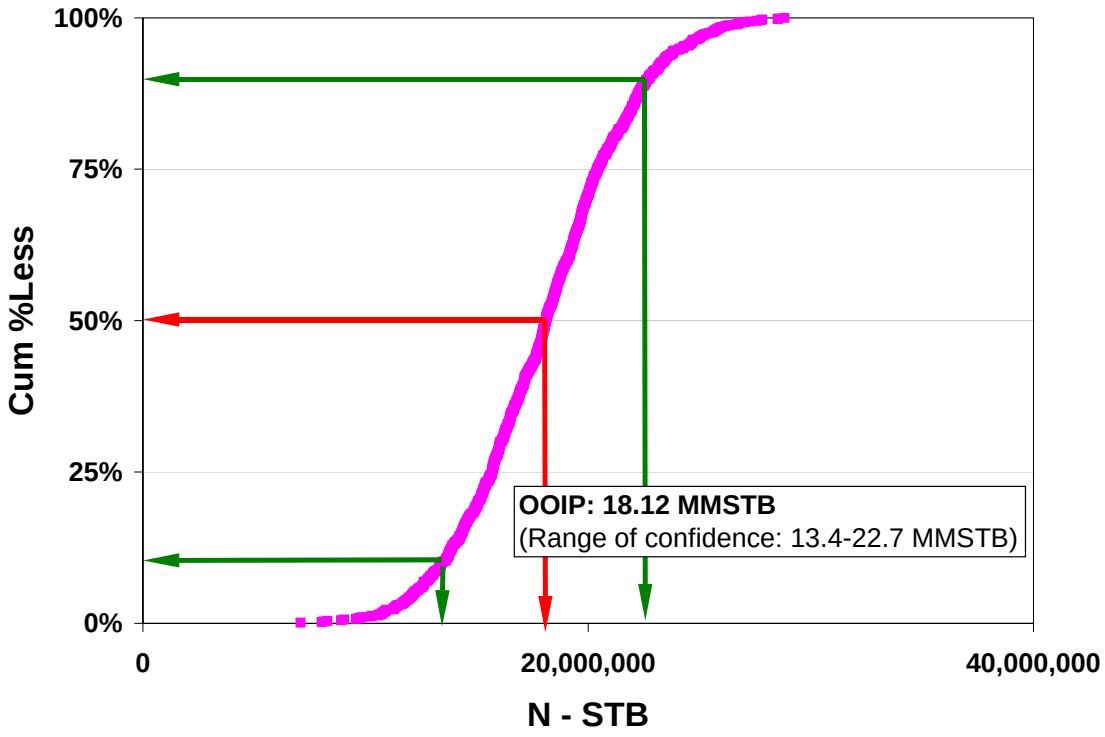

Fig. 5-3 – Estimation of original oil in place for Jacob pay formation using stochastic approach.

Besides the calculation of the original oil in place, we have also considered a recovery factor in order to estimate the cumulative production. We have chosen an

interval that represents a typical solution gas drive and water drive. For the solution gas drive a value of 10% recovery factor was assumed. And for the water drive case a recovery factor of 30% was assumed. So the interval of variation would be 10-30% with a mean of 20%. Our intention in doing these assumptions is to compare the results from this analysis with the estimated cumulative production in a later section (reserves by DCA). And therefore determine a most likely recovery factor and a most likely reservoir-drive mechanism governing the movement of fluids in the reservoir.

The formula used for estimating the cumulative production is just the product of the original oil in place times the recovery factor.

$$N_p = RF * OOIP \quad \text{..... (5.2)}$$

The distribution used for the recovery factor was a triangular one. There is no particular reason for using the named distribution, just for making the calculations a little bit easier.

According to the Society of Petroleum Engineers (SPE) the term “proved reserves” is defined as follows: “Proved reserves must be produced profitably under current economic conditions, operating methods, and government regulations.”
Since we are working with a reservoir that has been exploited for many years under all the previous years’ economic conditions and government regulations, we can consider the cumulative production obtained here as proved reserves.

Fig. 5-4 shows the results obtained using the stochastic approach. There is a 50% probability to recover 3.11 MMSTB with a range of confidence from 2.2 MMSTB (90% probability) to 4.1 MMSTB (10% probability).
We will keep these values in mind for the next section.

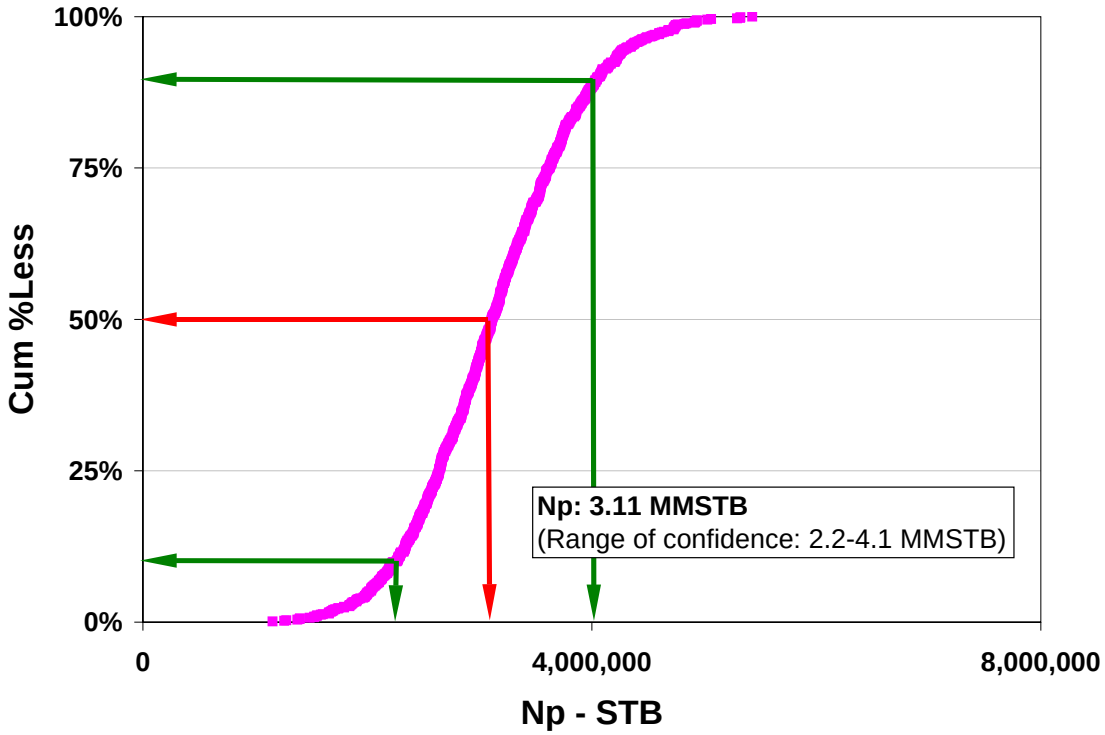

Fig. 5-4 – Estimation of cumulative production, using stochastic approach.

5.2 Production analysis

Production analysis is mandatory for any oil field and recording data production is also mandatory and is usually the most common available data in any oil field. However the Jacob field is particular since there are few records of accurate daily oil and water production data on a well-by-well basis.

The oil initial production was recorded for 90 wells. The area with higher initial production is located at the east central part of the lease (**Fig. 5-5**). The highest initial production recorded was 300 BOPD in the well 23A (completed in 1934). The zone with higher production rates is concentrated in the east part of the lease and in the surrounding areas the rates were just low in comparison.

We might think that having such different values of initial production would mean that we have two different reservoirs, however in plotting the same initial rates with respect to time we find that there is a trend of decrement in production as time

passes by (**Fig. 5-6**). The first “good” wells were drilled in the first 6 years of activities in the Jacob field. After that the wells started producing just below 10 bbl/d of oil. Another fact that calls our attention is the gap in time from 1970 to 1990, 20 years without exploring for new wells!

About field production, I had information of oil field production from 1956 to present (as of as Oct 2003). The plot of monthly data is shown in **Fig. 5-7**. The number of wells in current operation in the field is also added. A steady declination in the oil rate is observed until 1990 when the rate of declination drops very fast and in spite of having almost the same number of wells. This declination is even worse in 1998 when the rate drops below 10 bbl/month! However, by the end of 2002 the production increased and kept at acceptable levels, as a consequence of drilling two new wells (121A and 122A). In summer 2003 three wells were tested in order to determine the production potential. Those wells were 2A, 20A and 52A. Unfortunately until the end of this report no records were obtained from the oil field personnel.

The accounted oil cumulative production is **1,348,615 bbl** (From 01/01/56 to 10/01/03). Additionally 680,000 bbl were reported as production from this field from discovery to April 1937 (J. Turner’s Report available in the field files). For the rest of the years the production was not available. Therefore an accounted **2,028,615 bbl** were produced from this field.

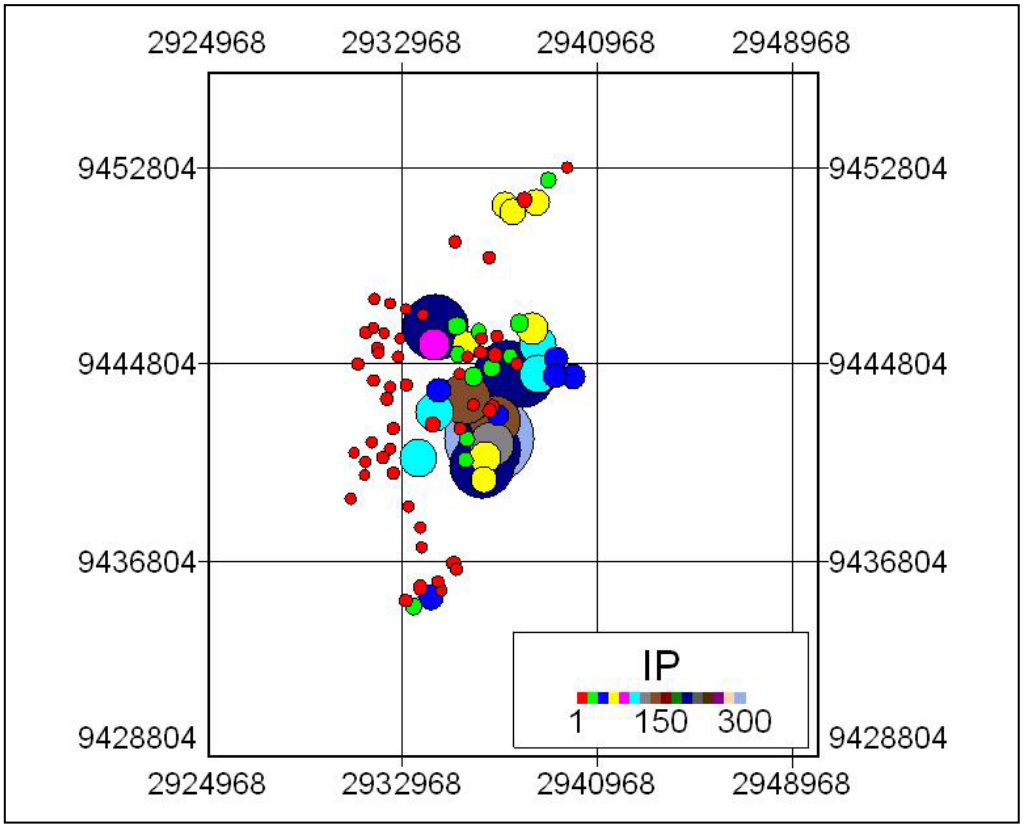

Fig. 5-5 – Bubble map of initial production.

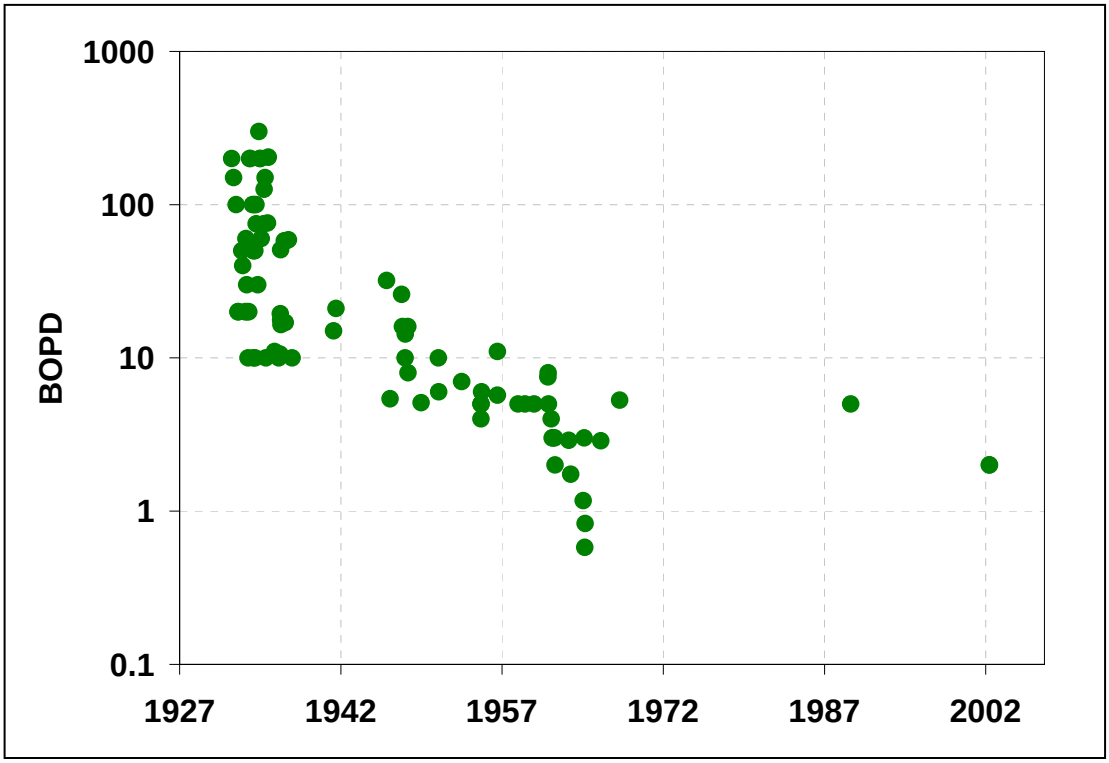

Fig. 5-6 – Trend of declination of initial production.

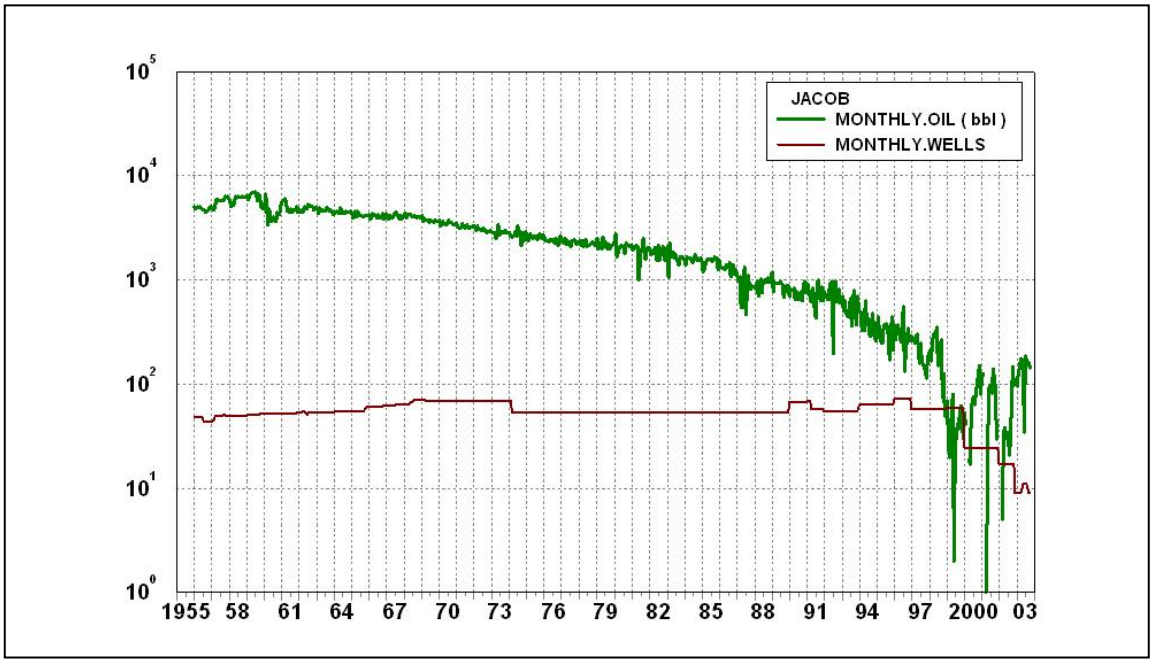

Fig. 5-7 – Monthly oil production for the Jacob field from 1956 to 10/2003.

In terms of production data on a well-by-well basis, I was able to gather information for 52 wells. Only once a year the production of oil and sometimes water was reported to the Rail Road Commission of Texas because of State regulations. This data can be found in the Appendix of this thesis.

The production data was recorded sporadically and since the early 70's. Having this kind of data it is impossible to perform a decline curve analysis neither to establish what type of rate declination the wells followed (e.g. exponential, hyperbolic, harmonic). However it is observed that in some of the wells the water rates recorded were high and in others the water rates were low and almost zero. In converting this data into water cut might explain better the production performance of this field.

5.3 Fluids distribution

In this section we use the oil and water saturations values from the cores and sidewall core data analyses to represent a spatial distribution of the fluids along the field.

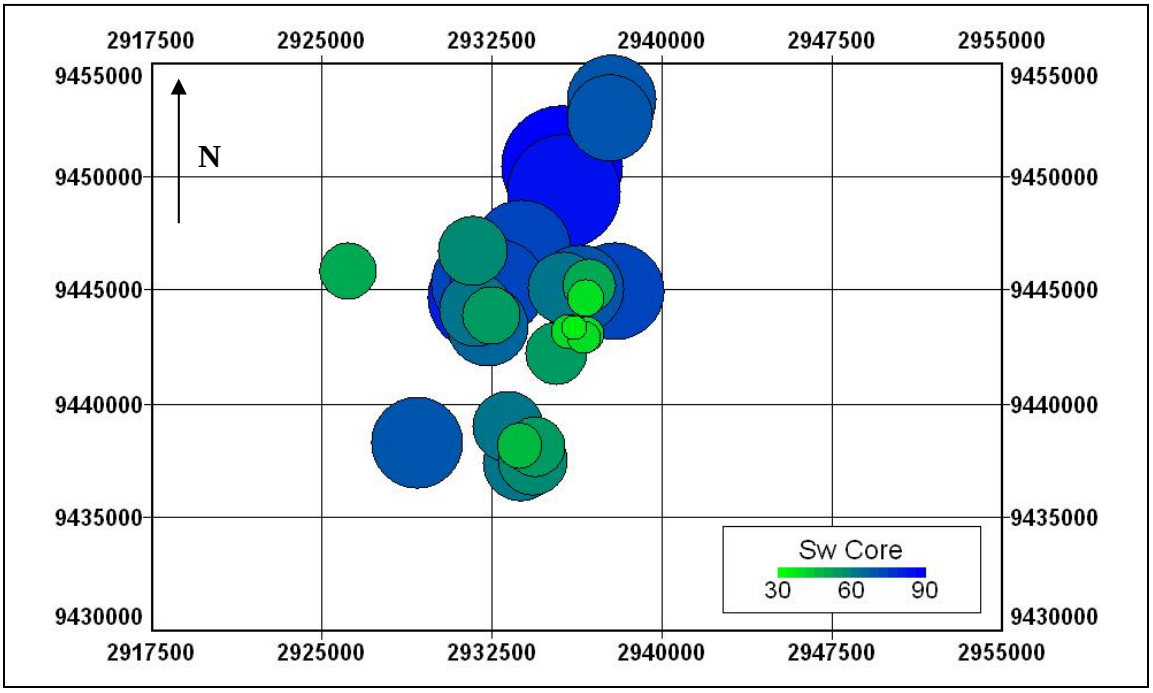

Fig. 5-8 – Bubble map for core water saturation.

Since water saturations are dynamic data and were obtained in a particular time plotting them in a grid system is meaningless (i.e. interpolating the data). A better representation, therefore, is a bubble map. Bubble maps for water saturation (**Fig. 5-8**) and oil saturation (**Fig. 5-9**) were obtained.

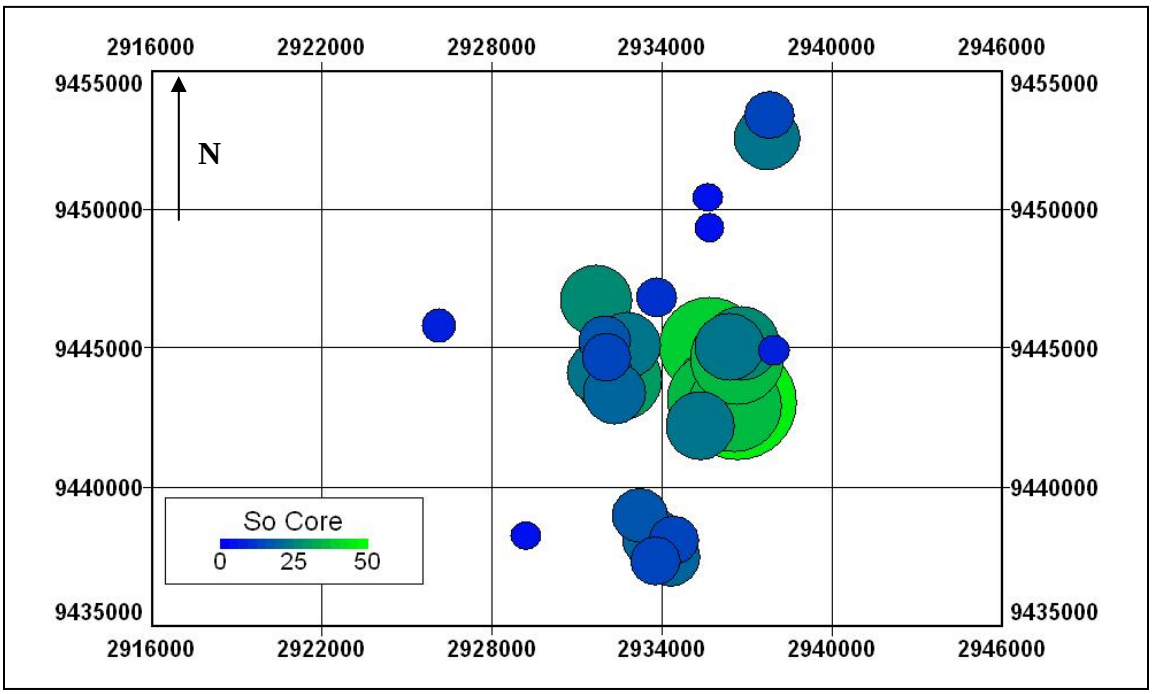

Fig. 5-9 – Bubble map for core oil saturation.

The higher water saturations were at the north part of the field and the low water saturations were found with no certain order. In terms of oil saturation, the east central part of the field showed high saturations (almost 50%), this coincides with the high rates obtained by the first wells drilled in this area.

A better picture of the saturations data can be appreciated in plotting them as a function of time. **Figs. 5-10** and **5-11** show how the saturations changed as the time passed. It seems that the water saturation tends to decrease instead of increase. However the range is between 50-60%. These values are in close agreement with those derived

from log analysis. For the oil saturation it is clearly observed that the first wells reached values of almost 40% oil saturation, however the last wells were in the average of 20%.

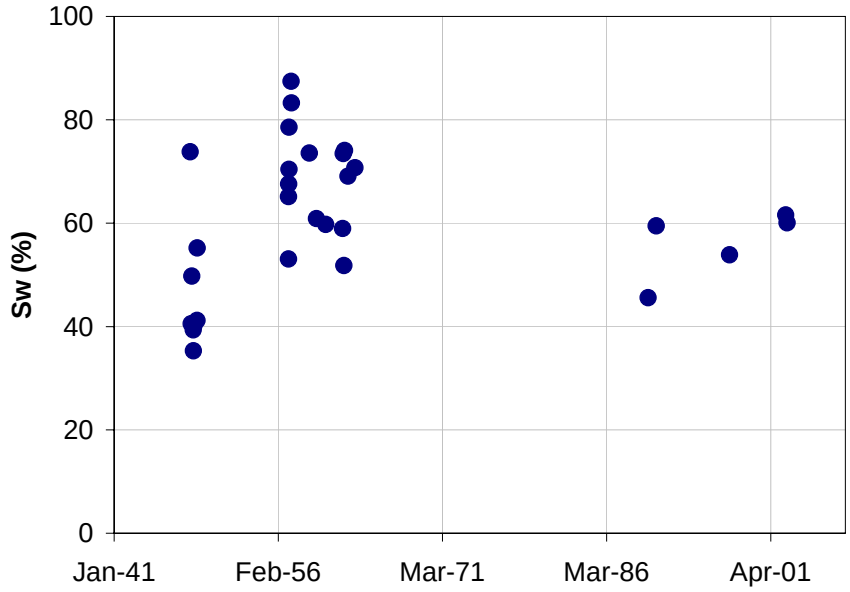

Fig. 5-10 – Core water saturation as a function of time.

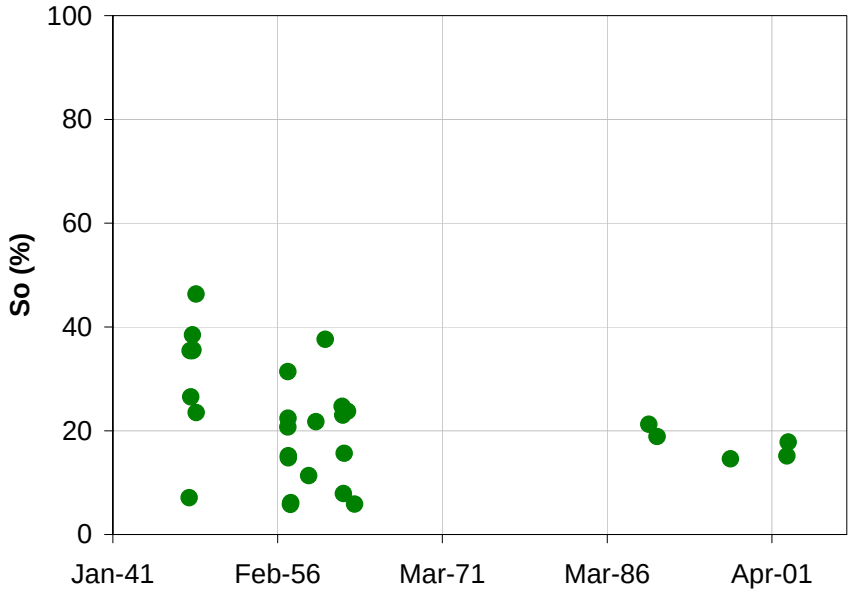

Fig. 5-11 – Core oil saturation as a function of time.

As it was mentioned previously, the production data on a well-by-well basis was recorded sporadically. There were periods of time having oil and water production therefore, the calculation of the water cut was possible. By making a contour map of the existing wells for several time periods the movement of fluids can be investigated.

In that sense, six grid (contour) maps were built as it is shown in **Figs. 5-12** and **5-13**. The earliest date was February 1975 and the latest February 1997. Recall from Fig. 5-7 that at late 1998 many wells were abandoned (production declined dramatically).

The blue areas represent the zones with high water cut and the green ones represent zones with low water cut. It is clearly observed that the water is moving from the northeast and from the southeast as well. Two facts can explain this behavior: the north east and the south east regions are the lowest parts of the monocline (from 3D modeling), the high correlation coefficient of vertical to horizontal permeability in the northeast region letting the water to flow in the vertical direction preferentially.

There is a clear change of water cut from 1975 to 1979. The water was moving from the northeast region preferentially and afterwards the water encroached from the southeast region. This behavior kept the same until 1997.

From the analysis of these plots we can conclude that there is a water encroachment from the lower part of the structure and there is room for extracting oil in the highest part. In the highest part of the structure there were wells having very low water cut. Even now, in that zone there are wells having low water cut (e.g. 27W: 21%, 122A: 12%, 121A: 0%).

It is important to observe that due to the interpolation methodology (inverse distance) the southwest area is showed as oil saturated. However, in this area only one well (25W) was drilled having very low oil saturation (Fig. 5-12). So, do not take that area as oil saturated.

In order to confirm that there is water encroachment from the southeast part of the reservoir it was ran several “swabbing” tests. The discussion follows in the next section.

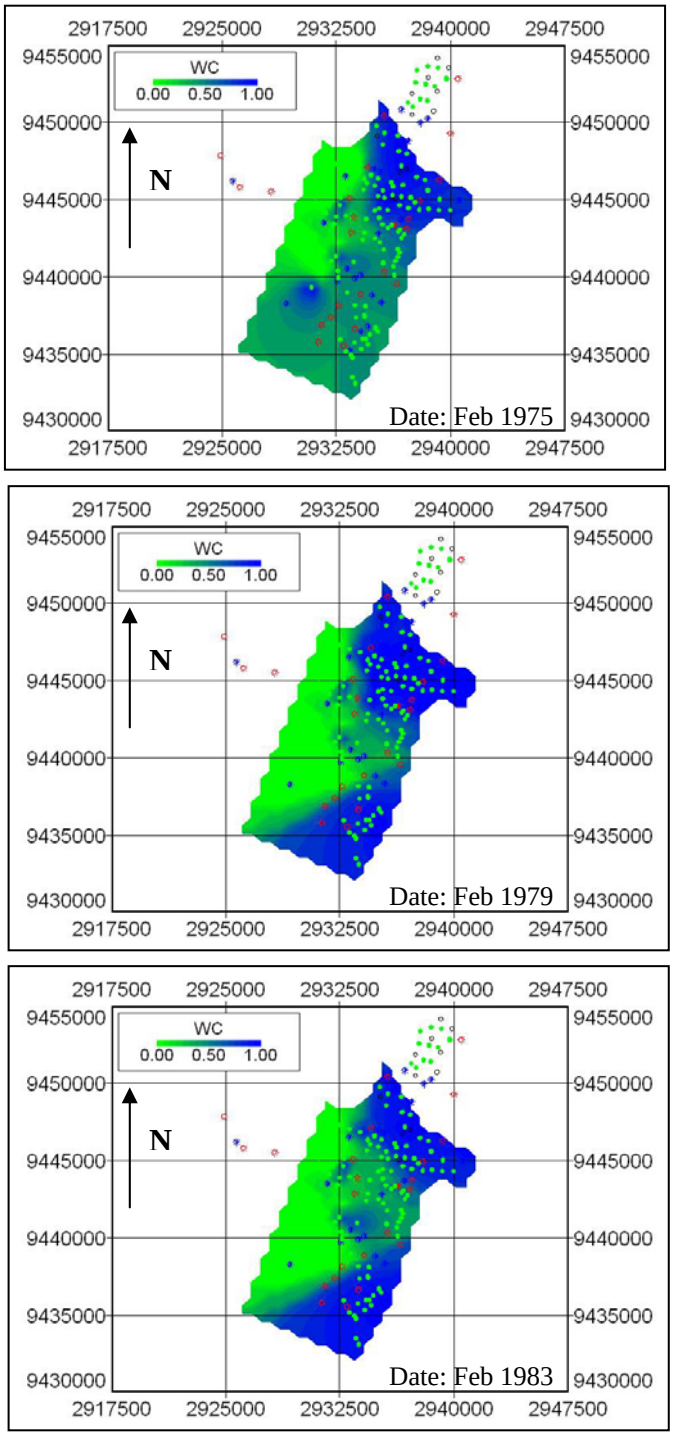

Fig. 5-12 – Grid maps for water cut (1st part).

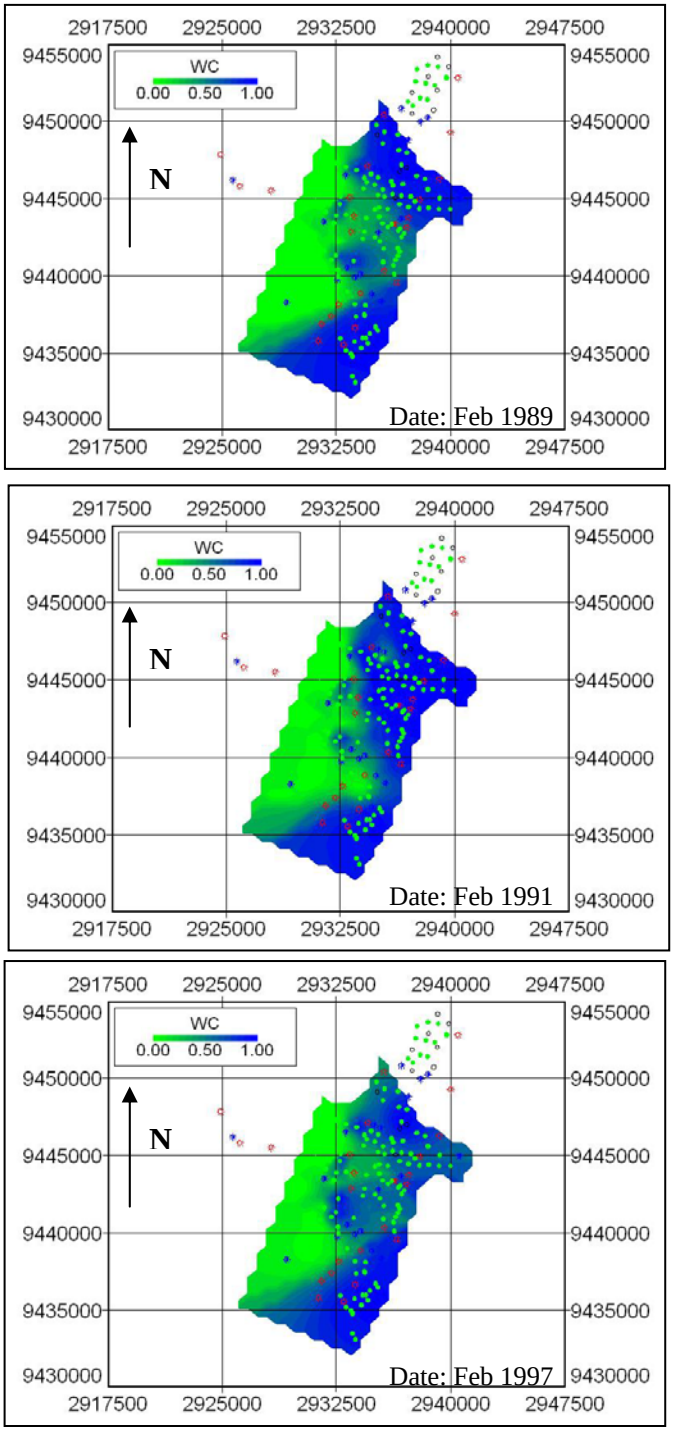

Fig. 5-13 – Grid maps for water cut (2nd part).

5.4 Analysis of fluid levels

The energy of the reservoir can be determined from pressure transient tests. In the absence of those tests, a fair indicator of energy (pressure) can be obtained from fluid levels in those wells that do not produce in a continuous manner.

In a set of 5 wells the fluid levels were recorded while “swabbing” the fluids in the wellbore (**Figs. 5-14**, and **5-15**).

In the well 117A (Fig. 5-14) the fluid levels raise almost up to surface and the fluid recovered is mostly oil. However some sand is present when swabbing relatively deep (almost below 600 ft).

Well 119A also behaves in the same manner as well 117A. In this case water is an issue while swabbing the fluids. As in the previous case water and sand are present when swabbing deeper than 600 ft.

Well 121A was completed in October 2003, so the swabbing activities shown in Fig. 5-14 are those of the first tests in trying to clean the well before installing the sucker rod system. This well also shows a good recovery of fluid level as time passes.

Well 122A also was completed in October 2003 and as in the previous well the plot showed in Fig. 5-15 shows the first swabbing tests. Observe that in this case the date interval is shorter than in the previous cases. The fluid level rose up to 600 ft.

Well 15-F (Fig. 5-15) shows also a good recovery of fluid level. Some times only water is recovered from the well. There is also an indication of free gas in the well. However, a good amount of oil was recovered from this well.

Well 15-F is located south from the other wells and it may be observed that more water is recovered from this well in comparison to the others. Also note that the 4 first wells are neighbors of the same area.

If we can assume that all the five wells belong to the same reservoir hydraulic unit, we can conclude that there is a support of energy by water encroaching from the south part of the field. This analysis strengthens the fluid movements analyzed in the previous section.

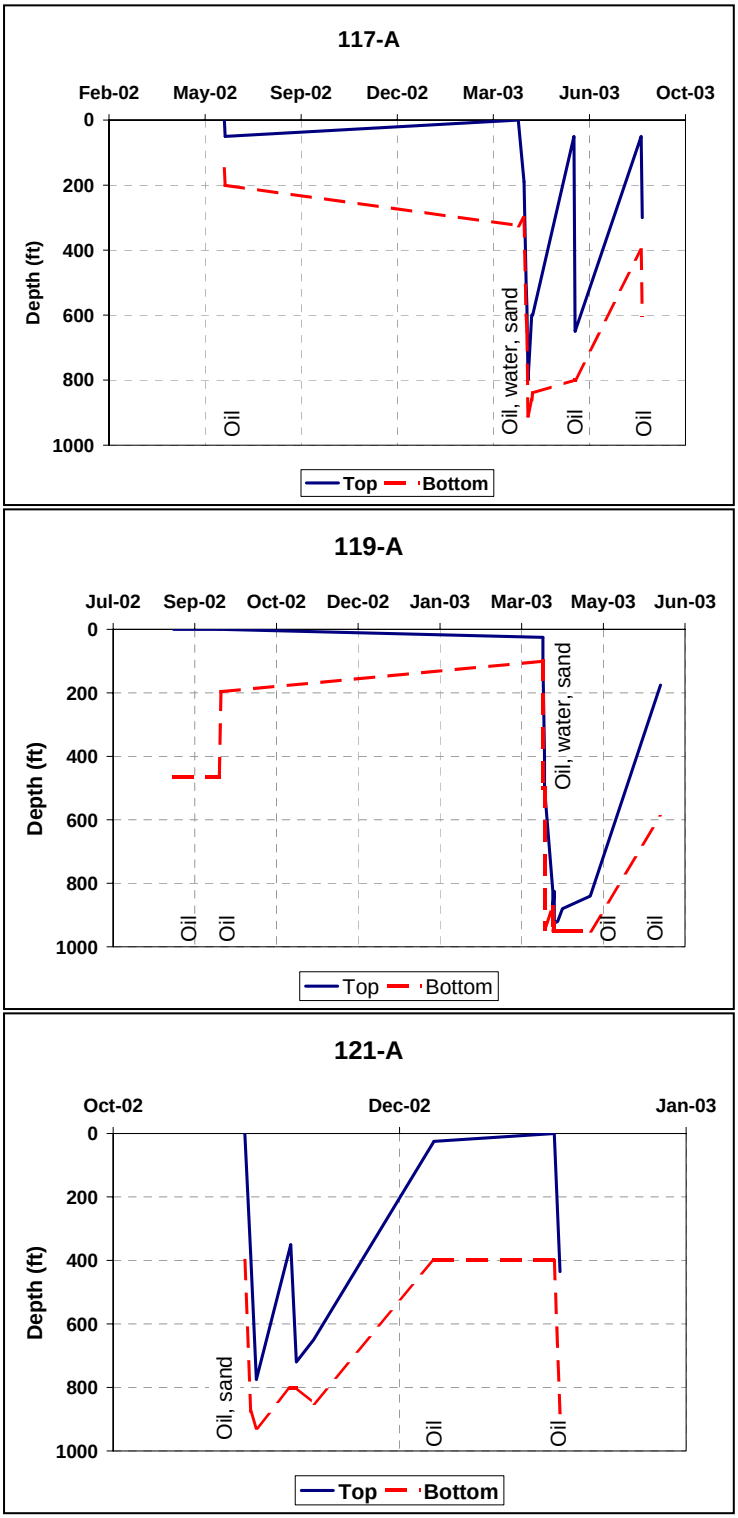

Fig. 5-14 – Analysis of fluid levels (1st part).

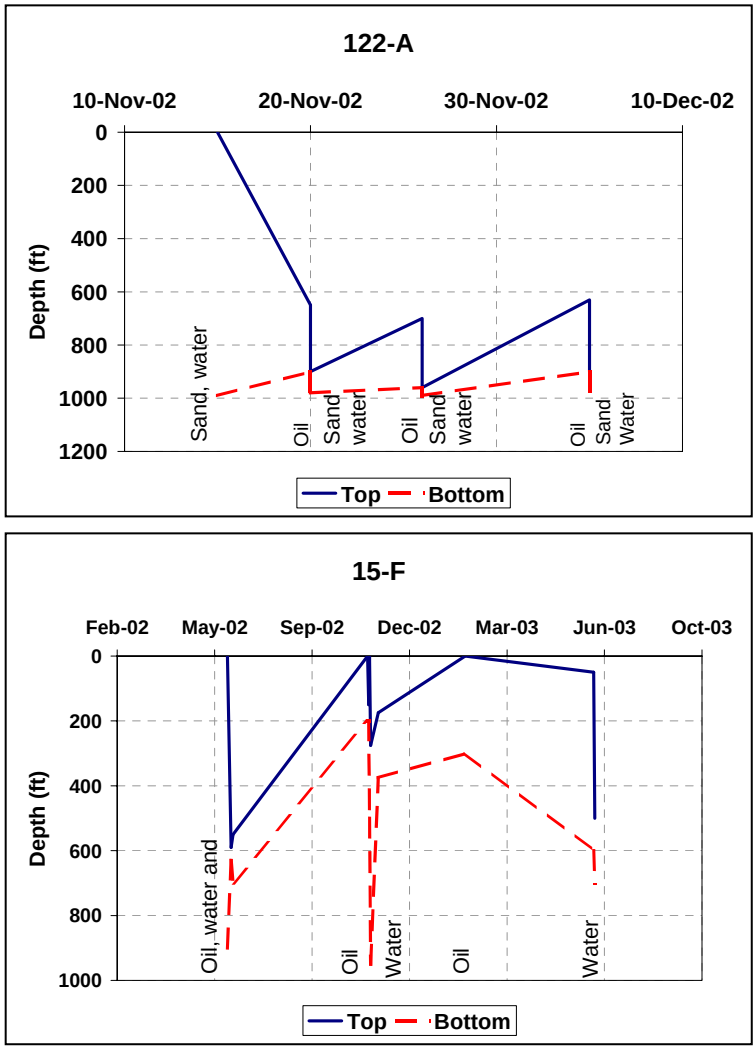

Fig. 5-15 – Analysis of fluid levels (2nd part).

5.5 Estimation of remaining reserves by DCA

The decline curve analysis (DCA) is used to forecast production and therefore determine the remaining reserves in the field. In the Jacob field it is possible to estimate the remaining reserves from the monthly production data available. Two scenarios were chosen depending upon which historical data to use for the regression analysis. The first scenario (**Fig. 5-16a**) used the historical data from 1990-2000. The second scenario (**Fig. 5-16b**) used the historical data from 1980-1990. The idea of using two different scenarios was due to the different rate of declination in those two periods of time.

It is important to outline that the main assumption in this analysis is that in the forecasted years the number of wells will not be increased. Another point is that it is assumed that the final rate (economic limit) is 1 bbl/day.

In the first scenario the remaining reserves are estimated to be 6.62 Mbbl (thousand of barrels), while in the second scenario a value of 10.60 Mbbl is estimated. We may say that being pessimistic the remaining reserves would be that of the first scenario.

These estimations will change if we change the parameters outlined above, such as, for example the economic limit or the number of wells.

Discussion: Estimated Ultimate Recovery (EUR)

Since we had not access to 19 years of production we estimated them by doing a regression analysis taking into account the first five years of production and the declination rate for the period 1956 to 1970 (when the company stopped drilling new wells). **Fig. 5-17** shows this regression analysis. The following assumptions were made: the rate for the first years of production was assumed to be constant at 371 STB/d (summing up gives 680 MSTB). The declination rate for the 19 years is assumed to follow the same rate as for the period from 1956 to 1970 (0.036 $year^{-1}$).

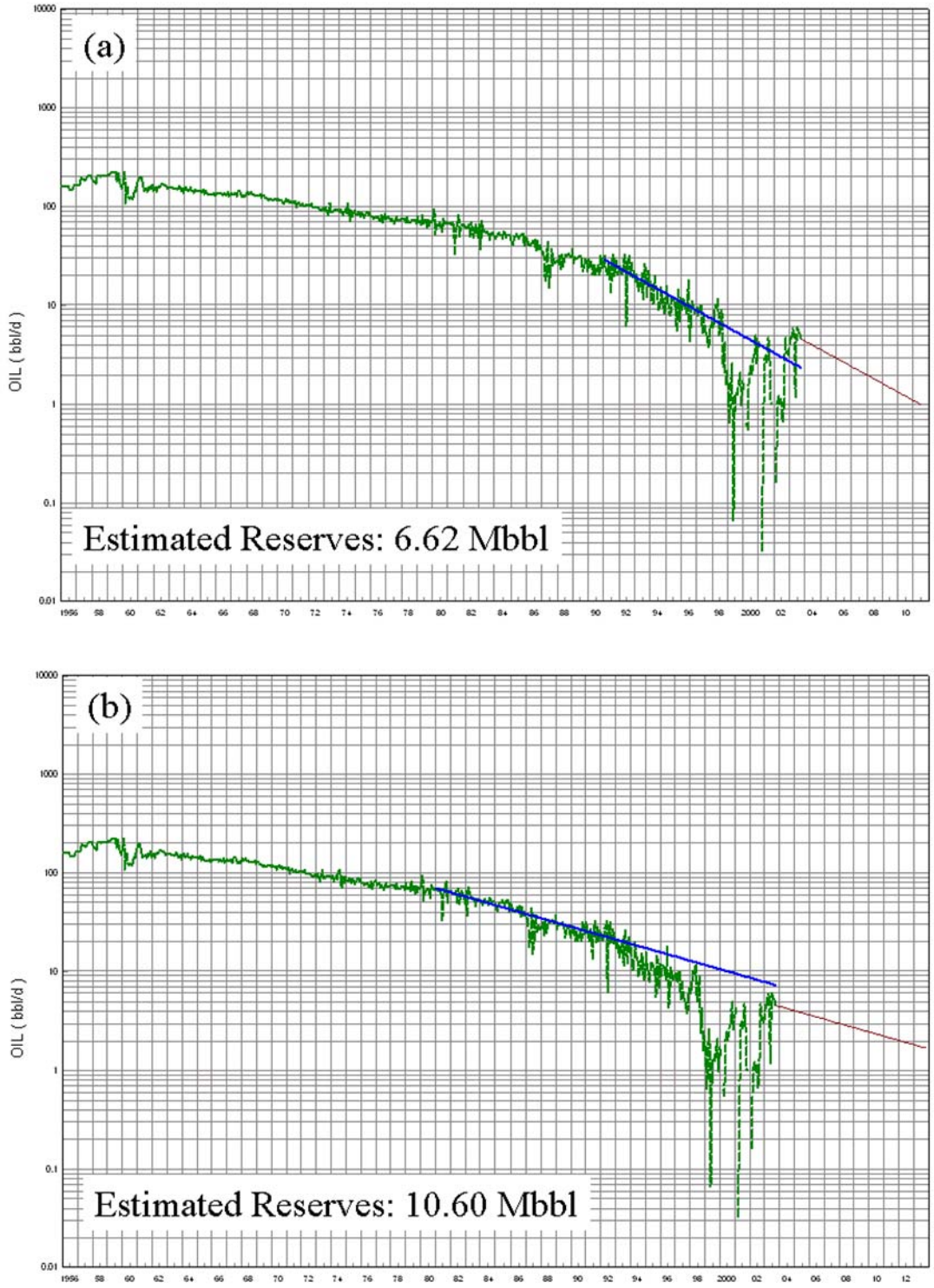

Fig. 5-16 – Estimation of remaining reserves as of October 2003, using historical data (a) 1990-2000, (b) 1980-1990.

The estimated value for the cumulative production gives 1.80 MMSTB of oil. If we trust on this value we can conclude that the estimated cumulative oil production for Jacob field might be on the order of 3.8 MMSTB.

Therefore the EUR for Jacob field is estimated to be 3.81 MMSTB.

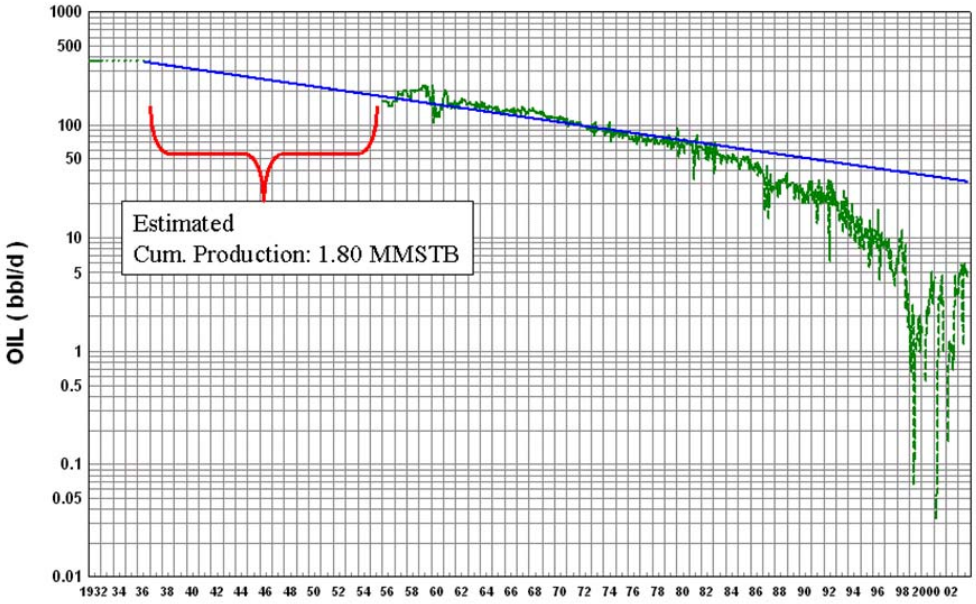

Fig. 5-17 – Estimation of production declination for the period 1937 to 1955. The blue line shows the regression line.

As it was estimated in section 5-1, the estimated cumulative production using the volumetric formula and the stochastic approach was more likely to be 3.11 MMSTB. This last value compared to 3.80 MMSTB obtained from the decline curve analysis can be considered a close agreement. We have to be aware of the uncertainties existing in our calculation especially in estimating the cumulative production for those 19 years of unknown data.

The estimated 3.11 MMSTB of cumulative production was calculated using a range of recovery factor. That range was from 10% to 30% with a mean of 20%. Since the estimated cumulative production from DCA is higher than the 3.11 MMSTB, the recovery factor may be higher than 20%, therefore indicating that the main reservoir-drive mechanism would by waterdrive.

CHAPTER VI

POTENTIAL DEVELOPMENT OPPORTUNITIES

6.1 Issues that undermine the proper development of the Jacob field

Before giving any recommendation regarding the potential development of the Jacob field, it is important to know what the particular situations of the oil field operations are, so a better understanding of the field as a whole can be achieved.

6.1.1 Surface facilities status

The surface area of the Jacob field is divided in three leases: "Ashley" to the east, "Williams" to the south and "Morrill" to the west (**Fig. 6-2**). There are 4 gathering stations in use and one, located in the Ashley lease, in stand-by. The wells currently in production are connected to the same pipeline. Therefore, at the gathering station there is no manifold that separates the production in order to perform individual production tests. That is the main reason why it is not possible to test the wells individually. Even if the pipes were connected individually, the facilities at the gathering stations are not in good conditions to allow a good test.

It was mentioned before that only 9 wells were in production in the Jacob field. Of those 9 wells, 6 wells are in pump-off (**Table 6-1**). However there are 10 wells with potential to be put on production again. Those wells were shut-in due to two main problems: production of sand and high water cut (there are no records of those high cuts yet).

In terms of sand production, I have analyzed three samples of wells facing this problem. Using the sieve analysis methodology[19] the mean size of the grains was determined (**Fig. 6-1**). From the analysis performed a poor sorting and not well-graded grains of the samples was established. The median grain size for the three wells was between 88-120 microns.

Having these values it is possible to recommend the installation of pre-packed screens that stop the production of sand. However it is a costly practice and not always has great success.

The water production was also noted as a production issue. If we observe the wells being shut-in due to high water cut (Table 6-1) and also check the production history of these wells we observe that only two wells have water production history (2A and 20A). The last water rates for those two wells were 20 bbl/d and 10 bbl/d respectively. A major problem in water production is its disposal. The surface installations are not well conditioned to store much water production.

In order to determine the rates of water production properly, we asked the field personnel to test three wells with potential of high water production: 2A, 20A and 52A. No record is available for those tests.

TABLE 6-1 – WELL STATUS AS OF JULY 2003

WELL	STATUS
Currently Pumping	
6-W	Sucker rod. 12/hr/day
26-W	Sucker rod. 12 hr/day
27-W	Sucker rod. 12 hr/day
32-W	Sucker rod. 12 hr/day
121-A	Sucker rod. 8 hr/day
122-A	Sucker rod. 11 hr/day
15-F	Swabbing once a month
119-A	Sucker rod.
31-W	Sucker rod. Once a month
Shut-In due to production issues	
117-A	Sand production. Wellbore full of oil
2-A	High water cut
20-A	High water cut
57-A	High water cut
22-W	High water cut
24-W	High water cut
16-W	Sand production
20-W	Sand production
12-A	Not P&A. No downhole equipment
56-A	Not P&A. No downhole equipment

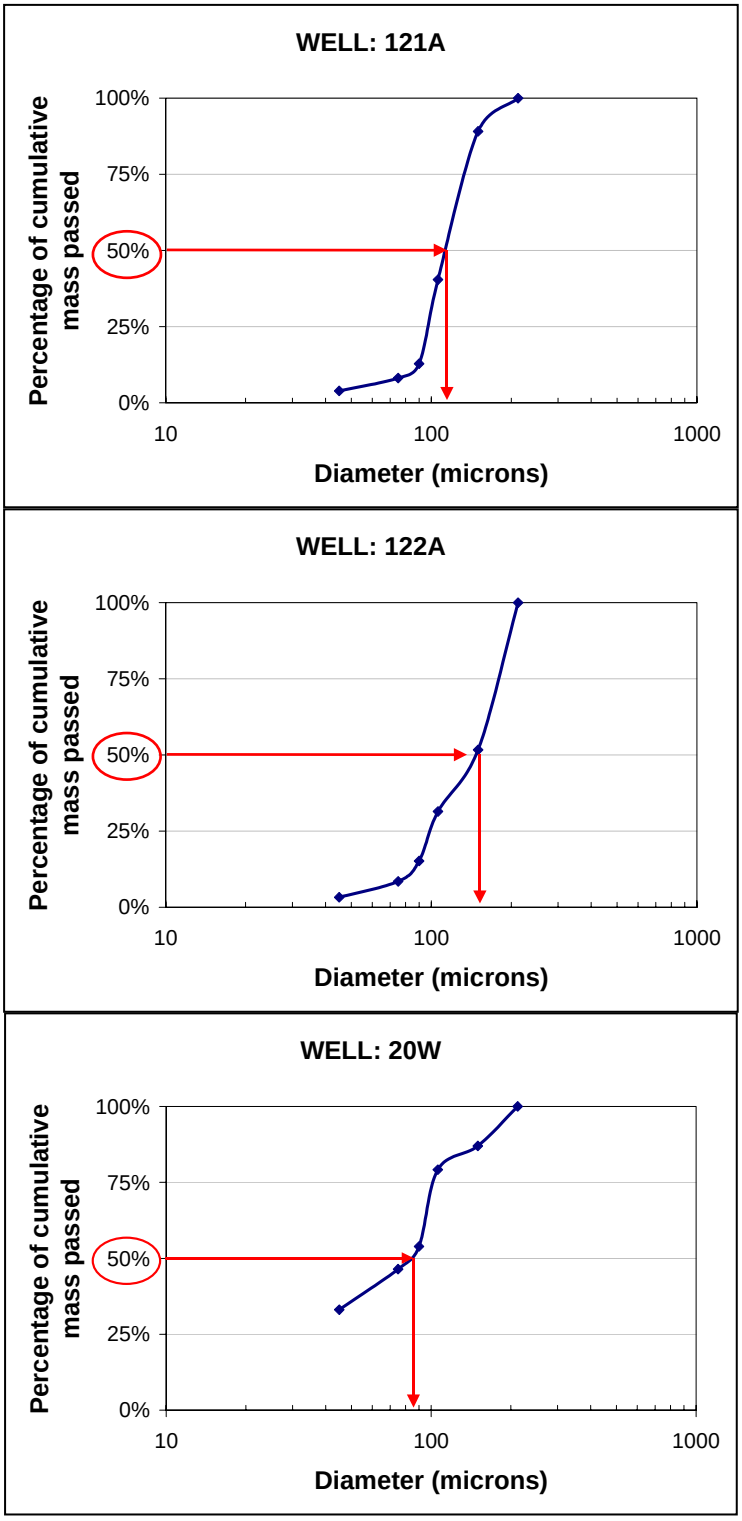

Fig. 6-1 – Grain size distribution analysis for wells 121A, 122A and 20W.

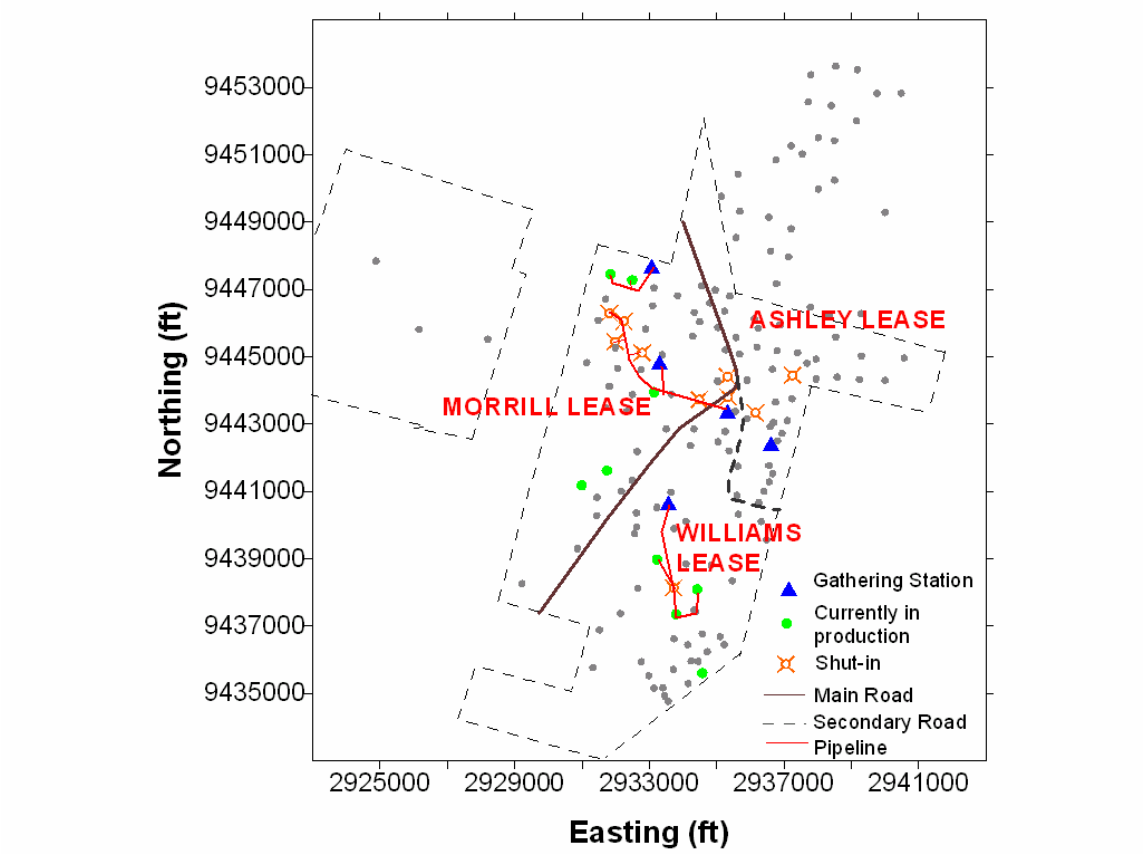

Fig. 6-2 – Surface facilities distribution of the Jacob field.

6.2 Potential development of the field

Maybe the most important part of the research is to identify potential opportunities in the Jacob field.

As it was explained in section 5.5 the recovery factor is in the range of 20% or higher. This high value gives us the idea of the status of depletion of the reservoir. Since the reservoir has pressure support it is expected to recover those 10.60 MSTB of oil and an unknown amount of water. Of course those remaining barrels of oil are not so attractive for the economy of the field due mainly to the time needed to recover them (10 years). Therefore just leaving the wells at their current operating condition is not a good business decision.

We have identified two main sets of opportunities that can be drawn from what it was studied: reconditioning existing wells and drilling new wells.

6.2.1 Reconditioning of existing wells

First, in a short period of term put back on production those wells having production issues to be resolved. For this field, having such a low oil production, adding just 1 barrel of oil per day may impact directly on its economy. For example if we can add the production of the 8 wells having production issues (Table 6-1), the reserves estimation is dramatically increased to 13.5 Mbbls in the worst case and 19.80 Mbbls in the best case.

Second, for the medium term look at by-passed oil: in a certain number of wells the Mirando sand showed oil and gas presence in the drilling cuttings. **Fig. 6-3** shows the location of those wells in Jacob field. 13 wells were identified with the Mirando sand as having oil and gas shows. Moreover, from an early cross section developed in section 2, we have identified that the Mirando sand becomes thicker towards the northwest direction (See Fig. 2-11, structural cross section along dip). If we see again Fig. 6-3 we realize that towards the same direction (northwest) there are more wells having showed oil and gas in the Mirando sand. The first activity needed is to perforate the existing wells and test the Mirando sand and determine its oil potential (of course it will be required to establish the condition of the casing and the cement as well as logging those wells). The second activity would be to drill a new well and core and test the Mirando sand and determine the reservoir quality. So far in all our analyses it showed a better quality than the actual pay formation.

Third, for the medium to long term implement a waterflooding pilot in the existing pay zone. This should be done especially in the northwest part of the structure. Investigate the communication between wells by observing the water breakthrough. But before doing that it is highly mandatory to have the surface facilities distributed properly and in good conditions. The location of injector wells can be accomplished by using the static reservoir models developed: the 3D model, the contour maps of gross and net

thickness, porosity and permeability. Especially the last one since we would like to avoid water channeling while waterflooding the reservoir.

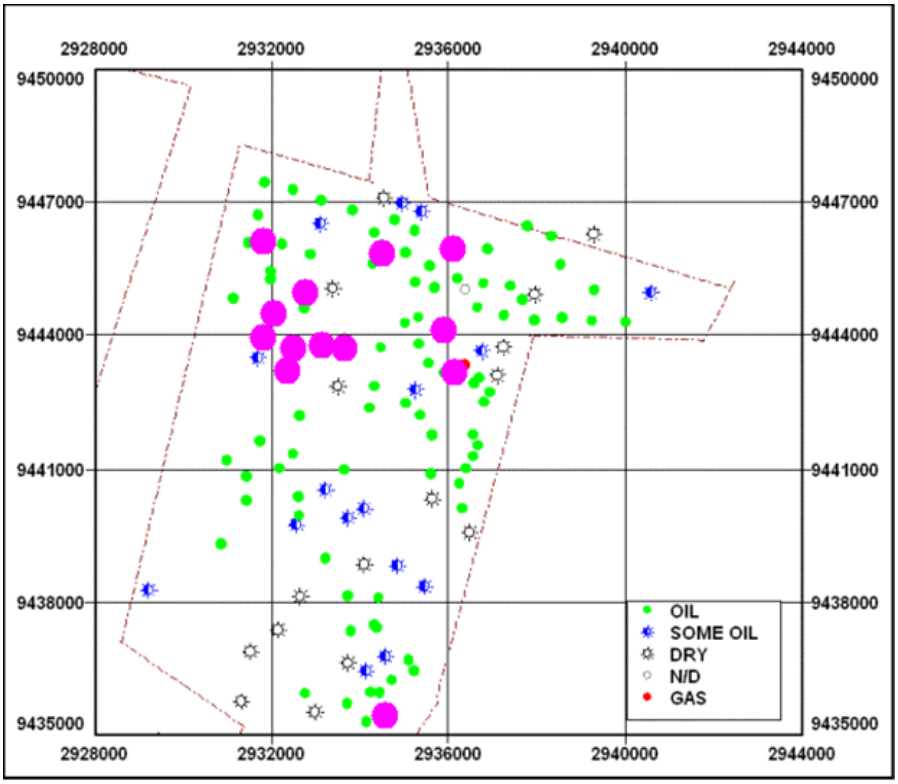

Fig. 6-3- Location of wells that showed oil and gas presence in the Mirando sand.

We would like to remark some questions that should be answered in the short term:

- How much water do we need to handle? (It requires testing production properly)
- How many wells have the casing in good conditions to be able to be shot?
- What is the quality of the water produced? Is it good enough to be re-injected or does it need treatment?
- Are the wells in Jacob field producing with all their potential? (We do not know how damaged the wells in the Jacob field are. Pressure transient tests give us clue answers in this regard).

Only by answering the previous questions might we take forward steps.

6.2.2 Drilling new wells

Infill drilling might be a good option for recovering the remaining reserves in the Jacob field. As it was shown the highest part of the structure (northwest) has areas of low water cut, so this area is attractive for infill drilling.

There is a key question to determine: how big is the drainage radius in Jacob wells? The dimensions of the reservoir can only be obtained by performing a pressure transient test or by having precise production data on a well-by-well basis. Once we have this information we can define the accurate drainage area and a better definition of how far a well can be located from another.

Also, there is plenty of surface area to investigate, but the need of seismic is extremely important to delineate the reservoir structure along the field and improve the model proposed. And therefore look not only for other areas but also for new horizons.

CHAPTER VII

CONCLUSIONS AND RECOMMENDATIONS

7.1 Conclusions

- It was confirmed that Mirando sand was formed in the Jackson Group while the Pettus sand was formed in the upper part of the Yegua formation. Both in the Eocene epoch corresponding to the Nueces River Basin of South Central Texas. They have the particularity of being young unconsolidated clastic sediments.
- By correlating existing well logs it was demonstrated that the formations underlying the Jacob field are continuous along the field. The presence of a continuous layer of lignite (San Miguel lignite) served as an excellent marker and also to define the environments of deposition of the Mirando and Pettus sands. The Mirando sand was deposited in a strandplain-barrier system, however the Pettus was deposited in a lagoonal system (the presence of a continuous layer of oyster shells confirmed this assumption). Because of this fact, the Mirando sand is expected to have better reservoir qualities than the Pettus.
- There were identified five electrofacies that characterized distinctively the rock types of the stratigraphic column of interest. The lignite was identified as EF 4, with particular high neutron porosity and low density, the Mirando sand as EF 6, having a characteristic high GR and high resistivity, and The Pettus as (EF 3 + EF5) showing a serrate GR shape with low resistivity values.
- The shale model that explains the shale character of the formation is that of dispersed clay, this behavior has direct impact in the productivity of the Pettus sand because of the high shale content.
- The analysis of well logs indicated high shale content especially in the Pettus sand (~30%) however the Mirando sand showed low content of shale (<10% in average). In terms of water saturation, the average value estimated for the Pettus formation was 55% and for the Mirando formation 40%.

- The investigation of the anisotropy of the reservoir indicates that there is a strong relationship between the horizontal to the vertical permeability, showing that the fluid has the same preference of flowing towards the vertical or the horizontal direction. In terms of areal anisotropy it was demonstrated that the data tends to be more correlated towards the northwest direction, giving us an idea that the reservoir is more homogeneous in that direction.
- With the aid of a 3D model built using shale content only, the monocline type of structure was confirmed as well as the areal and vertical distribution of shale along the field: in the areal sense, the Mirando sand showed its clean character all along the field, however the Pettus sand showed a moderate to high shale content all along the field. This visual aid can help us in future decisions in determining where to drill and/or where to place injector wells.
- The original oil in place for the Pettus formation was estimated to be 18.12 MMSTB.
- As of October 2003 the remaining reserves were estimated to be 10.6 MSTB. By doing a regression analysis of production data for the unknown period of 19 years we estimated that the EUR could be 3.81 MMSTB. By comparing these values with the volumetric analysis we were able to estimate the recovery factor to be in the order of 20% or higher. That value indicates that the main drive-reservoir mechanism might be waterdrive.
- The analysis of water cut grids along the field and as a function of time showed that there is a water encroachment from the lower parts of the structure. This behavior was confirmed by the analysis of fluid levels in the southern part of the field: the fluid levels easily reached the surface when the wells were shut-in and more water was recovered towards the south direction.
- Two main issues undermine the production improvement in the pumping wells of the Jacob field: sand production and water disposal. Only by solving these problems the production can be increased by 5 STB of oil per day.

7.2 Recommendations

- The fastest way to increment oil production in the Jacob field is by improving the surface facilities distribution and the handling of sand production and water production disposal.
- However at the current rates a low recovery (10 MSTB) is expected for the future 10 years, therefore a mid-term plan is needed. It should be concentrated in developing (waterflooding or infill drilling) the highest part of the structure (northwest area of the field), since it shows that the water did not encroached it yet.
- The long-term plan should be concentrated on investigating the oil potential of the Mirando sand. There were identified thirteen wells that showed oil and gas presence in the Mirando sand. The locations of those wells coincide with the area where the Mirando sand thickens (from cross sections). Therefore the first step in determining the oil potential must be by perforating the depth interval where the Mirando showed oil and gas presence. We suspect good results since this formation shows better reservoir characteristics than the current pay zone.
- The addition of data to the field database will dramatically add value to the present study. We suggest obtaining seismic information to better delineate the horizons and to look for deeper prospects. For the new wells keep always the core samples, those samples are very valuable when analyzing the geological settings of the reservoir. If possible running pressure transient tests will definitely give us key parameters to better characterize the formations (e.g. the current reservoir pressure, the extent of the reservoir, the wellbore damage, etc.).

REFERENCES

1. Barwis, J.H., McPherson, J.G., and Studlick, R.: *Sandstone Petroleum Reservoirs*, Springer-Verlag, New York (1990)
2. Wilson, M.D.: "Evaluating Diagenetically Complex Reservoirs," *Development Geology Manual*, D. Morton-Thompson and A.W. Woods (eds.), Methods in Exploration Series, AAPG, Tulsa, Oklahoma (1993) **10**, 314-320
3. Fisher, W.L., Proctor, C.V., Galloway, W.E., and Nagle, J.S.: "Depositional Systems in the Jackson Group of Texas: Their Relationship to Oil, Gas and Uranium," *Gulf Coast Association of Geological Societies Transactions*, (1970) **20,** 234-261
4. Schenk, C.J., and Viger, R.J.: "Geological Description of the Western Gulf Province (047)," US Geological Survey, http://cpg.cr.usgs.gov/pub/ (2002)
5. Anderson, R.D.F., Barnett, D.G., Briggs, K.S., Brundege, H.T., Cobb, W.R., *et al.*: "Nueces River Cross Section, Maverick to Kleberg Counties, Texas," South Texas Geological Society, San Antonio, Texas (1951)
6. Snedden, J.W.: "Stratigraphy and Environment of Deposition of the San Miguel Lignite Deposit Northern McMullen and Southeastern Atascosa Counties, Texas," M.S. thesis, Texas A&M University, College Station, Texas (1979).
7. Kaiser, W.R., Johnston, J.E., and Bach, W.N.: "Sand Body Geometry and the Occurrence of Lignite in the Eocene of Texas," 1977 Rocky Mountain Coal Symposium, Golden, Colorado, 10 May.
8. Boak, J.M.: "Geological Cross Sections," *Development Geology Manual*, D. Morton-Thompson and A.W. Woods (eds.), Methods in Exploration Series, AAPG, Tulsa, Oklahoma (1993) **10**, 300-304
9. Scheihing, M.H., and Atkinson, C.D.: "Lithofacies and Environmental Analysis of Clastic Depositional Systems," *Development Geology Manual*, D. Morton-Thompson and A.W. Woods (eds.), Methods in Exploration Series, AAPG, Tulsa, Oklahoma (1993) **10**, 263-268

10. Lee, S.H., Kharghoria, A., and Datta-Gupta, A.: “Electrofacies Characterization and Permeability Predictions in Complex Reservoirs,” paper SPE 78662 presented at the 1999 SPE Annual Technical Conference and Exhibition, Houston, Texas, 3-6 October.
11. Bassiouni, Z.: *Theory, Measurement, and Interpretation of Well Logs*, Textbook Series, **4**, SPE, Richardson, Texas (1994)
12. Ahmed, A.M, Hunt, E.R, Pursell, D.A., and McCain, W.D.: “Application of Multi-Well Normalization of Open Hole Logs in Integrated Reservoir Studies,” paper SPE 38263 presented at the 1997 SPE Western Regional Meeting, Long Beach, California, 25-27 June.
13. Heslop, K., and Heslop, A.: “Interpretation of Shaly Sands,” *Dialog Journal*, (April 2002) **10**, 1-14
14. Kelkar, M., and Perez, G.: *Applied Geostatistics for Reservoir Characterization*, SPE, Richardson, Texas (2002).
15. Mattax, C.C., McKinley, R.M., Clothier, A.T.: “Core Analysis of Unconsolidated and Friable Sands,” paper SPE 4986 available from SPE, Richardson, Texas (1975).
16. Monicard, R.P.: *Properties of Reservoir Rocks: Core Analysis*, Institut François Du Pétrole, Paris, France (1980)
17. Xue, G., Datta-Gupta, A., Valko, P.P., and Blasingame, T.A.: “Optimal Transformations for Multiple Regression: Application to Permeability Estimation from Well Logs,” paper SPE 35412 presented at the 1996 SPE Improved Oil Recovery Symposium, Tulsa, Oklahoma, 21 April.
18. Gringarten, E., and Deutsch, C.V.: “Methodology for Variogram Interpretation and Modeling for Improved Reservoir Characterization,” paper SPE 56654 presented at the 1999 SPE Annual Technical Conference and Exhibition, Houston, TX, October 3-6.
19. Maggard, B.J.: Laboratory Experiment Guide “Grain Size Distribution,” Petroleum Engineering 311 Lab. Texas A&M University. Spring 2003

APPENDIX

PRODUCTION DATA ON A WELL-BY-WELL BASIS

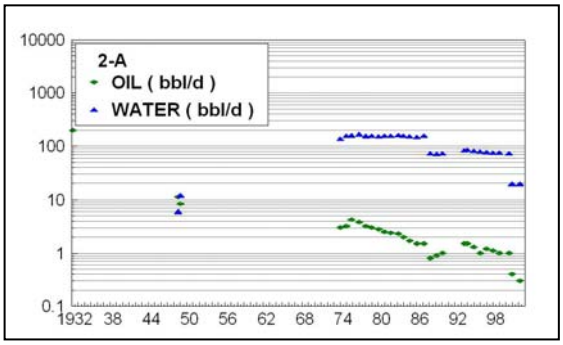
2-A
OIL (bbl/d)
WATER (bbl/d)
10000
1000
100
10
1
0.1
1932 38 44 50 56 62 68 74 80 86 92 98

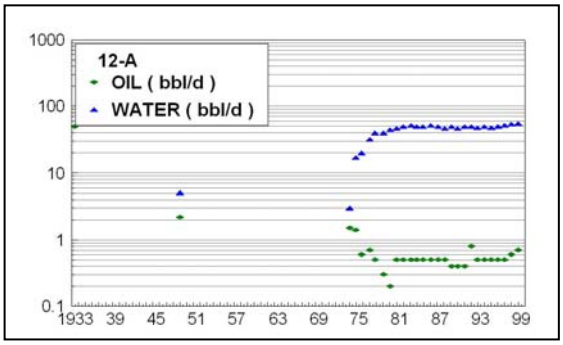
12-A
OIL (bbl/d)
WATER (bbl/d)
1000
100
10
1
0.1
1933 39 45 51 57 63 69 75 81 87 93 99

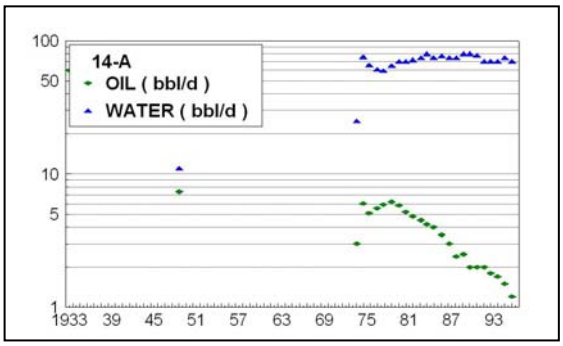
14-A
OIL (bbl/d)
WATER (bbl/d)
100
50
10
5
1
1933 39 45 51 57 63 69 75 81 87 93

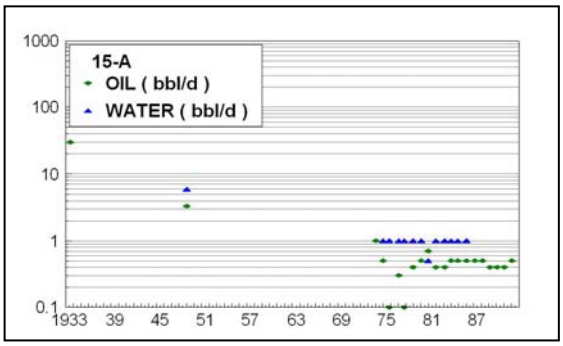
15-A
OIL (bbl/d)
WATER (bbl/d)
1000
100
10
1
0.1
1933 39 45 51 57 63 69 75 81 87

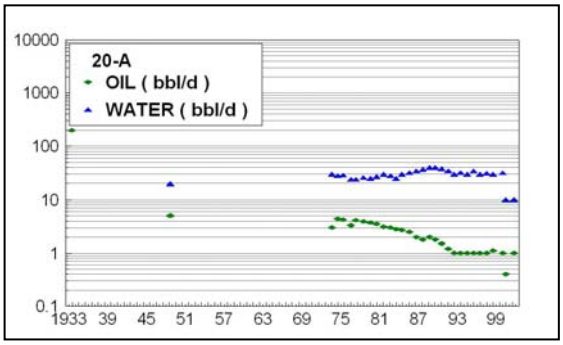
20-A
OIL (bbl/d)
WATER (bbl/d)
10000
1000
100
10
1
0.1
1933 39 45 51 57 63 69 75 81 87 93 99

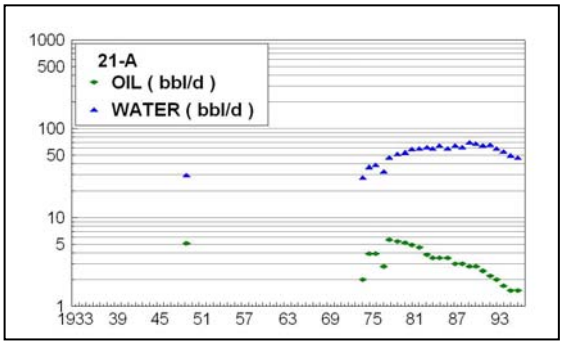
21-A
OIL (bbl/d)
WATER (bbl/d)
1000
500
100
50
10
5
1
1933 39 45 51 57 63 69 75 81 87 93

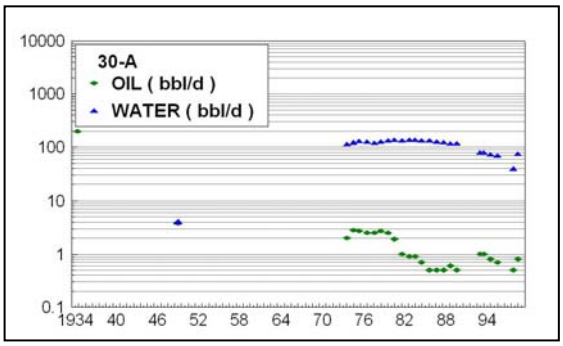
30-A
OIL (bbl/d)
WATER (bbl/d)
10000
1000
100
10
1
0.1
1934 40 46 52 58 64 70 76 82 88 94

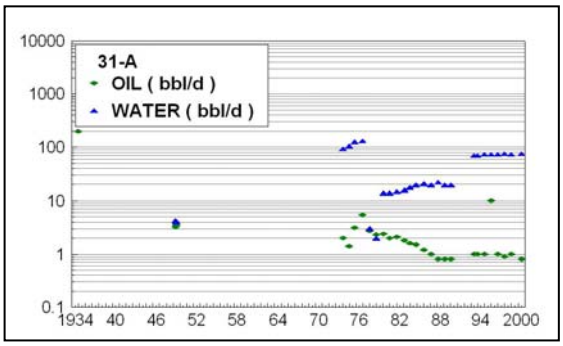
31-A
OIL (bbl/d)
WATER (bbl/d)
10000
1000
100
10
1
0.1
1934 40 46 52 58 64 70 76 82 88 94 2000

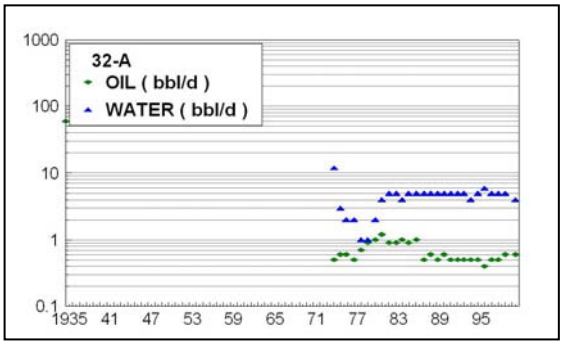
32-A
OIL (bbl/d)
WATER (bbl/d)
1000
100
10
1
0.1
1935 41 47 53 59 65 71 77 83 89 95

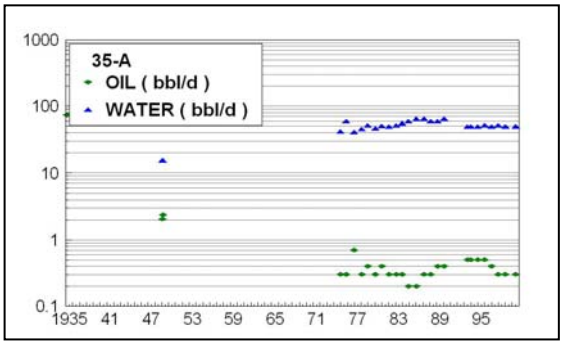
35-A
OIL (bbl/d)
WATER (bbl/d)
1000
100
10
1
0.1
1935 41 47 53 59 65 71 77 83 89 95

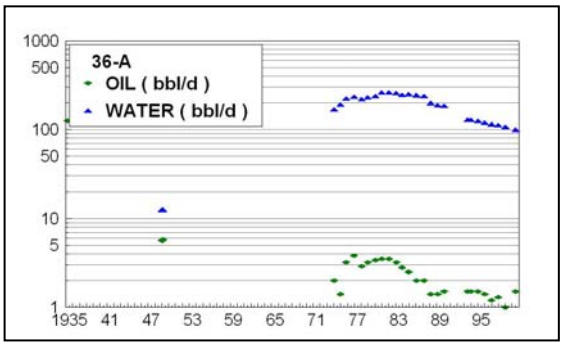
36-A
OIL (bbl/d)
WATER (bbl/d)
1000
500
100
50
10
5
1
1935 41 47 53 59 65 71 77 83 89 95

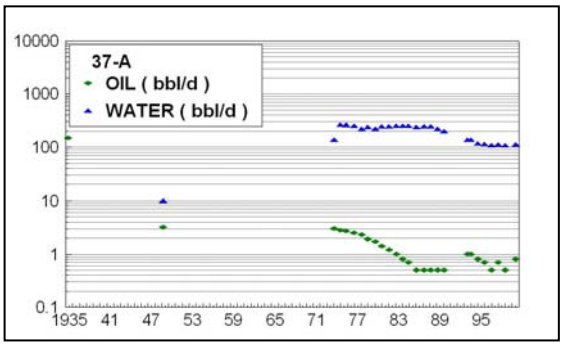
37-A
OIL (bbl/d)
WATER (bbl/d)
10000
1000
100
10
1
0.1
1935 41 47 53 59 65 71 77 83 89 95

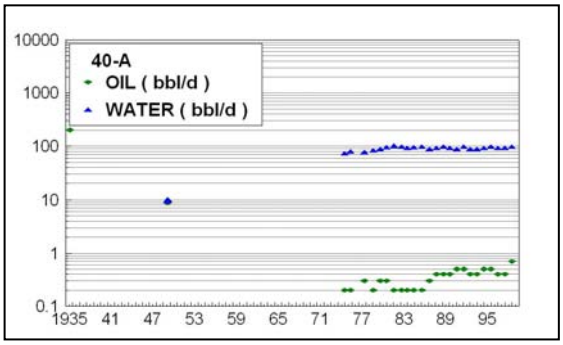
40-A
OIL (bbl/d)
WATER (bbl/d)
10000
1000
100
10
1
0.1
1935 41 47 53 59 65 71 77 83 89 95

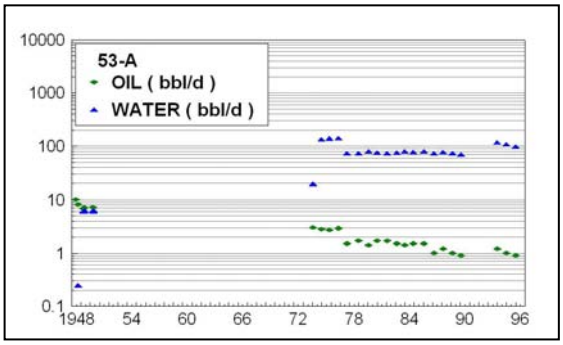
53-A
OIL (bbl/d)
WATER (bbl/d)
10000
1000
100
10
1
0.1
1948 54 60 66 72 78 84 90 96

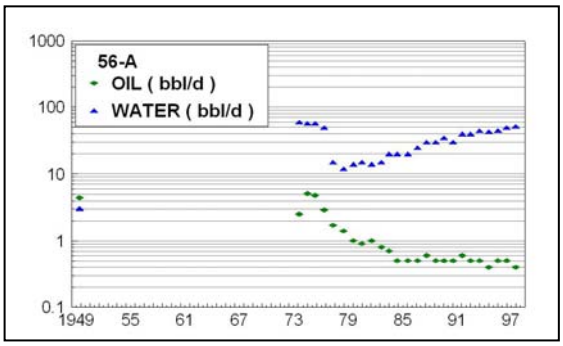
56-A
OIL (bbl/d)
WATER (bbl/d)
1000
100
10
1
0.1
1949 55 61 67 73 79 85 91 97

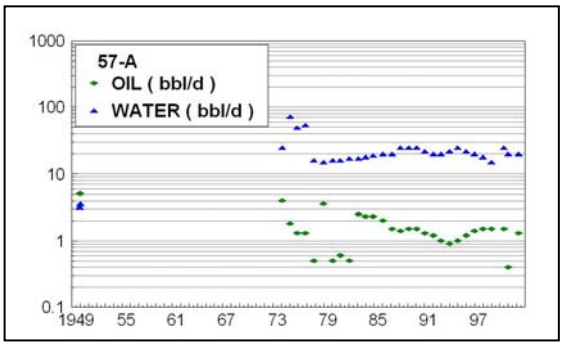
57-A
OIL (bbl/d)
WATER (bbl/d)
1000
100
10
1
0.1
1949 55 61 67 73 79 85 91 97

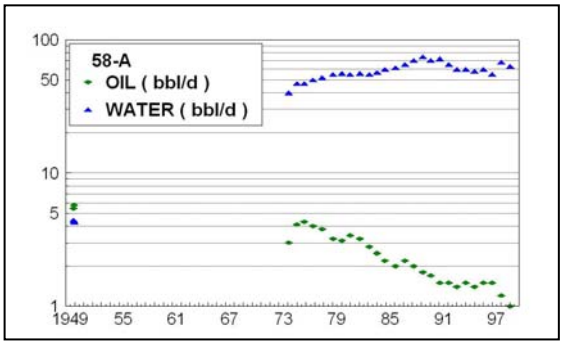
58-A
OIL (bbl/d)
WATER (bbl/d)
100
50
10
5
1
1949
55
61
67
73
79
85
91
97

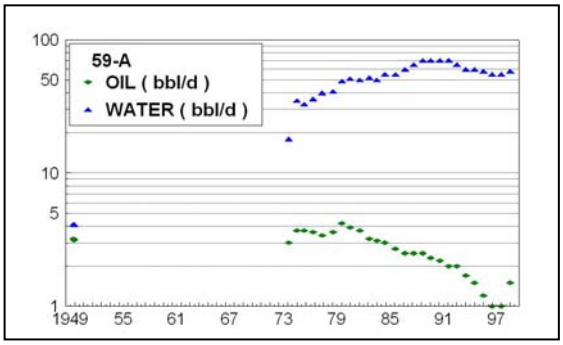
59-A
OIL (bbl/d)
WATER (bbl/d)
100
50
10
5
1
1949
55
61
67
73
79
85
91
97

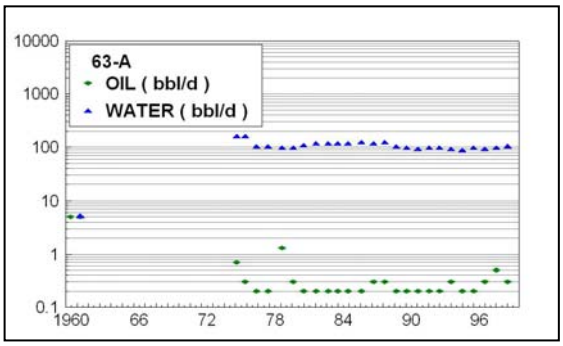
63-A
OIL (bbl/d)
WATER (bbl/d)
10000
1000
100
10
1
0.1
1960
66
72
78
84
90
96

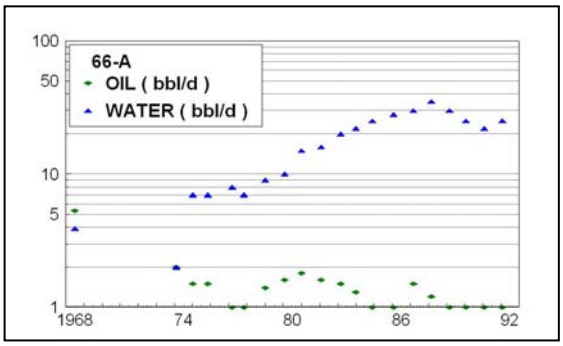
66-A
OIL (bbl/d)
WATER (bbl/d)
100
50
10
5
1
1968
74
80
86
92

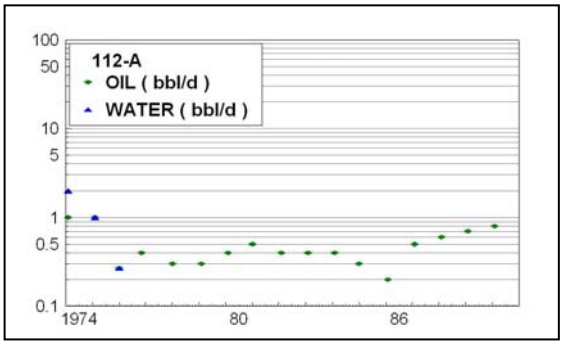
112-A
OIL (bbl/d)
WATER (bbl/d)
100
50
10
5
1
0.5
0.1
1974
80
86

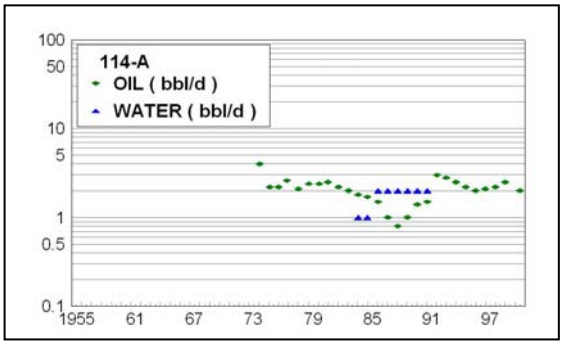
114-A
OIL (bbl/d)
WATER (bbl/d)
100
50
10
5
1
0.5
0.1
1955
61
67
73
79
85
91
97

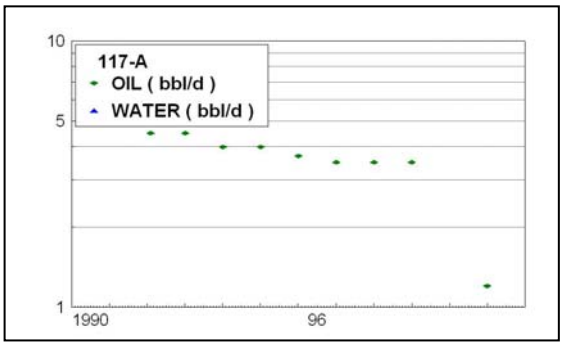
117-A
OIL (bbl/d)
WATER (bbl/d)
10
5
1
1990
96

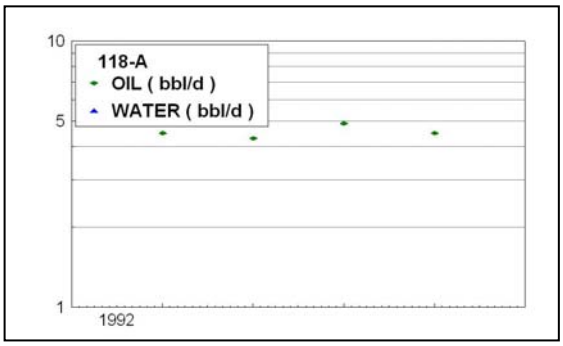
118-A
OIL (bbl/d)
WATER (bbl/d)
10
5
1
1992

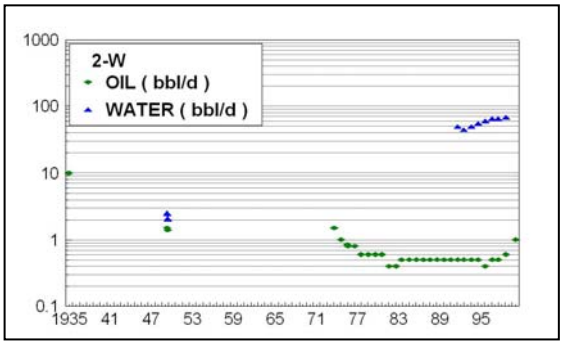
2-W
OIL (bbl/d)
WATER (bbl/d)
1000
100
10
1
0.1
1935 41 47 53 59 65 71 77 83 89 95

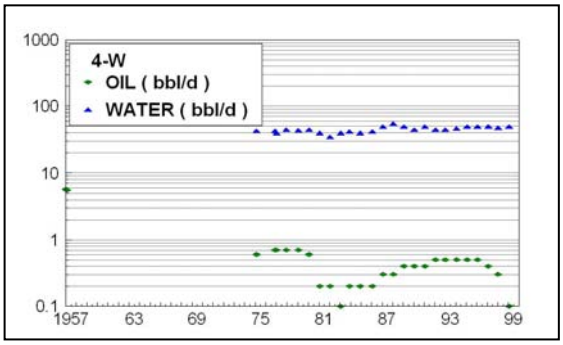
4-W
OIL (bbl/d)
WATER (bbl/d)
1000
100
10
1
0.1
1957 63 69 75 81 87 93 99

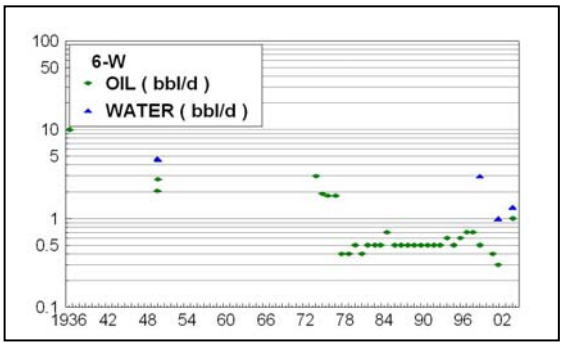
6-W
OIL (bbl/d)
WATER (bbl/d)
100
50
10
5
1
0.5
0.1
1936 42 48 54 60 66 72 78 84 90 96 02

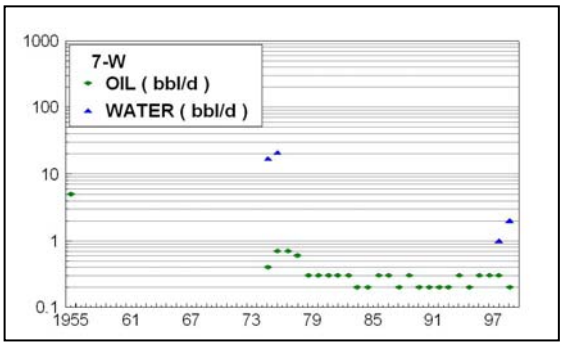
7-W
OIL (bbl/d)
WATER (bbl/d)
1000
100
10
1
0.1
1955 61 67 73 79 85 91 97

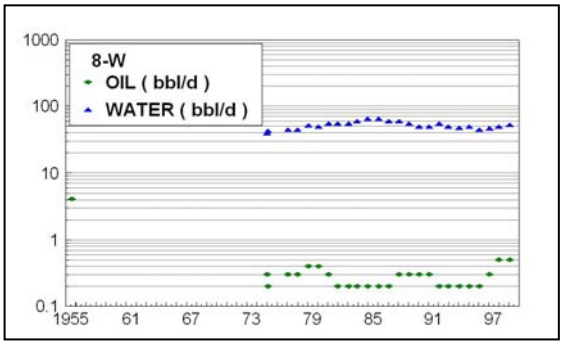
8-W
OIL (bbl/d)
WATER (bbl/d)
1000
100
10
1
0.1
1955 61 67 73 79 85 91 97

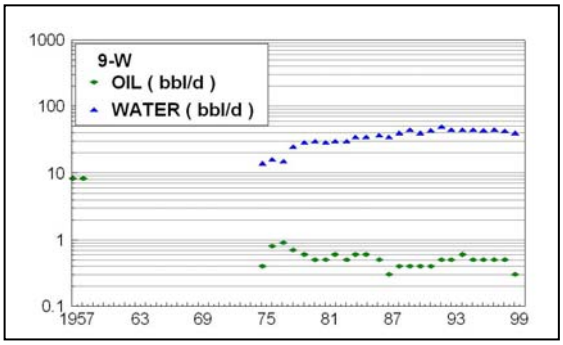
9-W
OIL (bbl/d)
WATER (bbl/d)
1000
100
10
1
0.1
1957 63 69 75 81 87 93 99

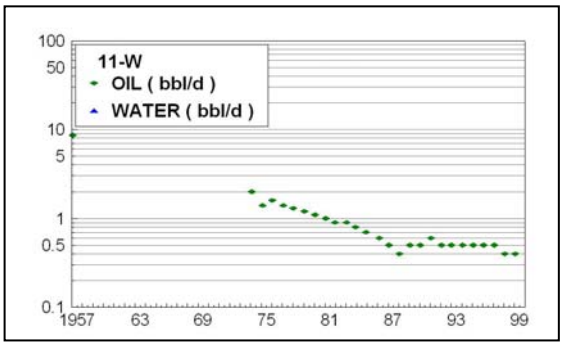
11-W
OIL (bbl/d)
WATER (bbl/d)
100
50
10
5
1
0.5
0.1
1957 63 69 75 81 87 93 99

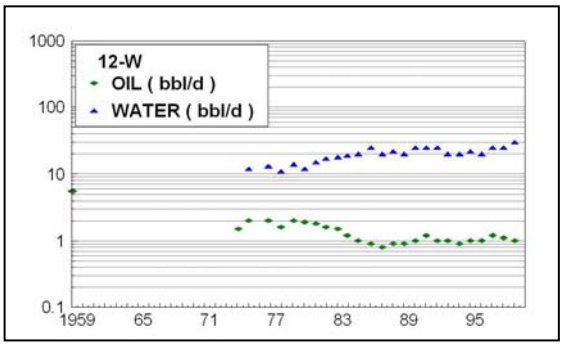
12-W
OIL (bbl/d)
WATER (bbl/d)
1000
100
10
1
0.1
1959 65 71 77 83 89 95

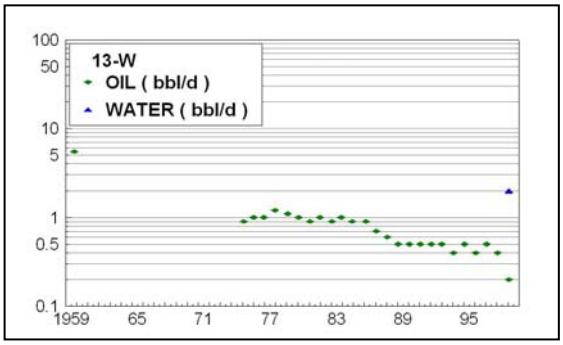
13-W
OIL (bbl/d)
WATER (bbl/d)
100
50
10
5
1
0.5
0.1
1959
65
71
77
83
89
95

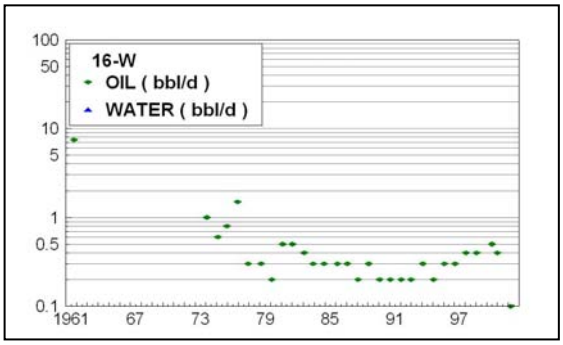
16-W
OIL (bbl/d)
WATER (bbl/d)
100
50
10
5
1
0.5
0.1
1961
67
73
79
85
91
97

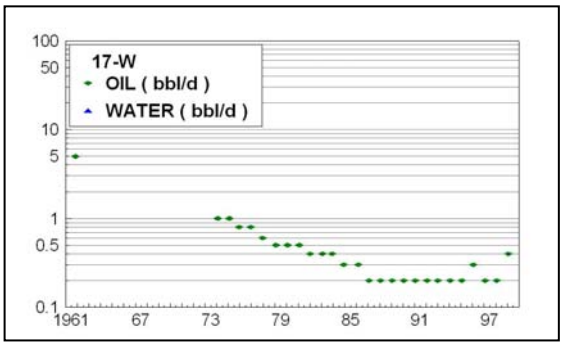
17-W
OIL (bbl/d)
WATER (bbl/d)
100
50
10
5
1
0.5
0.1
1961
67
73
79
85
91
97

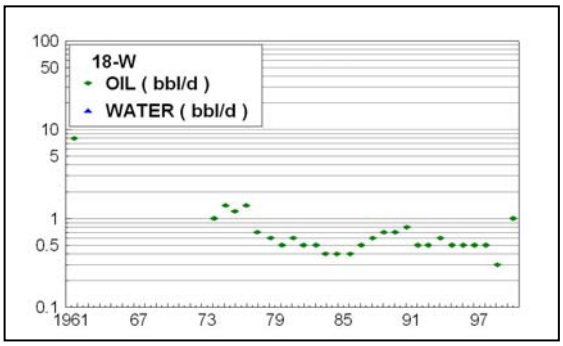
18-W
OIL (bbl/d)
WATER (bbl/d)
100
50
10
5
1
0.5
0.1
1961
67
73
79
85
91
97

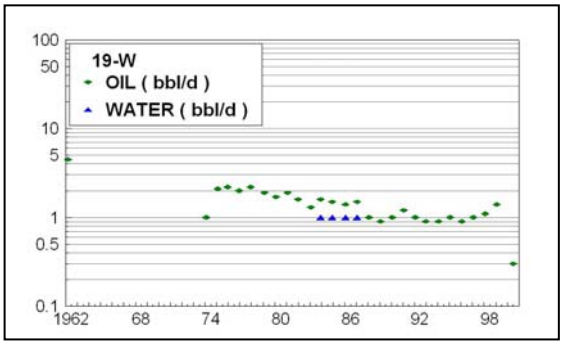
19-W
OIL (bbl/d)
WATER (bbl/d)
100
50
10
5
1
0.5
0.1
1962
68
74
80
86
92
98

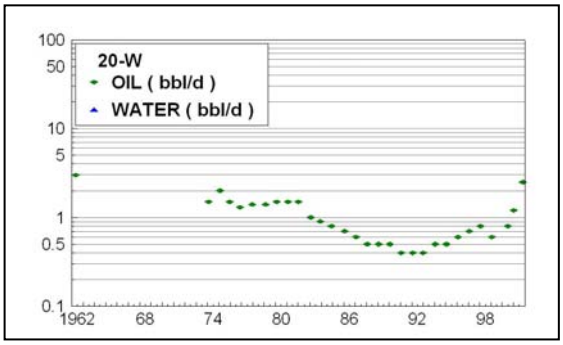
20-W
OIL (bbl/d)
WATER (bbl/d)
100
50
10
5
1
0.5
0.1
1962
68
74
80
86
92
98

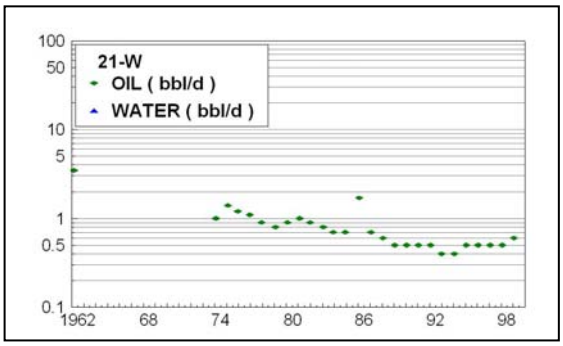
21-W
OIL (bbl/d)
WATER (bbl/d)
100
50
10
5
1
0.5
0.1
1962
68
74
80
86
92
98

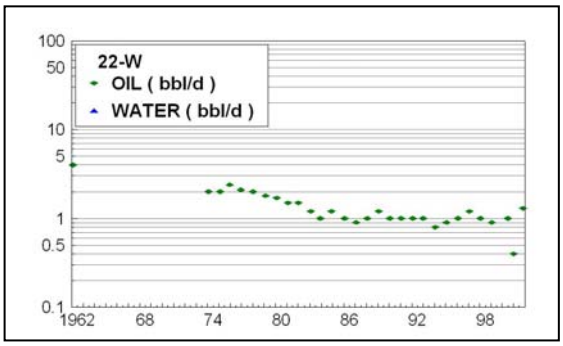
22-W
OIL (bbl/d)
WATER (bbl/d)
100
50
10
5
1
0.5
0.1
1962
68
74
80
86
92
98

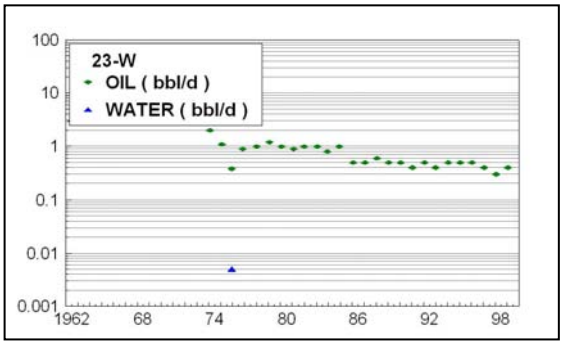
23-W
OIL (bbl/d)
WATER (bbl/d)
100
10
1
0.1
0.01
0.001
1962 68 74 80 86 92 98

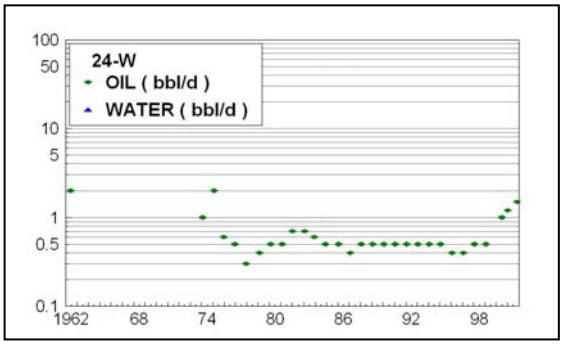
24-W
OIL (bbl/d)
WATER (bbl/d)
100
50
10
5
1
0.5
0.1
1962 68 74 80 86 92 98

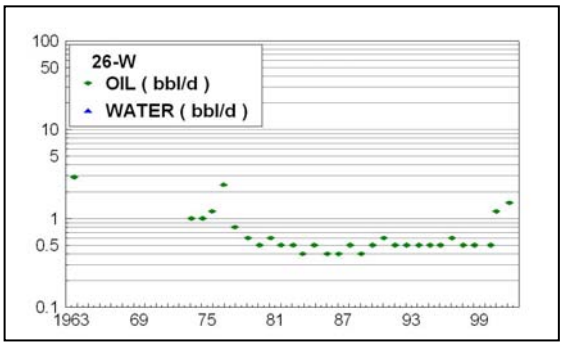
26-W
OIL (bbl/d)
WATER (bbl/d)
100
50
10
5
1
0.5
0.1
1963 69 75 81 87 93 99

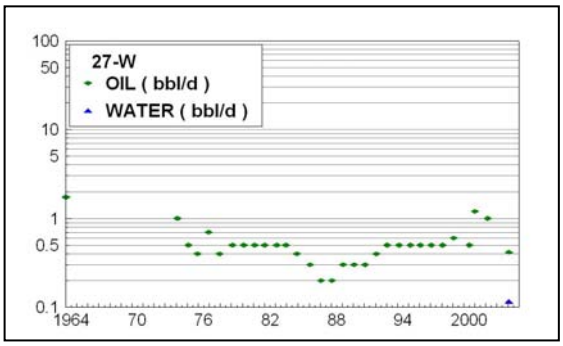
27-W
OIL (bbl/d)
WATER (bbl/d)
100
50
10
5
1
0.5
0.1
1964 70 76 82 88 94 2000

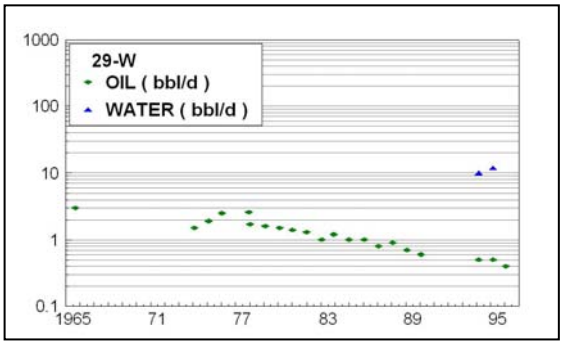
29-W
OIL (bbl/d)
WATER (bbl/d)
1000
100
10
1
0.1
1965 71 77 83 89 95

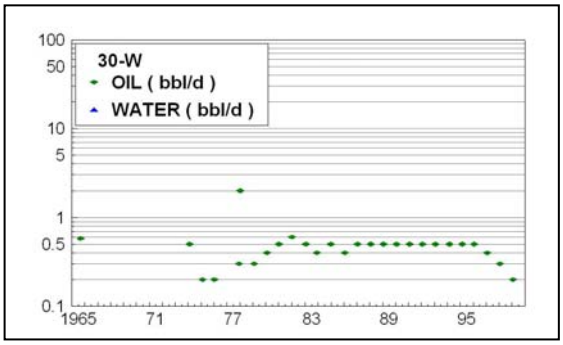
30-W
OIL (bbl/d)
WATER (bbl/d)
100
50
10
5
1
0.5
0.1
1965 71 77 83 89 95

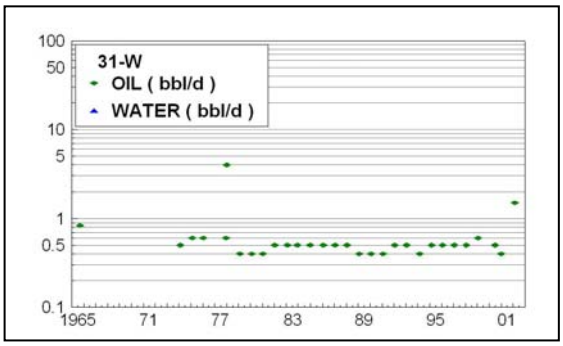
31-W
OIL (bbl/d)
WATER (bbl/d)
100
50
10
5
1
0.5
0.1
1965 71 77 83 89 95 01

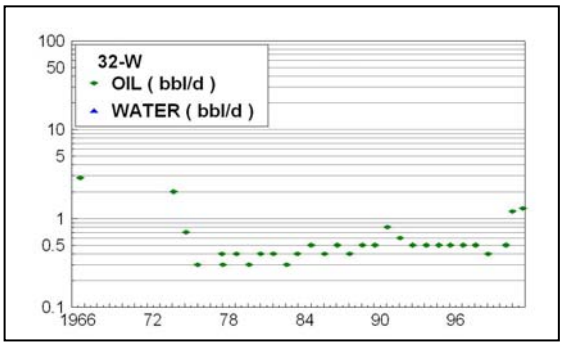
32-W
OIL (bbl/d)
WATER (bbl/d)
100
50
10
5
1
0.5
0.1
1966 72 78 84 90 96

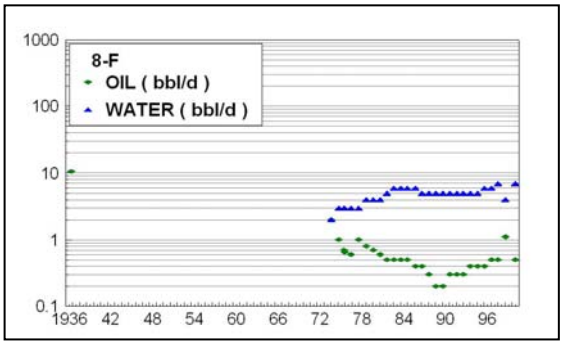
8-F
OIL (bbl/d)
WATER (bbl/d)
1000
100
10
1
0.1
1936 42 48 54 60 66 72 78 84 90 96

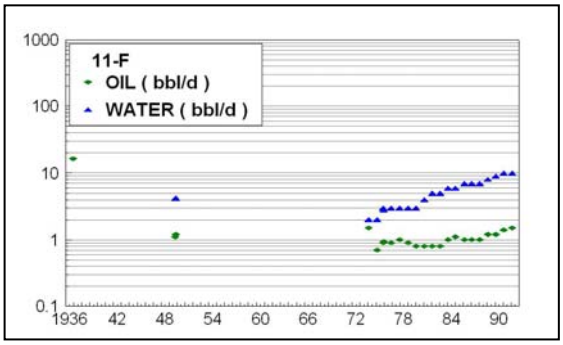
11-F
OIL (bbl/d)
WATER (bbl/d)
1000
100
10
1
0.1
1936 42 48 54 60 66 72 78 84 90

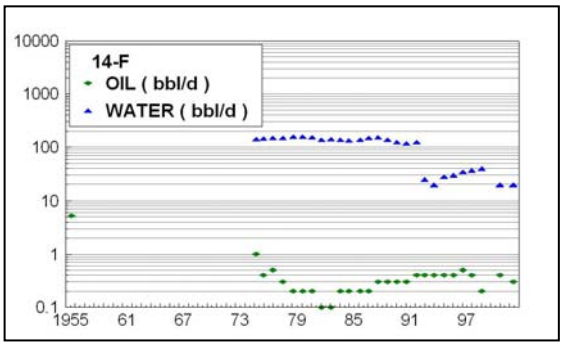
14-F
OIL (bbl/d)
WATER (bbl/d)
10000
1000
100
10
1
0.1
1955 61 67 73 79 85 91 97

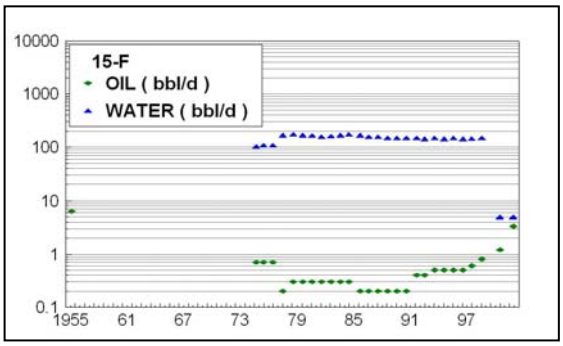
15-F
OIL (bbl/d)
WATER (bbl/d)
10000
1000
100
10
1
0.1
1955 61 67 73 79 85 91 97

VITA

Name:	Mirko Joshoe Hernandez Depaz
Permanent Adress:	Mz 16 Lt 14 Urb. Nicrupampa Huaraz, Ancash, Peru
Education:	B.S., Petroleum Engineering National University of Engineering Lima, Peru, 1996
Experience:	Repsol-YPF, San Jorge Basin, Argentina Reservoir Engineer (1998-2002) Schlumberger Anadrill, Lima, Peru MWD Engineer (1997-1998)